University of Alberta

Subsurface Hydrological Characteristics of an Overdeepened Cirque Glacier

by

Christine F. Dow

A thesis submitted to the Faculty of Graduate Studies and Research
in partial fulfillment of the requirements for the degree of

Master of Science

Department of Earth and Atmospheric Sciences

Fall 2009
Edmonton, Alberta

Examining Committee

Dr. Jeffrey Kavanaugh, Department of Earth and Atmospheric Sciences

Dr. Martin Sharp, Department of Earth and Atmospheric Sciences

Dr. Peter Steffler, Department of Civil and Environmental Engineering

Dedication

I would like to dedicate this thesis to my grandmother, Elizabeth Anderson (1924-2008). She was a wonderful women, looked up to and respected by all who knew her. She continues to be a great inspiration in my life.

Abstract

This thesis examines the hydrological characteristics of West Washmawapta Glacier, an overdeepened cirque glacier located in the Vermillion Range, B.C., Canada. Fieldwork involved drilling nine boreholes, which were surveyed with a borehole camera and instrumented with combinations of pressure transducers, thermistors and electrical conductivity sensors. Results show the cirque hydrology consisted of a predominantly subglacial, distributed drainage system. Hydraulic jacking occurred within the overdeepened region in both the summers of 2007 and 2008. Hydrological shut-down occurred very late, potentially due to the effect of the riegel on basal drainage, preventing flow out of the overdeepening at lower water pressures. Basal water temperatures were observed to fluctuate diurnally (up to 0.8°C) above the local pressure melting point, likely due to influx of geothermally-heated groundwater and insulation of water within a sediment aquifer. Varying basal water pressures and temperatures suggest that hydraulic potential and supercooling effects are often over-simplified in glacier studies.

Acknowledgements

I would like to first and foremost thank my supervisor, Dr. Jeff Kavanaugh, for the help he provided with this project and the thesis during my M.Sc. I received much assistance from Jeff with planning, organizing and implementing the field seasons for this project. In addition, he suggested many helpful edits during the writing of this thesis. Jeff also provided me with many invaluable opportunities for developing my science career, including various field assistant positions and support for attendance at several international conferences.

Justin Beckers is gratefully acknowledged for field assistance in 2007 and 2008, particularly for his wire-coiling and inclinometer-pulling skills among many others. In addition, I would like to thank the collaborators of the Helmet Mountain Cirque Project, Dr. Kurt Cuffey, Johnny Sanders and Dr. Kelly MacGregor, for advice, support and good company in the field.

Financial and logistical support for this M.Sc. project and the related fieldwork was provided by Alberta Ingenuity, the Natural Sciences and Engineering Research Council of Canada, the Canadian Circumpolar Institute, the National Science Federation, the University of Alberta Graduate Student Association, the Institute of Geophysical Research and the Faculty of Graduate Studies and Research at the University of Alberta. I gratefully acknowledge their support.

Many people have assisted in the completion of this thesis. In particular, I had several very helpful conversations with Dr. Martin Sharp during this project. In addition Roy Coulthard, Jess Vaughan, Hannah Milne, Faye Wyatt, Ben Gready, Dr. John England, Dr. Nick Barrand, Inka Koch and Alex Gardner all contributed useful discussions and/or help with this project.

Finally, I would like to thank my family and friends for their support and encouragement, which was invaluable throughout the process of completing this thesis and M.Sc.

Contents

List of Tables

List of Figures

List of Symbols

B	Conductivity cell constant	cm^{-1}
C_c	Conductance	Ω^{-1}
C_s	Specific heat capacity of water	$4.2 \times 10^6\,\mathrm{J\,m^{-3}\,K^{-1}}$
E_{pmp}	Heat energy to keep water at the pressure melting point	$\mathrm{m\,kg\,s^{-3}}$
E_w	Heat production from water flow	$\mathrm{kg\,s^{-3}}$
G	Gain (V_{out}/V_{in})	unitless
H	Ice thickness	m
K	$1 + \beta\, C_s$	unitless
L	Latent heat of fusion	$3.34 \times 10^5\,\mathrm{J\,kg^{-1}}$
P_i	Ice overburden pressure	Pa
P_w	Water pressure	Pa
Q	Water flux	$\mathrm{m^3\,s^{-1}\,m^{-1}}$
R_r	Reference resistor	Ω
R_s	Resistance of sensor	Ω
R_w	Resistance of wire	Ω
V_{in}	Datalogger excitation voltage	mV
V_{out}	Sensor output voltage	mV
Z_s	Elevation of the ice surface	m
$\dot{f}$	Rate of freezing	$\mathrm{kg\,s^{-1}\,m^{-2}}$
g	Acceleration due to gravity	$9.81\,\mathrm{m\,s^{-2}}$
s	Distance along the direction of equipotential	m
x	Distance along the vertical plane of s	m
z	Elevation above a reference datum level	m
α_b	Horizontal gradients of glacier bed elevation	unitless
α_b^*	Hydraulic slope threshold at ice overburden pressure	unitless
$\alpha_{b\gamma}^*$	Hydraulic slope threshold at varied water pressures	unitless
$\alpha_b^\dagger$	Supercooling slope threshold at ice overburden pressure	unitless
$\alpha_{b\gamma}^\dagger$	Supercooling slope threshold at varied water pressures	unitless
α_s	Horizontal gradients of ice surface elevation	unitless
β	Pressure melting point coefficient	$\mathrm{K\,Pa^{-1}}$
γ	Fraction of ice overburden pressure	unitless

Δh	Change of water pressure head height	m
θ_{TPK}	Triple point temperature	$273.16\,\mathrm{K}$
ϕ	Hydraulic potential	Pa
ϕ_0	Reference hydraulic potential	Pa
$\nabla\phi$	Hydraulic potential gradient at overburden pressure	$\mathrm{kg\,m^2\,s^2}$
$\nabla\phi_\gamma$	Hydraulic potential gradient at varied water pressures	$\mathrm{kg\,m^2\,s^2}$
ρ_i	Density of ice	$917\,\mathrm{kg\,m^{-3}}$
ρ_w	Density of water	$1000\,\mathrm{kg\,m^{-3}}$
σ	Conductivity	$\mu\mathrm{S\ cm^{-1}}$

List of Abbreviations

AWS = Automatic Weather Station
DEM = Digital Elevation Model
EODH = englacial overdeepening drainage hypothesis
GPR = Ground Penetrating Radar
HST = hydraulic slope threshold
PMP = pressure melting point
SST = supercooling slope threshold
WWG = West Washmawapta Glacier

Chapter 1

Introduction

1.1 Overview

Cirques are features found in almost every mountainous landscape. They often consist of an overdeepened bowl with an amphitheatre-like headwall. Although there is little consensus on their initial formative mechanism (see e.g. Benn and Evans, 1998; Bennett *et al.*, 1999; Turnbull and Davies, 2006), glacial erosion processes are widely recognized as being highly influential in the development of cirque bowls (e.g. Olyphant, 1981; Holmlund, 1991; Bennett *et al.*, 1999; Oskin and Burbank, 2005). As a result, an understanding of cirque glacier dynamics is necessary to comprehend the evolution of these overdeepened features.

Glacier hydrology affects ice dynamics through enhanced sliding and sediment deformation (e.g. Piotrowski, 2003), and subglacial erosion through weathering and removal of basal material (e.g. Roberts *et al.*, 2002; Alley *et al.*, 2003a). Despite the importance of glacier hydrology in these systems, little research has been conducted into the hydrological characteristics of cirque

glaciers. However, some related studies have been carried out for overdeepenings under valley glaciers (e.g. Hodge, 1976; Hantz and Lliboutry, 1983; Hooke *et al.*, 1988; Fountain, 1994; Iken *et al.*, 1996; Hanson *et al.*, 1998). The most widely cited hypothesis for the hydrological characteristics of overdeepenings was developed by Hooke and others (Hooke *et al.*, 1988; Hooke, 1991; Hooke and Pohjola, 1994) at Storglaciären, a small polythermal glacier in Sweden. This overdeepening hypothesis (hereafter referred to as the 'englacial overdeepening drainage hypothesis' or EODH) stipulates that if the adverse slope of a riegel (a barrier of bedrock that bounds an overdeepening at the down-valley end) is sufficiently steep, subglacial water will be forced into the englacial system, thus bypassing the overdeepening, as shown in Figure 1.1. The EODH, if applied to overdeepened cirque glaciers, has significance for erosion and weathering patterns in the cirque bowl, as basal erosion would be difficult to maintain with a primarily englacial hydrological system. It is therefore important to establish whether the drainage pattern suggested by the EODH is ubiquitous for overdeepened cirque and valley glaciers, or only applicable to a subset of overdeepened glaciers, if any.

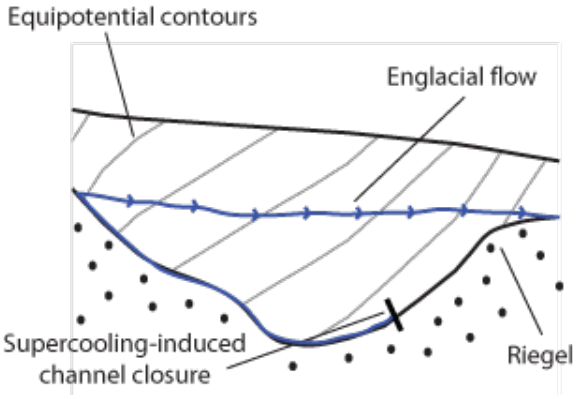

Figure 1.1: Simplified model of englacial flow over an overdeepening instigated by blockage of subglacial channels due to a steep adverse slope.

1.2 Review of glacial hydrology

Water flowing on the surface of glaciers is sourced primarily from surface ablation and precipitation (Stenborg, 1973; Fountain, 1998). In many cases, much of this supraglacial water is routed through subsurface (i.e. englacial and subglacial) drainage systems, within which the fluid is stored or transported in various types of networks. The process of water evacuation through different drainage systems and basal conditions is complex. For example, drainage pathways can consist of englacial conduits, subglacial linked-cavities, basal water films, subglacial channels or flow through basal sediment, among others. It is widely recognized that many of these drainage systems can co-exist under the same glacier (e.g. Fountain, 1993; Hubbard *et al.*, 1995; Hubbard and Nienow, 1997; Fountain and Walder, 1998). In addition, both englacial and subglacial drainage systems are temporally and spatially variable, so it is rare that only one water flow model should be applied to a glacial system (Vivian, 1980).

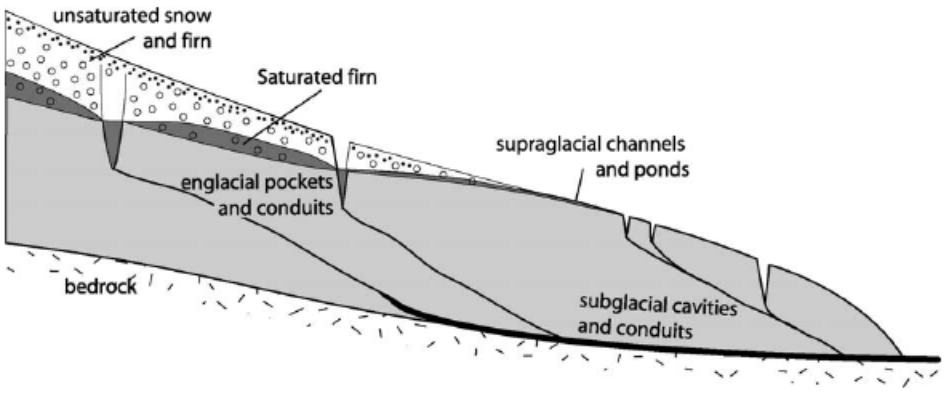

Figure 1.2: Schematic of the main hydrological systems within a glacier. From Jansson *et al.* (2003), originally adapted from Röthlisberger and Lang (1987).

In this chapter, I will describe several types of glacial drainage networks, and also the effects of adverse basal slopes on the evacuation of water out of glacial systems. The latter is particularly important in overdeepening drainage systems. Glacier drainage systems consist of supraglacial, englacial and sub-

glacial components, as depicted in Figure 1.2. This thesis focuses on the subsurface hydrology of cirque glaciers, and so supraglacial drainage will only be minimally discussed.

1.2.1 *Englacial drainage*

Conduits

Water penetrates to the bed of a glacier through moulins (Stenborg, 1973; Hooke, 1989), crevasses (Weertman, 1973; Boon and Sharp, 2003), or conduits (channels) within the ice (Röthlisberger and Lang, 1987; Fountain and Walder, 1998). The latter generally form at the base of crevasses and propagate down into the ice through micro-fractures or ice veins (Fountain and Walder, 1998). Figure 1.3 shows one process by which an englacial channel might develop at the base of a crevasse.

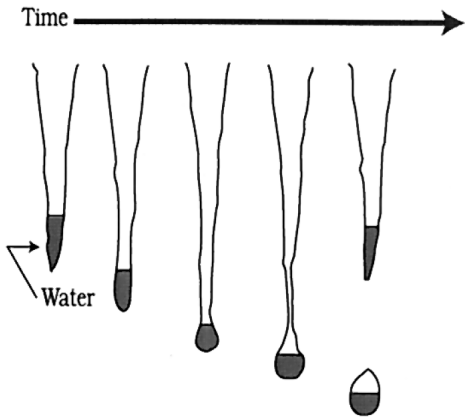

Figure 1.3: Formation of an englacial channel flowing at the base of a crevasse. Over time, the crevasse closes due to ice deformation but the channel persists because of sufficient water flow preventing closure. From Fountain and Walder (1998).

Englacial channels, once initiated in moulins or crevasses, generally propagate perpendicularly to equipotential contours within the glacier (see Shreve, 1972). Englacial channels are thought to form an upward-branching arborescent network (Fig. 1.4) and reach the glacier bed somewhat downstream of

where they entered the system (Shreve, 1972; Fountain, 1993; Fountain and Walder, 1998).

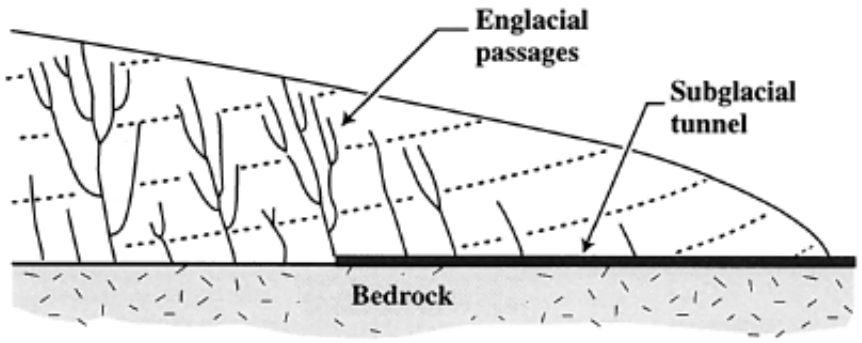

Figure 1.4: Arborescent network of englacial channels flowing (solid lines) perpendicular to equipotential contours (dotted lines). From Fountain and Walder (1998).

Englacial fractures

Borehole video observations by Fountain *et al.* (2005a,b) at Storglaciären identified englacial fractures that functioned as a major water transport system. Similar fractures were noted by J. Harper (http://research.gg.uwyo.edu/joelh/benchglacier/video.html) during borehole video surveys at Bench Glacier, Alaska in 2002. One of the Bench Glacier voids opened during the field season at a depth of 138 m; it was not related to surface crevasse features.

It is not clear how englacial fractures form or whether they originate at the bed of the glacier, within the ice itself, or from the downward extension of surface crevasses (Fountain *et al.*, 2005b). The fractures generally follow old strain features such as palaeo-crevasses (crevasses closed through ice deformation). The englacial fractures also tend to be hydraulically active, which prevents their closure by ice deformation (Fountain *et al.*, 2005a,b).

Englacial pore flow

An alternative mechanism for the formation of englacial conduits is from water flow through pores in the ice. Nye and Frank (1973) argued that water should be able to flow through three- and four-grain ice intersections, rendering temperate glaciers (glaciers with ice entirely at the pressure melting point) essentially permeable. Although water along ice-grain boundaries was identified by Raymond and Harrison (1975), the intersections were found to have extremely low water velocities. Slow flow was due to the small size of veins ($\sim$5-10 μm) that equated to a hydraulic conductivity of around 0.1 mm a^{-1} for bubbly ice (Raymond and Harrison, 1975), and 0.9 mm a^{-1} for finer-grained blue ice (Nye and Frank, 1973). Lliboutry (1971) argued that if the glacier was fully permeable, viscous dissipation of frictional heat resulting from water flow would soon create a glacier full of vertical holes and rapidly melt the entire body of ice. Instead, Lliboutry (1971) suggested that vein passages are blocked by ice deformation and refreezing in grain intersections, which limits the distance that water can be transmitted through ice pores to a length scale of a few ice grains (Lliboutry, 1971).

1.2.2 *Subglacial drainage*

Subglacial drainage systems typically develop, both spatially and temporally, from relatively constricted networks, such as linked-cavity systems, towards more efficient networks, such as channelized systems during the summer months (Nienow *et al.*, 1998a). This drainage network development is due to the competition between the frictional melting of basal ice from water flow, and the creep closure of ice. The capacity of the subglacial drainage system therefore evolves along with seasonal changes in the volume of water input (Paterson,

1994).

Linked-cavity drainage

Lliboutry (1964) suggested that when ice slides over rough basal topography, subglacial cavities form. Basal water fills cavities because they are at a lower pressure than areas that are in direct contact with the ice. As water input into the system increases, previously isolated water-filled cavities become connected by small conduits, and water flow is enabled through an anastomosing, highly distributed system (Lliboutry, 1968; Iken and Bindschadler, 1986). Distributed systems (e.g. Fig. 1.5a) are inefficient at transporting subglacial water (Walder, 1986), and are therefore characterized by high water pressures (Lliboutry, 1968; Lappegard and Kohler, 2005). With even greater influxes of meltwater into the system, water pressure in linked-cavities can, in some circumstances, exceed the ice overburden pressure, allowing the ice to be lifted off the bed. This 'hydraulic jacking' can reduce basal friction and increase the glacier velocity (Iken *et al.*, 1983; Röthlisberger and Lang, 1987).

Channelized drainage

Once greater volumes of water begin to flow through the basal system, cavities can become more closely linked and form channels (Walder, 1986; Mair *et al.*, 2002b). Röthlisberger (1972) first conceptually examined development of pressurized conduits both at the bed of a glacier and within the ice. The size of a channel is determined by the relationship between the melting of conduit walls through viscous dissipation of heat, and creep of ice into the conduit. At the same discharge, larger channels will have a lower water pressure than smaller channels; under such conditions, larger channels will draw water away from smaller channels (Röthlisberger, 1972). As a result, the subglacial melt-

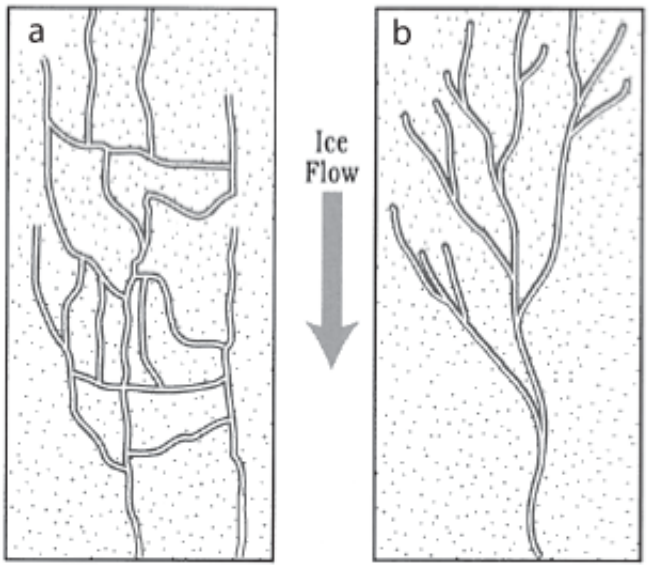

Figure 1.5: Plan view of a simplified a) distributed linked-cavity drainage system and b) channelized drainage system. After Fountain and Walder (1998).

water system often tends towards an arborescent network of efficient channels (Shreve, 1972), as shown in Figure 1.5b. Towards the end of the summer season, decreasing volumes of water input into a highly developed basal network can result in water flowing through conduits at atmospheric pressure (Röthlisberger, 1972).

Basal conduits generally either cut into overlying ice (R-channels) or into the bedrock below (N-channels), as described by Weertman (1972). The former are argued to be more prevalent due to frequent changes in basal drainage conditions that can alter the locations of basal channels (Röthlisberger and Lang, 1987). N-channel development would likely require a drainage system with very stable channel locations (Walder and Hallet, 1979), although they have also been argued to form connections in linked-cavity systems, which tend to be less stable (Kamb, 1987; Walder and Hallet, 1979).

Weertman flow

In both distributed and channelized drainage systems, Weertman (1972) argued that water, produced at the base of hard-bedded glaciers from frictional and geothermal heat, forms a film that flows in a thin ($\sim$1 mm) layer over the bed of the glacier. The thin layer of water is routed into cavity- or channelized-drainage systems, providing a mechanism for movement of water from isolated areas of the glacier bed. Weertman (1972) also argued that if water in R-channels exceeds overburden pressure at times of rapid increases in water volume, the conduits will have insufficient time to fully adjust to the rate of flow, and water will spread out into a film. Nye (1973), however, argued that the roughness and semi-permeability of bedrock or debris at the glacier bed would cause inherent instability in a water film that would favour development of a linked-cavity or channelized system. Alternatively, Walder (1982) argued that differences in the thickness of glacial ice affect the basal melt rate, which leads to non-uniform thickness of water sheets and therefore instability.

Soft-bedded hydrology

Both subglacial cavity and conduit drainage hypotheses are based on the premise of ice lying on a hard bed. However, many glaciers and ice-sheets overlie soft permeable sediments (see e.g. Boulton and Jones, 1979; Paterson, 1994; Stone and Clarke, 1998; Harrison and Post, 2003). The presence of sediment can greatly affect the flow paths of subglacial water. Fluid can travel through pores in sediment by Darcian flow (Iken and Bindschadler, 1986; Paterson, 1994); however, due to the small size of pore spaces in sediment, the velocity of flow and capacity of fluid transport with Darcian flow is often highly restricted (Lliboutry, 1983; Iken and Bindschadler, 1986; Walder

and Fowler, 1994). With larger volumes of water input, there are various hypotheses for water flow in a sediment-based environment. Walder and Fowler (1994) have suggested that water can flow in canals at the ice-sediment interface, which behave like hard-bed conduits. Similarly, cavity-based flow is argued to be possible on a soft bed (Kamb, 1987). However, Paterson (1994) suggested that a canal-based drainage system in sediment is not stable and might be vulnerable to drainage re-organization. Alternative sediment water flow theories include drainage through small channels (or 'pipes') that form within sediment, and drainage through macroporous horizons. The pipes are created through fine sediment eluviation and allow a faster version of Darcian pore-water flow (Clarke, 1987b). A macroporous horizon forms when sediment grains are re-aligned by water flow, creating larger pore spaces and increasing the hydraulic conductivity of the sediment, which also allows faster Darcian flow (Clarke, 1987b).

Warm, hard-bedded glaciers move primarily through water-lubricated sliding at the bed and visco-plastic deformation of the ice (Paterson, 1994). Soft-bedded glaciers, however, can also move through basal sediment deformation (Clarke, 1987b; Iverson *et al.*, 1995). The shear stress from overlying ice is often sufficiently high to overcome the yield strength of basal sediment causing it to actively deform (Iverson *et al.*, 1994; Fischer and Clarke, 2001). Deformation is determined by the basal shear stress and pore-water pressure within the sediment (Iverson *et al.*, 1999). Once pore-water pressures approach overburden pressure, sediments often become very weak and deform readily (Iverson *et al.*, 1995).

Winter and spring flow

Input of water into glacial systems usually occurs primarily through the summer months when temperatures are high enough to melt surface snow and ice (Röthlisberger and Lang, 1987). However, throughout the year, water can also be provided to the subglacial system through geothermally-driven melting of basal ice and groundwater influx (Hooke *et al.*, 1985; Paterson, 1994). As the latter water inputs are generally fairly small, subsurface drainage systems are argued to become increasingly constricted through ice deformation during the winter months (Röthlisberger and Lang, 1987; Fountain and Walder, 1998).

In spring, the first meltwater to the glacier bed usually encounters a low-capacity, undeveloped hydrological system (Röthlisberger and Lang, 1987). As the drainage system does not have sufficient time to develop in response to greater volumes of water, input of water into an undeveloped basal system allows greater lubrication at the bed by flooding rough basal topography (Bindschadler, 1983). Basal lubrication sometimes causes a temporary increase in ice velocity, which persists until the drainage network adjusts to the increased volume of water flow (Iken *et al.*, 1983; Röthlisberger and Lang, 1987). Initiation of basal pressure changes with meltwater input at the beginning of the melt season, and the resulting increases in ice velocity, are often referred to as 'spring events' (Röthlisberger and Lang, 1987).

1.2.3 *Borehole hydrology*

Englacial and subglacial drainage systems are notoriously difficult to access (Hubbard and Nienow, 1997; Sharp *et al.*, 1998), and each method of investigating them has limitations (Clarke, 1987a). Dye tracing can illuminate water flow velocities within the glacier and can determine whether water storage is occurring within the drainage network (e.g. Hooke *et al.*, 1988; Fountain, 1993;

Nienow *et al.*, 1998b; Hasnain *et al.*, 2001; Schuler *et al.*, 2004). However, dye tracing cannot generally be used to definitively differentiate between types of glacial drainage networks (Sharp *et al.*, 1998; Gordon *et al.*, 2001), which is an important aspect of investigating overdeepening hydrology. Ground penetrating radar (GPR) surveys have been used to elucidate various aspects of subglacial hydrological systems. Changes in the reflection-phase of radar wavelets can indicate dielectric contrasts between water and ice, caused by changes in radar velocity as the wave travels through different materials (e.g. Arcone *et al.*, 1995; Stuart *et al.*, 2003; Matsuoka *et al.*, 2007). GPR surveys, however, are difficult to implement in glaciers with high volumes of englacial pore meltwater (Plewes and Hubbard, 2001). Pro-glacial studies of meltwater out-flow have been used to assess flow pathways through glaciers and the relationship between water discharge and ice velocity (e.g. Elliston, 1973; Collins, 1979a; Gurnell and Fenn, 1985; Willis *et al.*, 1998; Swift *et al.*, 2005). However, pro-glacial measurements do not typically allow differentiation between different types of drainage networks within a glacial system. In several studies, tunnels have been dug allowing *in situ* examination of subglacial hydrology (e.g. Vivian, 1980; Hooke *et al.*, 1985; Lappegard and Kohler, 2005). Tunneling studies, however, are argued to potentially significantly alter the local subglacial environment so that care must be taken when analysing data from such sites (Hooke *et al.*, 1985). For studies of overdeepening hydrology, tunneling would not be a practical approach due to limited access to the overdeepened region of the glacier. There have been various efforts at modeling water flow through overdeepenings and up adverse slopes (e.g. Lliboutry, 1983; Röthlisberger and Lang, 1987; Creyts, 2007). However, the limited research into overdeepening hydrology means that the models have only been minimally tested.

Borehole hydrology is another method for investigating subsurface hydrology (e.g. Gordon, 1977; Hodge, 1979; Hantz and Lliboutry, 1983; Iken and Bindschadler, 1986; Fountain, 1994; Hubbard *et al.*, 1995; Stone and Clarke, 1998; Harper *et al.*, 2005; Rutter, 2005). Boreholes, which are typically drilled to the glacier bed with hot water, allow *in situ* investigation of subglacial hydrology by facilitating installation of a wide range of hydrological and mechanical sensors (see e.g. Stone *et al.*, 1993; Iverson *et al.*, 1994; Kavanaugh and Clarke, 2000; Oldenborger *et al.*, 2002; Fudge *et al.*, 2008). Additionally, englacial networks can be examined with borehole camera systems (e.g. Engelhardt *et al.*, 1978; Pohjola, 1994; Copland *et al.*, 1998; Fountain *et al.*, 2005b).

There are limitations with borehole investigation of glacial systems. A borehole only allows access to a small region of the ice bed within a large glacial system (Sharp *et al.*, 1998); how representative conditions at that location are of conditions on a larger scale remains unclear (Kavanaugh and Clarke, 2006). Some have argued that by drilling a borehole to the bed of a glacier, the basal hydrology is disturbed and the resulting *in situ* measurements cannot be trusted (e.g. Sharp *et al.*, 1998; Smart, 1998). Smart (1998) also noted that open boreholes are subject to water influx from the surface, which will alter interpretation of basal water pressure changes; however, once the borehole has frozen closed or is plugged, *in situ* measurements accurately represent changes in water pressure within the borehole (Murray and Clarke, 1995). Studies have found spatially consistent changes in water pressure across arrays of boreholes (e.g. Smart, 1998; Harper *et al.*, 2005; Fudge *et al.*, 2008). Such consistency indicates that use of boreholes for investigating subglacial hydrology is a valid technique (Hubbard and Nienow, 1997). Rutter (2005) also argued that instrumentation of boreholes is the only method that allows continuous changes

in subglacial hydrological conditions to be observed in a relatively undisturbed environment. On the other hand, the advection of boreholes with the flow of ice results in a spatial signal of the subsurface glacial hydrological system in addition to a temporal signal, which over long periods of time or for relatively fast flowing glaciers should be taken into account (e.g. Engelhardt *et al.*, 1978). For this study of West Washmawapta Glacier (WWG) hydrology, I chose to use boreholes as the primary method of investigation. The boreholes allow visual estimation of englacial drainage systems and *in situ* instrumentation of basal hydrological systems. These techniques allowed differentiation between basal and englacial flow systems within the overdeepening. Dye tracing was not possible at WWG due to permit restrictions.

Changes in the water level (or pressure head) in a borehole are a convenient visualization for change in basal water pressure at that location (Hodge, 1976; Murray and Clarke, 1995), as the pressure head value can be directly compared with the ice overburden pressure. The pressure head (Δh; SI units: m) is related to the water pressure (P_w; SI units: Pa) in the following manner:

$$P_w = \rho_w g \Delta h, \tag{1.1}$$

where ρ_w=1000 kg m^{-3} is the density of water, g=9.81 m s^{-2} is acceleration due to gravity, and Δh is the change of water height in the borehole relative to the elevation of the borehole base, the pressure head is then defined as

$$\Delta h = \frac{P_w}{\rho_w g}. \tag{1.2}$$

Boreholes are typically labeled as 'connected', 'unconnected' or 'alternating' depending on observed changes in pressure head and other measurements (e.g.

Murray and Clarke, 1995; Smart, 1998; Gordon *et al.*, 2001). If virtually no water pressure head change occurs in the borehole and the level of water is close to overburden pressure, the borehole is defined as unconnected to a basal hydrological system (see e.g. Smart, 1998). Instead, if fluctuations in pressure head occur (typically on a diurnal timescale), the borehole is labeled as connected to a basal hydrological system (Hodge, 1976). Given the temporally and spatially variable nature of subglacial drainage systems, boreholes can be connected at some times and not at others. Alternating connection can occur on short timescales, and can be dependent on basal water pressure (e.g. Fountain, 1994; Hubbard *et al.*, 1995; Rutter, 2005). Sometimes changes in the flow regime at the glacier bed or movement of the ice can result in boreholes connecting to the system long after they were drilled (e.g. Hodge, 1979; Smart, 1998; Stone and Clarke, 1998).

1.2.4 *Hydraulic potential*

Flow of water through a glacial network, whether englacial or subglacial, is determined by the hydraulic potential in the system. Information about basal water pressure throughout a glacier, volume of water entering and exiting subglacial systems and water velocity are necessary to calculate true hydraulic potential gradients in a system. However, as these data are difficult to come by in studies of subglacial hydrology, equations of estimated hydraulic potential are used as an alternative. The following sections examining estimated hydraulic potential equations and estimated water flow thresholds are based upon the assumption that information of water flux throughout the glacial system is not available. The following equations have been used for many years in the study of subglacial hydrology to circumvent the latter limitation and are also applied within this study. Following Shreve (1972), the equation

for estimated hydraulic potential (ϕ) in a subglacial system is

$$\phi = P_w + \rho_w g z. \tag{1.3}$$

Here z the elevation above a reference datum level. Assuming that basal water pressure is uniformally at ice overburden pressure ($P_i = \rho_i g H$, where H is the ice thickness and $\rho_i = \sim 917\,\mathrm{kg\,m^{-3}}$ is the density of ice), the subglacial hydraulic potential gradients $\nabla\phi$ are

$$\nabla\phi = (\rho_w - \rho_i)\, g\alpha_b + \rho_i g \alpha_s. \tag{1.4}$$

Here α_b and α_s are horizontal gradients of the ice surface and glacier bed elevations (i.e. the bed and ice-surface slopes). Water flows from high to low potential, driven primarily by the ice surface gradients.

During summer months, basal water pressures are commonly observed to fluctuate diurnally (e.g. Elliston, 1973; Hubbard *et al.*, 1995; Schuler *et al.*, 2004; Fudge *et al.*, 2008), and although overburden pressure is often reached, water pressures are rarely temporally or spatially static during the glacier melt-season in connected areas of the bed (Shreve, 1972). In unconnected areas of the bed, however, steady pressures at, or near, the flotation level are common (e.g. Smart, 1998). Due to the variations of water pressure within many glacial systems, equations 1.3 and 1.4 are not necessarily accurate representations of subglacial hydraulic potential gradients. Here follows an equation for hydraulic potential gradients with uniform variations of basal water pressure. This approach is also not fully representative of a glacial system with spatially varying water pressures. However, as mentioned above, the lack of information about water flow volumes and velocities through glacial systems result in

the use of equations based primarily on ice surface slopes and changes in ice thickness (i.e. known quantities in many glacial systems). Hydraulic potential gradients incorporating uniformally varied water pressures can be calculated with

$$\nabla\phi_\gamma = \rho_w g\alpha_b + \gamma\left[\rho_i g\left(\alpha_s - \alpha_b\right)\right]. \tag{1.5}$$

Here, γ=P_w/P_i is a uniformally varied fraction of flotation.

1.2.5 *Water flow thresholds*

In the absence of a cirque glacier, water entering a cirque overdeepening would simply accumulate, forming a lake. With a glacier present, sufficiently steep ice surface slope gradients can drive subglacial water up the adverse riegel slope and out of the overdeepening, when assuming that ice thickness and ice surface slopes are the primary controls for water flow in the glacial system. However, water flow is complicated by changes in the freezing point depression of water as it flows up a riegel. Two thresholds for water flow up an adverse slope can thus be established in accordance with these factors: I refer to these as 1) the hydraulic slope threshold (HST) and, 2) the supercooling slope threshold (SST).

Hydraulic slope threshold

When the freezing-point thermodynamics of water are not taken into account, the limit of uphill basal water flow is defined by contours of equipotential within the ice. Water will tend to flow perpendicularly to lines of equal potential, driven by a combination of gravity and pressure of the overlying ice. On an adverse slope that reaches a particular steepness threshold, hydraulic

gradients prevent further uphill flow. Following Hooke (2005), the hydraulic potential (ϕ) is taken in relation to direction s, here defined to lie along a line of equipotential:

$$\frac{d\phi}{ds} = \rho_i g \frac{d\left(Z_s - z\right)}{ds} + \rho_w g \frac{dz}{ds}. \tag{1.6}$$

Here Z_s is the elevation of the ice surface. As s is defined, $d\phi/ds$ is equal to zero; this allows Equation 1.6 to be rearranged as

$$\left(\rho_i - \rho_w\right) \frac{dz}{ds} = \rho_i \frac{dZ_s}{ds}. \tag{1.7}$$

The dip in the equipotential surface with respect to direction x, which is defined as the horizontal distance (in the same vertical plane as s), is obtained by multiplying both sides of Equation 1.7 by ds/dx:

$$\frac{dz}{ds}\frac{ds}{dx} = \left(\frac{\rho_i}{\rho_i - \rho_w}\right) \frac{dZ_s}{ds}\frac{ds}{dx}. \tag{1.8}$$

Noting that

$$\frac{dz}{ds}\frac{ds}{dx} \cong \frac{dz}{dx} \tag{1.9}$$

is the dip in the equipotential contour at point z and

$$\frac{dZ_s}{ds}\frac{ds}{dx} \cong \frac{dZ_s}{dx} \tag{1.10}$$

is the surface slope, α_s, the dip of the equipotential plane is calculated by extracting dz/dx from Equation 1.8:

$$\frac{dz}{dx} = -\left(\frac{\rho_i}{\rho_w - \rho_i}\right) \alpha_s. \tag{1.11}$$

Equation 1.11 states that, for $\rho_i \approx 917\,\mathrm{kg\,m^{-3}}$, the equipotential plane dips at ∼11 times the ice surface slope in the opposite direction. Taking z to be coincident with the glacier bed, the hydraulic slope threshold α_b^* is therefore

$$\alpha_b^* = -\left(\frac{\rho_i}{\rho_w - \rho_i}\right)\alpha_s. \tag{1.12}$$

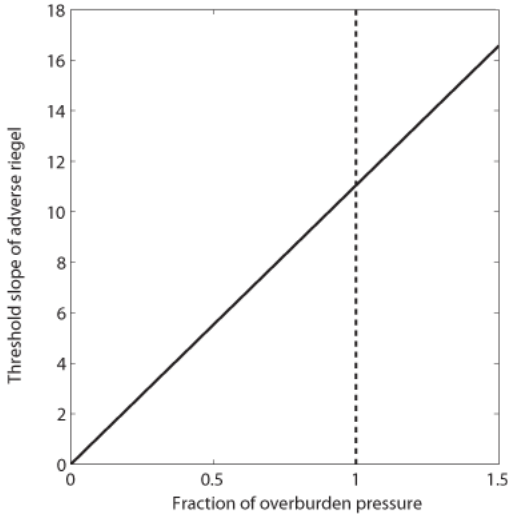

Figure 1.6: Hydraulic slope thresholds at different basal water pressures (plotted as fractions of overburden). The thresholds are the angle of the basal slope that would block water flow when multiplied by the surface slope and taken to be in the opposite direction as the surface slope (unitless).

The negative sign in Equation 1.12 shows that the slope must be adverse to the dip of the surface slope in order to block flow.

Equations 1.6-1.12 stipulate that basal water pressures are everywhere equal to ice overburden pressure. Again, ignoring the effects of water flow volumes and velocities in addition to spatially varying water pressures, HSTs can also be calculated for uniformally varied water pressures:

$$\alpha_{b\gamma}^* = -\gamma\left(\frac{\rho_i}{\rho_w - \rho_i}\right)\alpha_s. \tag{1.13}$$

As Figure 1.6 shows, when water pressures exceed overburden pressure, the

HST would have to be steeper to block uphill water flow.

Supercooling slope threshold

The hydraulic slope threshold described by Equation 1.12 is a gravity-driven threshold and does not take account of thermodynamical properties of the basal water. Water can exist at temperatures below 0°C due to factors such as pressure and presence of solutes in the water (Lliboutry, 1976; Tsang and Hanley, 1985). The rate of change of the melting point with increased pressure (β) is described by the Clausius-Clapyron equation:

$$\beta = \left(\frac{1}{\rho_i} - \frac{1}{\rho_w}\right)\frac{\theta_{TPK}}{L}. \tag{1.14}$$

Here $\theta_{TPK} = 273.16\,\mathrm{K}$ is the triple point temperature and $L = 3.34\,\mathrm{x}\,10^5\,\mathrm{J\,kg^{-1}}$ is the latent heat of fusion. When calculated for pure water, Equation 1.14 results in a freezing point depression of $0.0742\,\mathrm{K\,MPa^{-1}}$. However, for air saturated water, the rate of change is $0.0980\,\mathrm{K\,MPa^{-1}}$ (Lliboutry, 1976). Even if glacier meltwater is not entirely saturated with air, there will be some air content due to bubbles in the ice and water input from the surface. Therefore, the most appropriate rate is likely to be between these two values of β (Lliboutry, 1976).

When a parcel of water that is at the local pressure melting point (PMP) moves from an area of high pressure (e.g. a region of thick ice) to an area of lower pressure (a region of thinner ice), as would occur when flowing up a riegel, the temperature of that parcel of water becomes lower than the PMP in the new locality. The water is therefore 'supercooled'. If water flows sufficiently slowly, it equilibrates to the local temperature through conduction (Röthlisberger and Lang, 1987), frictional heating (Alley *et al.*, 1998), and latent heat release during freezing (Tsang and Hanley, 1985). In the latter

case, frazil ice forms in supercooled water by nucleating onto suspended particles. This suspended ice then accretes to the glacier sole or the underlying substrate as anchor ice (e.g. Svensson and Omstedt, 1994; Hammar and Shen, 1995; Cook *et al.*, 2006).

In order to determine the rate at which water will freeze when flowing at a lower temperature than the local pressure melting point, viscous dissipation of heat from flow of the water (E_w) must be taken into account. Alley *et al.* (1998) write this as

$$E_w = -Q\nabla\phi. \tag{1.15}$$

Here Q (units: $\mathrm{m^3\,s^{-1}\,m^{-1}}$) is the flux of the water. At this discharge (assumed constant), the heat energy required to keep the water at the pressure melting point (E_{pmp}) is defined as

$$E_{pmp} = Q\Delta P_w \beta C_s. \tag{1.16}$$

Here C_s=4.2 x 10^6 $\mathrm{J\,m^{-3}\,K^{-1}}$ is the specific heat capacity of water. Ignoring geothermal heating, and heating associated with glacier sliding and ice and sediment deformation, the rate of freezing $\dot{f}$ is given as

$$\dot{f} = \frac{(E_{pmp} - E_w)\cos\alpha_b}{L}. \tag{1.17}$$

It is not clear whether disregarding geothermal heating and sliding-related heating is a reasonable assumption. However, in line with the equations following Alley *et al.* (1998), and given that information about geothermal heating and sliding-related heating are difficult to come by, this assumption will be carried forward. Defining water pressure as the ice overburden pressure (P_i), and substituting Equations 1.15 and 1.16 into Equation 1.17 yields

$$\dot{f} = \frac{Qg\left[\rho_i K\left(\alpha_s - \alpha_b\right) + \rho_w \alpha_b\right]\cos\alpha_b}{L} \tag{1.18}$$

(where $K = 1 + \beta C_s$). In order to establish the supercooling slope threshold, $\dot{f}$ is set to 0 (i.e. melting and freezing are assumed equal), and Equation 1.18 is solved for α_b:

$$\alpha_b^\dagger = \frac{\rho_i K}{\rho_i K - \rho_w}\alpha_s. \tag{1.19}$$

According to Equation 1.19, the supercooling slope threshold (SST; $\alpha_b^\dagger$) is reached when $\alpha_b^\dagger = -1.2\alpha_s$ for air-saturated water, or $\alpha_b^\dagger = -1.7\alpha_s$ for pure water. If the slope of the bed is greater than these values (depending on the air saturation of the water), freezing occurs, and ice will accrete onto channel walls or glacial substrate, blocking (or at least narrowing) the path of flow up the adverse slope (Röthlisberger and Lang, 1987; Alley *et al.*, 1998). The SST is more restrictive on water flow up an adverse slope than the HST as the threshold slope angles are significantly smaller for the former.

1.3 Englacial overdeepening drainage hypothesis

The most widely cited overdeepening drainage hypothesis originates from work carried out by Hooke and others (Hooke *et al.*, 1988; Hooke, 1991; Hooke and Pohjola, 1994) at Storglaciären, Sweden. This polythermal glacier flows through one main overdeepening and three smaller overdeepenings (Fig. 1.7). Hooke and others' englacial overdeepening drainage hypothesis (EODH) was based on the following arguments:

1. Restrictions in basal flow result from the freezing of supercooled basal water during flow up adverse slopes (Hooke *et al.*, 1988).

2. Due to this restriction, basal water pressures will rise as flow is blocked by a steep riegel (Hooke, 1991).

3. As a result, water will find alternative, lower pressure englacial flow-paths (Hooke, 1991; Hooke and Pohjola, 1994). Hooke and Pohjola (1994) argued that englacial channels (which have circular cross-sections) will close more slowly than broad, low basal channels and will therefore have a lower pressure, encouraging flow from the basal system to the englacial system.

4. The englacial channels propagate over the overdeepened area until the riegel tip is reached and subglacial drainage can be re-established (Hooke and Pohjola, 1994).

Hooke (1991) argued that, for these reasons, overdeepenings with sufficiently steep riegels (i.e. those that reach the SST) will have a primarily englacial drainage system in the overdeepened area (Fig. 1.1).

1.3.1 *Storglaciären*

The EODH was developed by Hooke and others through several research campaigns at the main overdeepening at Storglaciären. Dye tracing was carried out by Hooke *et al.* (1988) and Seaberg *et al.* (1988), who found that flow of dye through the main overdeepening at Storglaciären was delayed relative to the rest of the drainage network. The drainage system the dye traveled through was argued to be englacial, as it appeared in a stream with low sediment load (Hooke *et al.*, 1988). Within the main overdeepening, basal pressures were

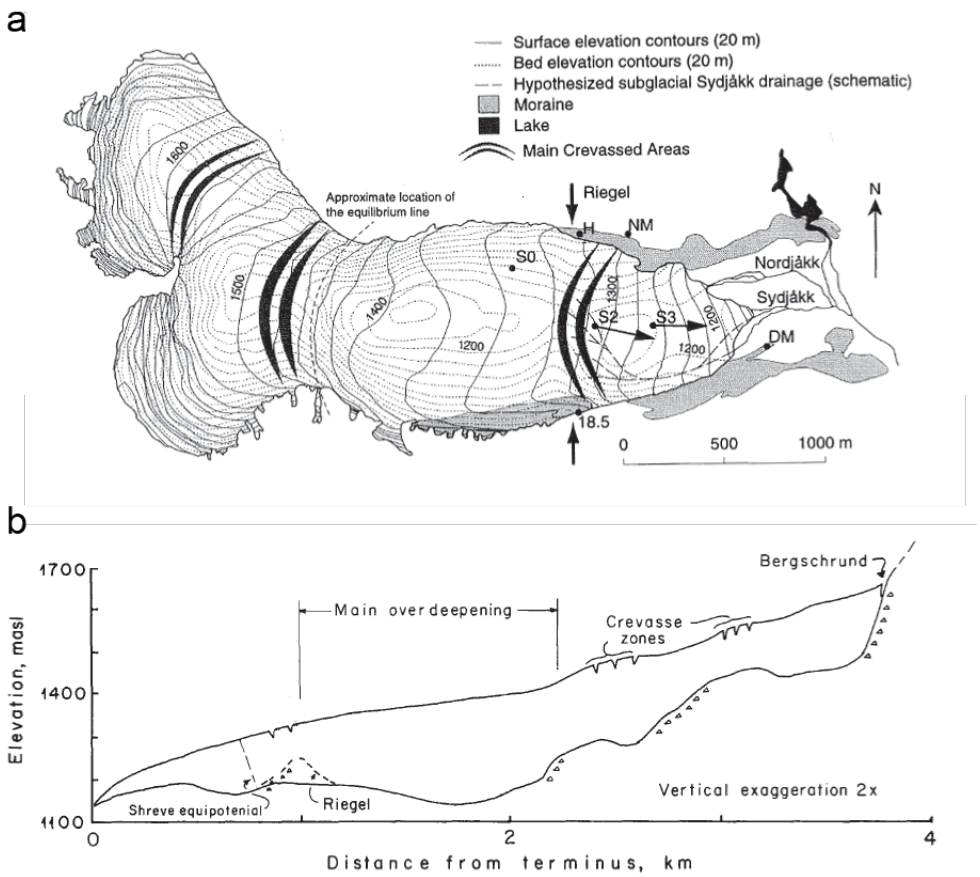

Figure 1.7: a) A plan view map of Storglaciären, Sweden with surface contours (solid lines) and basal contours (dotted lines). The main overdeepening riegel is noted. From Hanson *et al.* (1998). b) A cross-section of Storglaciären with the main overdeepening and areas of major surface crevassing noted. After Hooke (1991).

found to be near-flotation with little diurnal variation; down-stream of the riegel, basal pressures were lower and varied diurnally (Hooke *et al.*, 1989). Hooke *et al.* (1989) argued from this evidence that there was a distributed basal drainage system in the overdeepening, with basal water flow between a layer of till and the base of the ice. Somewhat contradictorily, Hooke (1991) argued the presence of till was due to the primarily englacial flow system in the overdeepening, which would limit sediment transport out of the riegel. Drilling records from 47 boreholes in the main overdeepening at Storglaciären indicated that 66% of the boreholes intersected englacial conduits, and that only 13% of these boreholes drained subglacially, often slowly (Hooke and Po-

hjola, 1994). From the evidence at Storglaciären, most water flow out of the main overdeepening appeared to be englacial (Hooke and Pohjola, 1994).

1.3.2 *Additional evidence for englacial drainage in overdeepened regions*

Several studies of glaciohydraulic supercooling and overdeepening hydrology have cited the EODH as a primary mechanism for water flow in glacial overdeepenings. Alley *et al.* (1997) summarized glaciohydraulic supercooling freeze-on in relation to basal sediment accretion and mentioned that once channels on an adverse slope are plugged, englacial flow will result and reduce accretion rates. Alley *et al.* (1998) suggested that englacial flow over an overdeepening is one potential effect of steep adverse riegels; however, near-marginal flow around the overdeepening or flow in basal cavities and films were also mentioned in that study as possible alternatives to englacial flow. Dye through-flow delay and storage was attributed to an englacial system within the overdeepening at Aletschgletscher in a study by Hock *et al.* (1999). Lawson *et al.* (1998) suggested that water was diverted into an englacial system within the overdeepening of Matanuska Glacier, Alaska. However, Lawson *et al.* (1998) also provided evidence of a distributed basal network in the Matanuska overdeepening and meters of basal sediment accretion from supercooling freeze-on. The latter observation would suggest that a subglacial flow system is the primary drainage network within the Matanuska overdeepening.

There are also some adaptations of the EODH, although still involving primarily englacial flow. Fountain and Walder (1998) argued that over time englacial channels can migrate down through the ice and become pinned at the head and terminus of an overdeepening (Fig. 1.8). Recently, Creyts (2007)

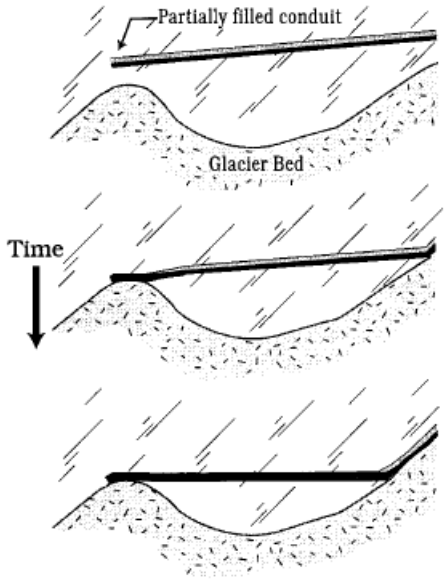

Figure 1.8: Schematic indicating evolution of an overdeepening englacial system where a migrating englacial channel eventually becomes pinned at the overdeepening head and tip of the riegel. The englacial channel then flows horizontally through the ice. From Fountain and Walder (1998).

modeled glaciohydraulic supercooling on slopes of various gradients. As part of the model, an 'englacial aquifer' was introduced, which was argued to result from flow from a high-pressure basal network into an englacial network through pores in the ice or basal fractures.

1.3.3 *Evidence for subglacial drainage in overdeepened regions*

Not all studies of overdeepening hydrology have advocated the EODH as the primary mechanism for drainage. In an overdeepening, Lliboutry (1983) argued that water is likely to flow towards the margins (driven by surface slopes), where the riegel is typically less steep. Near-marginal overdeepening flow was also suggested by a series of borehole pressure head measurements from Glacier

d'Argentière in the French Alps (Hantz and Lliboutry, 1983). Röthlisberger and Lang (1987), on the other hand, suggested that basal passages deeper in the overdeepening would be the preferential route of water flow. Both Alley *et al.* (2003a) and Clarke (2005) discussed glaciohydraulic supercooling and freezing of channels on adverse slopes but did not mention the possibility of an englacial system developing as a result. Iken *et al.* (1996) found, from borehole pressure head measurements and slug tests, that the drainage system in the overdeepening at Gornergletscher, Switzerland was basal. Towards the margin of Gornergletscher, subglacial drainage was fairly efficient, whereas drainage towards the middle of the overdeepening was slow and highly inefficient (Iken *et al.*, 1996). The overdeepened South Cascade Glacier was also reported to lack an englacial drainage system, with boreholes instead connecting to a high-pressure subglacial water network (Hodge, 1976). Working on the same glacier, Fountain (1994) discovered that subglacial conduits ran towards the margin of the overdeepening, avoiding the deepest area. The EODH was developed from evidence from the largest of four overdeepenings at Storglaciären (Hooke *et al.*, 1988; Hooke, 1989; Hooke and Pohjola, 1994). A smaller overdeepening at Storglaciären is located towards the glacier terminus (Fig. 1.7) and was studied by Hanson *et al.* (1998). They reported little evidence of widespread englacial drainage in this smaller overdeepening. Instead, they argued it had a dominantly basal drainage system with water flowing over the riegel only at times of high pressure.

1.4 Overall aims and application

The EODH suggested by Hooke *et al.* (1988) implies that, because most of the water in the overdeepened region flows englacially, little basal erosion is taking place. In addition, a primarily englacial drainage system could substantially impact ice dynamics in the region of the overdeepening (e.g. Bindschadler, 1983; Iken *et al.*, 1983). It is not clear however, whether it is possible for water to flow easily from a subglacial to an englacial system, even with the presence of a steep riegel.

The equations presented in this chapter for hydraulic potential gradients and supercooling slope thresholds are potentially limited in their application to subglacial hydrological systems. The possible problematic assumptions of these equations are that water is at a uniform overburden pressure throughout that glacial system and that the volume and flux of water through the system are not important factors.

In order to test whether the overdeepening drainage hypothesis is widely applicable, and to assess the suitability of hydraulic potential equations developed by Shreve (1972) and supercooling slope threshold equations developed by Alley *et al.* (1998), the subsurface hydrology of West Washmawapta Glacier, a small cirque in the Vermillion Range, B.C. Canada is examined. Through borehole camera investigation and basal instrumentation, aspects of the overdeepening hydrological system are determined.

The major research questions of this study are:

1) What are the characteristics of the drainage system? Does meltwater flow along the glacier bed or within englacial conduits?
2) What effect does the riegel have on subsurface drainage networks?

3) Do the hydraulic potential gradients of West Washmawapta Glacier suggest that water will flow up and over the riegel?

4) Is supercooled water likely to flow up and over the riegel at West Washmawapta Glacier?

5) Are the equations for hydraulic potential developed by Shreve (1972), and supercooling slope thresholds developed by Alley *et al.* (1998) appropriate for analysing the subsurface hydrological system at West Washmawapta Glacier?

1.5 Thesis structure

Chapter 2 introduces the field site, West Washmawapta Glacier, in the Vermillion Range, B.C., Canada. The methods for investigating the subsurface hydrology of this small cirque glacier are discussed. Field-based methods included the drilling of boreholes that were surveyed with a borehole camera and instrumented with a combination of pressure transducers, thermistors and conductivity meters.

Chapter 3 reports the field data collected during the investigation of the WWG subsurface hydrological system. These data include borehole camera logs for nine boreholes, and basal instrument results from four boreholes that reached the glacier bed.

The primary purpose of Chapter 4 is to discuss the englacial overdeepening drainage hypothesis suggested by Hooke and others (Hooke *et al.*, 1988; Hooke, 1991; Hooke and Pohjola, 1994). The EODH is tested by examining the results from the subsurface hydrology survey of WWG. The underlying assumptions of the EODH are discussed in relation to changes in supercooling slope thresholds with varying basal water pressure, and the temperature of the water flowing within an overdeepening.

Chapter 5 examines the features of the subglacial hydrological system at WWG from summer 2007 to summer 2008, including a late shut-down, hydraulic jacking and diurnally varying basal water temperature. The features that potentially impact the erosion patterns of the cirque are highlighted.

Chapter 6 lays out the conclusions of this investigation of WWG cirque hydrology. The main features of the hydrological system are reported. In addition, the implications of this research for erosion at WWG, and the implications for hydrological characteristics of other overdeepened glaciers are discussed.

Chapter 2

Field Setting and Methods

2.1 Field site

West Washmawapta Glacier (WWG) is located at the boundary between Kootenay and Yoho National Parks in the Vermillion Range, B.C., Canada, at 51° 10.35′ North, 116° 20′ West. This small ($\sim$1 km^2) temperate cirque glacier is situated in a bowl-like overdeepening with a maximum ice depth of $\sim$200 m (Fig. 2.1). The cirque bowl is eroded into the north-east flank of Helmet Mountain and has a steep headwall rising $\sim$500 m above the glacier surface. The median elevation of the cirque glacier is approximately 2500 m above sea level, and the ice surface spans an elevation range of $\sim$350 m. Historical aerial photographs show that WWG was joined with the opposing Washmawapta Icefield as recently as 50 years ago. Helmet Mountain and the overdeepened glacier bowl consist of Cambro-Ordivian shales with limestone inter-banding, from the McKay Group (Currie, 1975). The area surrounding WWG, including the rock underlying the Washmawapta Icefield, is Cambrian limestone of the Ottertail formation (Currie, 1975).

Regional temperatures are on the range of 10°C for the summer average and

-12°C for the winter average. Maximum summer temperatures reach ∼20°C; minimum winter temperatures are approximately -25°C (measured at Automatic Weather Station 1). The mean annual snowfall for the WWG region is ∼7 m (pers. communication, Parks Canada).

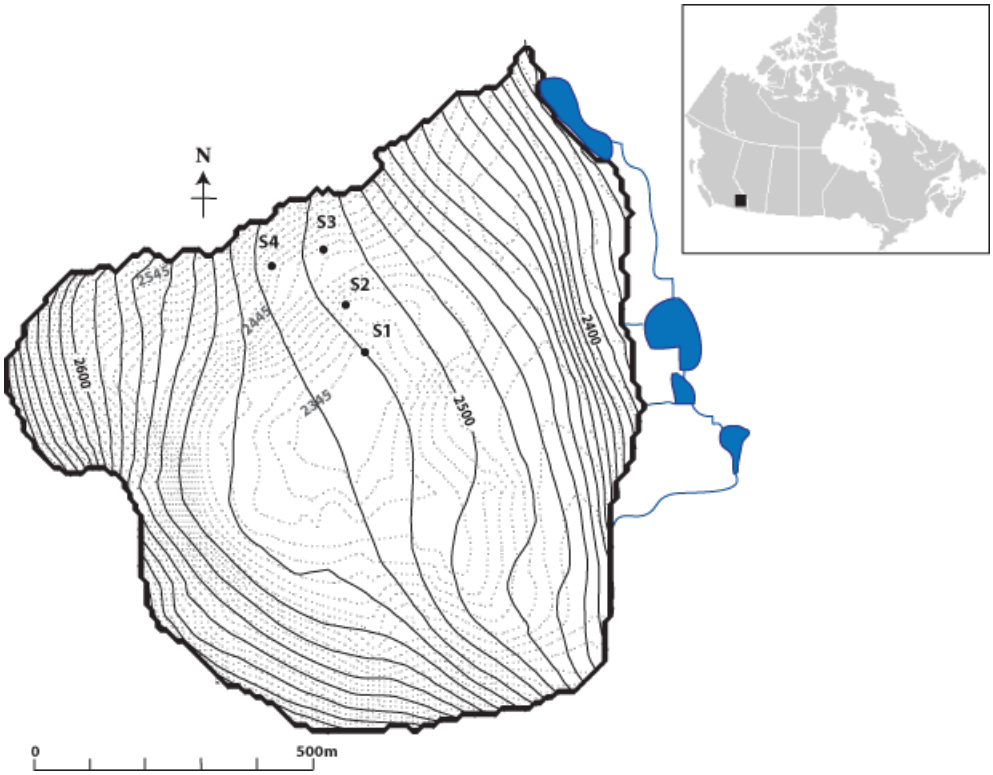

Figure 2.1: Map of West Washmawapta Glacier showing the location of the borehole drilling sites. The blue areas at the glacier terminus are proglacial lakes and streams indicating the main glacier water outlets. The solid lines are the glacier surface contours and the dashed lines are basal contours (both at 10 m intervals).

2.1.1 *Field campaign*

The Helmet Mountain Cirque project is a collaboration between U.C. Berkeley, California; Macalaster College, Minnesota; the United States Geological Survey (U.S.G.S.); and the University of Alberta. The ice flow and erosional characteristics of WWG, including modeling of the glacier force-balance, is the focus of research by J.W. Sanders and Dr. K. Cuffey (U.C. Berkeley).

The proglacial hydrological system is investigated by Dr. K. MacGregor (Macalaster College) to establish the glacier sediment-flux. Dr. Brian Collins of the U.S.G.S. is investigating erosion of the cirque headwall through use of a LiDAR system.

The cirque glacier subsurface hydrology is the focus of this M.Sc. project. My study contributes to the collaboration through investigations of both the spatially and temporally changing subglacial hydrology and the impact of the overdeepening hydrology on WWG erosion characteristics.

A field camp was established on the moraine ridge between West Washmawapta Glacier and Washmawapta Icefield in the summer of 2006 and was re-occupied in 2007 and 2008. The primary field season for this study of subsurface hydrology was in August 2007. A re-visit in 2008 allowed the collection of annual data and the re-drilling of boreholes for ice strain measurement.

2.1.2 *Glacier characteristics*

Due primarily to the shallow surface slope in the center of the glacier (approximately -3°), the velocity of the cirque glacier reaches a maximum of only ∼9 m a year. WWG flows roughly perpendicularly to the riegel (a bedrock ridge that has an adverse slope of ∼12°), towards the north-east. Repeat borehole inclinometry measurements and preliminary glacier flow modelling by J. Sanders suggest that, in the faster flowing near-margin region, roughly half of the observed surface flow rate is attributable to basal motion.

Glacier water input in the early melt-season (May and June) is primarily from snow patches on the headwall that melt and flow into a substantial bergschrund (pers. communication, J.W. Sanders), a crevasse that separates ice from the rock headwall (Paterson, 1994). From trends of water flow rills on

the glacier surface, it appears that supraglacial water flows towards the lateral margins of the cirque. Several moulins, located on the northern and southern tips of the riegel, drain a substantial volume of the surface meltwater into the ice subsurface.

Water is discharged from WWG at several places along the glacier terminus, as shown in Figure 2.1. The greatest volume of water appears to be discharged from a stream situated towards the southern margin of the cirque. Significant discharge might also occur into a pro-glacial lake at the northern margin. Average discharge from WWG during August 2007 was $\sim 0.4\,\mathrm{m}^3\,\mathrm{s}^{-1}$ (pers. communication, K. MacGregor).

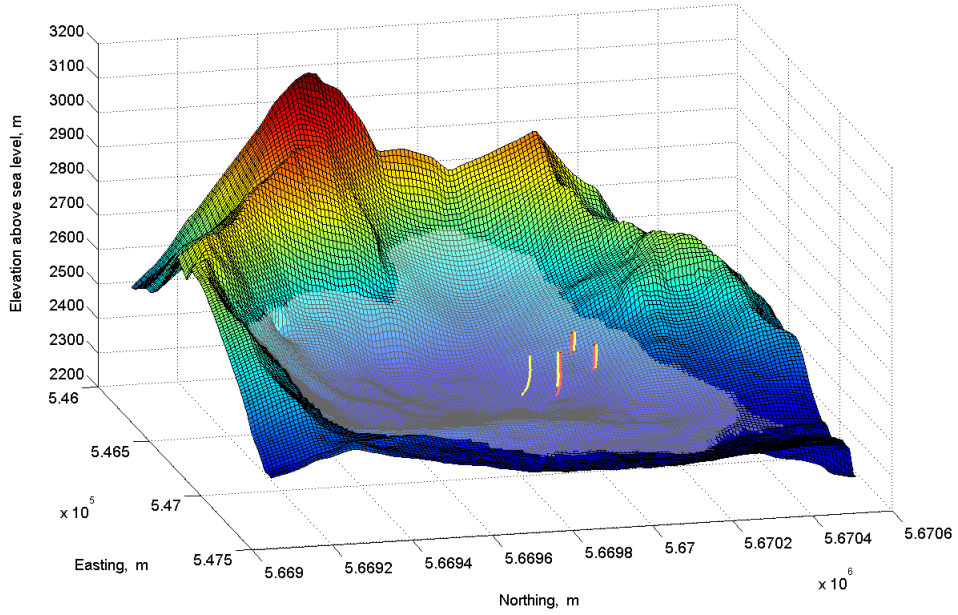

Figure 2.2: A DEM of Helmet Mountain and West Washmawapta Glacier. The opaque outline is the surface of the glacier. Yellow lines are the repeat inclinometry boreholes. Red lines are the instrumented boreholes. Plots of boreholes include the geometric shape measured at depth.

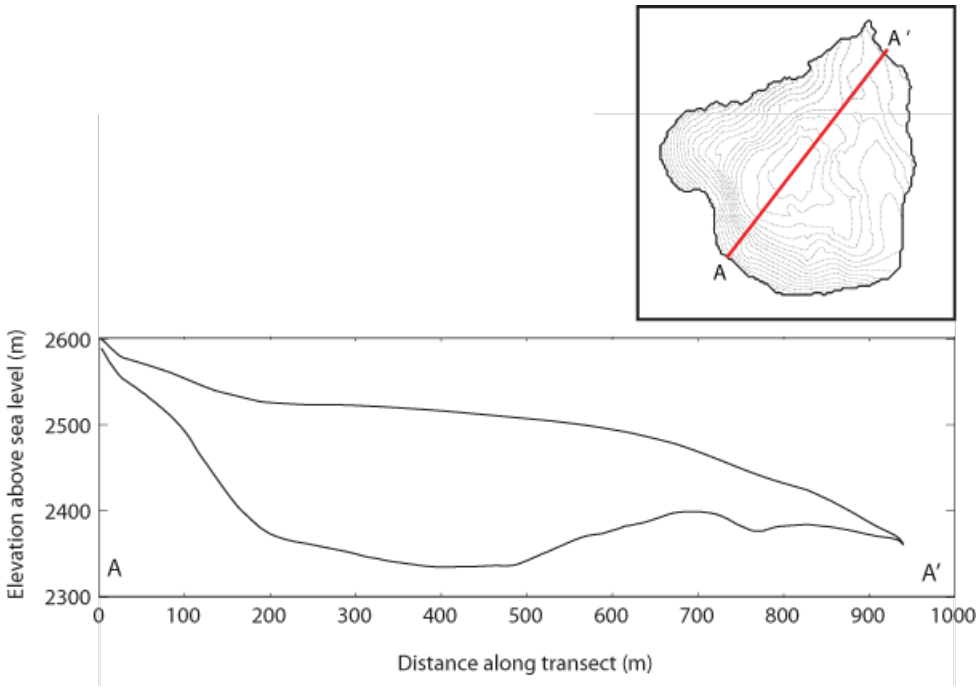

Figure 2.3: A cross-section of West Washmawapta Glacier through the overdeepening from A to A' (red line on the plan-view map).

2.2 Hydraulic potential

During the summer of 2006, the U.C. Berkeley team ran 22 GPR transects on the surface of WWG using a 5 MHz Narod Impulse Transmitter from Icefield Instruments, Inc. The relatively low survey frequency was necessary to penetrate through the water-saturated ice to the glacier bed. From point depths determined from two-way travel times, an interpolation of the glacier bed was calculated by J.W. Sanders. Global Positioning System (GPS) measurements, using a Trimble R7 system, were taken to establish the elevation of the ice surface. A digital elevation model (DEM) of the ice surface and Helmet Mountain headwall was then created by incorporating aerial photograph pair analysis and photogrammetry by HJW Geospatial, Inc. Figure 2.2 shows the surface and basal DEMs of West Washmawapta Glacier; borehole locations and geometric forms are also included. Figure 2.3 shows a cross-section of WWG through the overdeepening.

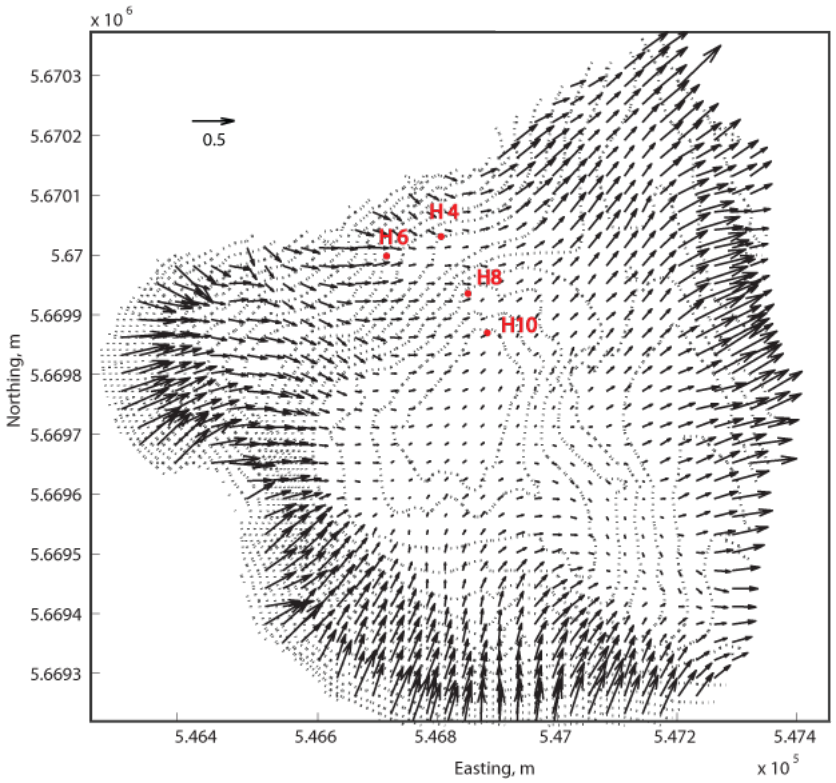

Figure 2.4: A map of WWG hydraulic potential gradients at ice overburden pressure. The dashed lines are the basal contours (in 15 m intervals). The red dots are the locations of the instrumented boreholes. The scale shows 0.5 m of hydraulic potential change per meter.

Hydraulic potential gradients were calculated from the WWG DEMs using Equation 1.4, which assumes that the subglacial water pressure is equal to the ice overburden pressure everywhere. The surface slopes and basal slopes were linearly interpolated onto a 10 m grid. Results of these hydraulic potential gradient calculations are shown in Figure 2.4. In this plot, the longer arrows indicate the regions of stronger hydraulic potential. Exact water flow paths are not calculated or assessed for WWG as the areas of water input, subglacial water volumes and basal conditions are not known.

2.3 Boreholes

In the summer of 2007, ten boreholes were drilled with a hot water drill on the northern side of WWG, up-glacier from the riegel (Fig. 2.4); the drilling rate was manually controlled, with care taken not to rest the drill on the tip during drilling. The first borehole (H1) was used as a calibration hole for pressure transducers and will not be discussed further. The remaining boreholes were used for instrument studies (H4, H6, H8 and H10) and repeat inclinometry (H2, H3, H5, H7 and H9).

2.3.1 *Borehole locations*

Surface conditions at WWG restricted hot-water drilling to a small (∼200 m x ∼150 m) region on the northern side of the glacier. Although the south-east side of the cirque glacier had abundant surface water, this area was both heavily crevassed and too steep to safely move the drill. The riegel was also a heavily crevassed region which prevented movement of the drill to this area. Drilling in the center of the glacier was precluded by a lack of surface meltwater; on the northern side of the cirque, drilling was limited to afternoon hours, when meltwater production was highest.

The locations of the boreholes were chosen to allow investigation of variations in subsurface drainage characteristics as the ice thins towards the glacier margin and as the hydraulic potential gradients, according to Figure 2.4, become stronger. Four sites for borehole drilling were chosen, located on an approximately 100 m spaced grid. These are shown on Figure 2.1. Three of the sites trended across the glacier in a transect from near-marginal thin ice to the deeper center of the cirque bowl. This transect ran approximately perpendicularly to the main flow direction of the ice. A fourth borehole site was

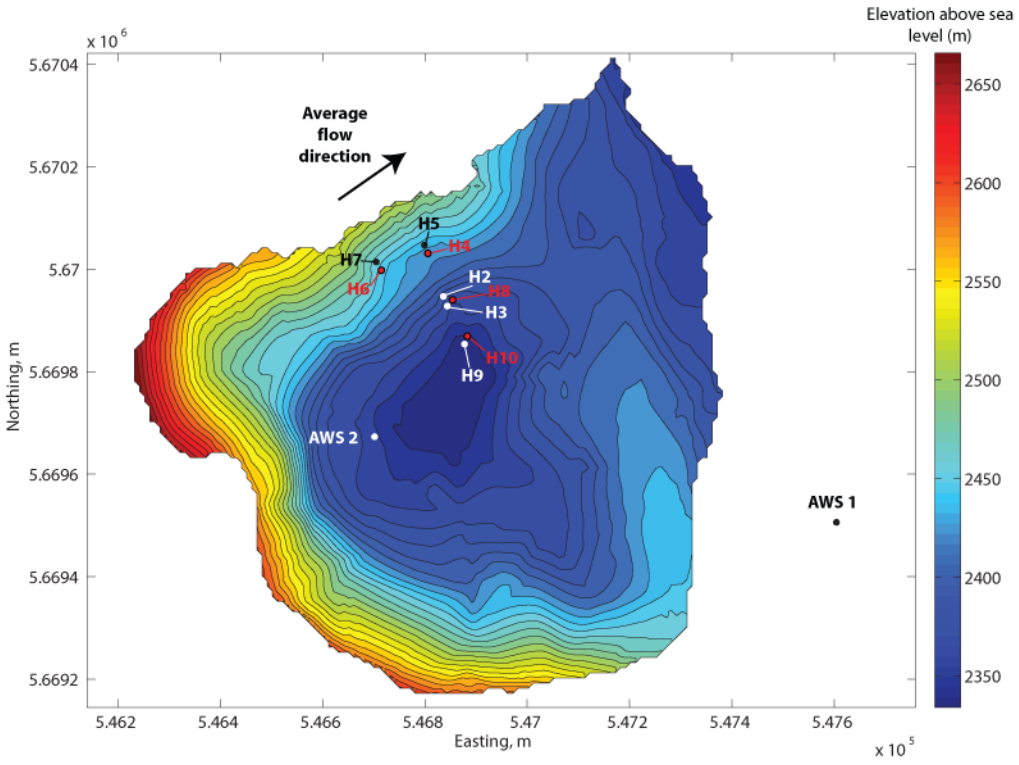

Figure 2.5: Basal contour map of WWG (at 13 m intervals) with the instrumented boreholes plotted in red and the repeat inclinometry boreholes plotted in white/black. The location of the moraine weather station (AWS 1) and the glacier weather station (AWS 2) are also plotted.

located further up-glacier from the riegel near the margin of the glacier. At all but one of these sites, two boreholes were drilled; three boreholes were drilled at site 2. Of the nine boreholes, five (H4, H5, H8, H7 and H8) reached the bed, as indicated by high turbidity levels observed in borehole video footage. Three of the boreholes (H2, H3 and H10) were blocked by rocks, with H2 and H3 failing to reaching the bed. The locations of the boreholes on the ice surface were surveyed with a Trimble R7 GPS in both 2007 and 2008, allowing displacements over this interval to be calculated. Locations of the instrumented and repeat inclinometry boreholes are plotted in Figure 2.5. The depths of the boreholes ranged from 54 m (H7) to 150 m (H10); borehole depths are given in Table 2.1 and Figure 3.1.

2.3.2 *Borehole camera*

All nine boreholes were surveyed with a Marks Products, Inc. GeoVISION, Jr.^{TM} borehole video camera (model number: GVJR H-D M2). The borehole camera was used to identify englacial features within the boreholes that could constitute an active part of the glacier drainage system, and also to examine the glacier bed. The camera was lowered down the borehole, and the video image was both monitored in real-time and recorded. Active monitoring allowed features in the borehole to be viewed carefully by adjusting the lowering speed of the camera. Depth increments (in feet) were recorded on the film and also noted manually from the marked cable. The depths of features were later logged, and converted to meters, by reviewing the footage. (The 'feet' reading on the borehole camera was more accurate than the 'meter' reading. As a result, original video logs were recorded in feet and depths later converted to meters.) The borehole camera logs were compared with the borehole drilling record, allowing voids to be linked to observed drops in borehole water level or the appearance of bubbles in the hole during drilling.

Many of the boreholes could not be fully surveyed with the borehole camera. Boreholes H2, H3 and H10 were blocked by rocks, and high turbidity levels in H4, H5, H6 and H7 meant that features at the base of these boreholes could not be seen. In H9, a constriction in the shaft a short distance above the bed (at $\sim$135 m) prevented passage of the camera. Restrictions in time and the potential for near-surface borehole freeze-closure prevented either delaying the borehole video surveys (which would have allowed sediments stirred up by drilling to settle) or repeat video surveys of the boreholes.

2.3.3 *Inclinometry*

Inclinometry was used to determine the geometric form of the boreholes at WWG (H10 excepted) upon completion of drilling. In four of the boreholes (H2, H3, H5 and H7), weighted aircraft wire was installed so the boreholes could be re-drilled the following year for repeat inclinometry. Repeat inclinometry of boreholes allowed the rates of ice deformation and basal sliding at WWG to be estimated.

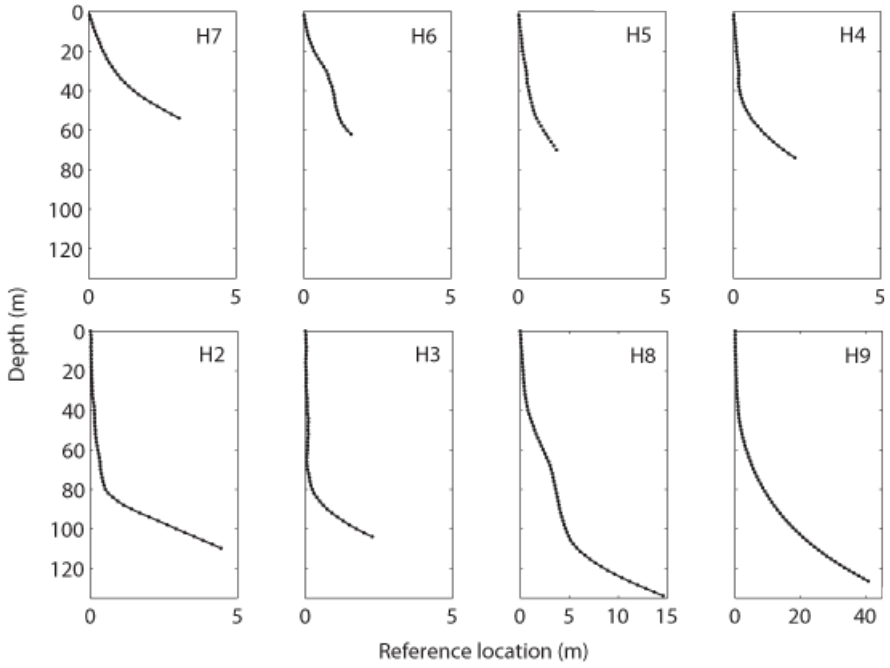

Figure 2.6: Geometry of boreholes H2-H9 from inclinometer measurements. The plots show the reference location from the top of the borehole as a function of depth.

For these borehole surveys, measurements were taken at 2 m increments with an Icefield Tools Corporation MI3 AUTOSHOT^{TM} inclinometer. Full inclinometry could not be completed for H2 and H3, as the boreholes were blocked by rocks. In addition, H10 was not surveyed due to rock blockage. Below a depth of ∼40 m, most of the boreholes began to dip away from vertical (Fig. 2.6), potentially due to cooling of the drill hose, changes in ice properties,

or melt-out of englacial rock debris. The inclinometry data were used to calculate the true depth of the ice in the regions of the drilled boreholes, thus providing validation and correction of the WWG basal DEM.

2.4 Borehole instrumentation

In order to examine the characteristics of the subsurface hydrological system at WWG, instruments were installed in a number of boreholes during the 2007 field season. Boreholes H4, H6 and H8 were instrumented with pressure transducers, thermistors and conductivity sensors (see Fig. 2.7 for an illustration of the borehole instrumentation); H10 was instrumented with a single pressure transducer. This latter hole was blocked by a rock ∼100 m above the bed, so changes in temperature and conductivity were unlikely to be recorded (for the depth of the pressure transducer installation relative to the borehole depth, see Table 2.1, and for the offset calculation, see Appendix B). For clarity, individual instruments will be referred to in relation to the borehole they occupy. For example, the pressure transducer, thermistor and conductivity sensor installed in borehole H6 will be referred to as P6, T6 and C6, respectively. Four-conductor (4C) and two-conductor (2C) wire (22/24 AWG, unshielded Coleman Signal Electric Cable) was attached to the instruments. For instrument wire type, wire lengths and installation information see Table 2.1. The limitations with using this wire for subglacial instrumentation are discussed in Appendix A.

A test borehole drilled in the 2006 field season was found to have frozen at ∼6 feet depth within one week. As a result, I assume that the tops of the boreholes drilled in 2007 also froze shut during a similar period of time at a similar depth. The borehole instrument data presented are therefore analysed

under the assumption that, disregarding outflow through an englacial system, there was no active flux of the water level in the borehole.

The following sections include descriptions of the data loggers and of the instruments installed at the bed of the glacier. Appendix B describes the calibration process for each instrument type.

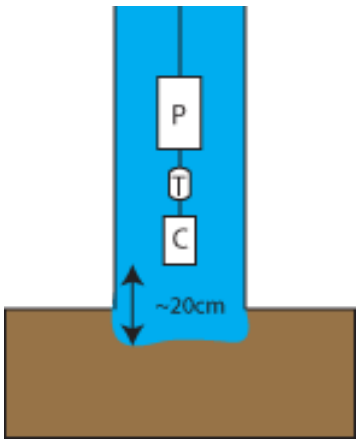

Figure 2.7: Schematic of the instrumentation of a borehole at WWG. The conductivity sensor (C) was installed ∼20 cm from the base of the borehole. The thermistor (T) was installed ∼5 cm above the top of the conductivity sensor. The pressure transducer (P) was installed ∼5 cm above the thermistor.

2.4.1 *Dataloggers*

The instruments were wired into three Campbell Scientific CR1000 Dataloggers. Power for each of the dataloggers was supplied by a 12 V, 7.5 Ah battery that was recharged by a 10 W solar panel. The loggers were programmed to take measurements every 2 minutes, during both the winter and summer seasons. For quality control purposes, the dataloggers recorded battery voltage and panel temperature in addition to instrument voltage outputs.

Inspection of the data revealed a number of artefacts, including shifts in values at times when instruments were added or removed, and periods of significant noise. These issues (and the solutions employed to correct them) are discussed in Appendices A and B.

Table 2.1: Borehole instrument characteristics

Borehole	H4	H6	H8	H10
Borehole surface elevation	2502.6 m	2510.4 m	2502.7 m	2504.7 m
Borehole depth	77.3 m	65.3 m	137 m	150 m
Borehole basal elevation	2425.3 m	2445.1 m	2365.7 m	2354.7 m
Instrument installation day ('07)	226	227	229	236
Pressure transducer				
Installation depth	76.5 m	64.6 m	136.2 m	70.9 m
Wire length	250 m	250 m	250 m	250 m
Wire type	4C	4C	4C	4C
End of record ('08)	208	197	208	237
Thermistor				
Installation depth	76.6 m	64.7 m	136.3 m	n/a
Wire length	250 m	230 m	185 m	n/a
Wire type	2C	4C	2C	n/a
End of record ('08)	237	230	237	n/a
Conductivity sensor				
Installation depth	77.1 m	65.1 m	136.7 m	n/a
Wire length	250 m	250 m	250 m	n/a
Wire type	2C	2C	2C	n/a
End of record ('08)	237	230	237	n/a

2.4.2 *Pressure transducers*

Omega Engineering Inc. (PX302-300AV) pressure transducers were used to examine changes in water pressure in boreholes H4, H6, H8 and H10. Changes in pressure can be interpreted as variations in water flow through the glacial system when compared to records of air temperature change (here used as a proxy for meltwater input into the glacial system). Temporal variations in pressure can often be identified as arising from flow in either a basal or englacial system. As noted in Chapter 1, borehole pressure is expressed in units of pressure head (m) for clarity, although this does not indicate changes in the actual borehole water level due to freeze-closure of the boreholes.

2.4.3 *Thermistors*

YSI 44033 RC thermistors were installed in boreholes H4, H6 and H8 during August 2007 to monitor the temperature of water in the boreholes. Most studies of glacial hydrology assume that basal water is at the local pressure melting point (e.g. Flowers and Clarke, 2002; Flowers *et al.*, 2003). However, water moving from the overdeepened regions of the glacier could potentially be supercooled (e.g. Alley *et al.*, 1997, 1998; Lawson *et al.*, 1998). The thermistors were originally installed to determine whether supercooled water was flowing up from the overdeepening into the region of the boreholes.

Comparisons of subglacial water temperatures and pro-glacial stream temperatures can indicate changes in temperature as water moves through the glacial system. During summer 2008, point temperature measurements were taken of various glacial outlet streams with a Traceable RTD Platinum Thermometer (model 15-077-55). This thermometer has an accuracy of $\pm 0.1\%$ (or 0.2°C). Due to anabranching (observed under the ice tongue), some of the measured pro-glacial streams were possibly from the same outlet.

2.4.4 *Electrical conductivity sensors*

Electrical conductivity sensors were installed at the base of WWG boreholes to establish the provenance of meltwater flowing through the boreholes (i.e. whether it was primarily part of an englacial or a basal flow system). The conductivity of glacial meltwater is commonly used to determine the dissolved ion concentration in the liquid. As water that flows basally in a glacial system will gain reactive ions from sediments or rocks (Stone and Clarke, 1998), Collins (1979a) argued that, in general, subglacial flow leads to relatively high meltwater conductivity values (e.g. $>\sim 65\ \mu\mathrm{S\,cm^{-1}}$), although the average conductivity of any glacial basin is highly dependent on the subglacial rock

lithology. Factors such as high-velocity water flow, or flow over basal material that has been leached of ions, will lead to lower electrical conductivity values within basal water (Fenn, 1987). Low conductivity water (e.g. $<\sim 5\ \mu\mathrm{S\,cm^{-1}}$) can also indicate that water is flowing englacially and is not in extensive contact with sediments (Fenn, 1987). Patterns within the conductivity data series can assist in differentiation between basal and englacial flow systems. For example, diurnal changes in conductivity suggests that water is traveling basally; conversely, the flow of englacial water within relatively stable pathways will prevent much diurnal variation of conductivity (Collins, 1979a).

The electrical conductivity sensors used in this study were fabricated by the Department of Chemistry Machine Shop (University of Alberta), and were installed at the base of H4, H6 and H8 during August 2007.

2.5 Weather stations

Two automatic weather stations (AWS) ran throughout the 2007 summer field season at WWG. The first station (AWS 1) was located on a recessional moraine $\sim$0.5 km from the glacier toe (Fig. 2.5), at an elevation of 2422 m above sea level. AWS 1 recorded air temperature (minimum, maximum and average); other instruments installed on AWS 1 are not relevant for this study and are therefore not discussed. Air temperature was averaged and recorded every hour with a sample taken every five seconds using a HMP45 C212 Temperature and Relative Humidity Sensor from Campbell Scientific. AWS 1 recorded throughout the winter and therefore can be used in conjunction with the full annual borehole instrument record.

A second weather station (AWS 2) was located in the glacier accumulation zone $\sim$0.3-0.4 km from the borehole sites, at an elevation of 2526 m (Fig. 2.5).

AWS 2 recorded air temperature (minimum, maximum and average) every fifteen minutes with measurements taken every minute, also using a HMP45 temperature-humidity sensor from Campbell Scientific. AWS 2 only recorded during the 2007 summer season.

2.6 Summary

West Washmawapta Glacier is a small overdeepened cirque glacier located in B.C., Canada. This project aims to establish the subsurface hydrology of this small glacier using boreholes drilled to the glacier bed with a hot water drill. In these boreholes, inclinometry surveys were completed for eight holes and borehole video surveys for nine holes. Pressure transducers, conductivity sensors and thermistors were installed in four of the boreholes. Additional data were collected from automatic weather station air temperature records.

Chapter 3

Field Data

3.1 Introduction

This chapter presents field data from the 2007 and 2008 investigations at West Washmawapta Glacier. First, borehole camera logs are discussed and the main observed features pertinent to the project aims highlighted, including the occurrence and character of englacial channels and fractures. The instrument data are then presented, including borehole pressure, electrical conductivity and water temperature time-series over a full annual cycle.

3.2 Borehole camera

The primary role of the borehole video camera was to determine the characteristics of any viable water pathways intercepted by hot-water drilling at WWG. Englacial voids observed in the WWG boreholes are classified into two main categories: channels (features with roughly circular cross-sections assumed to form through water flow; Section 3.2.1), and englacial fractures (generally planar features assumed to result primarily from ice stress conditions; Section 3.2.2). In addition, the camera was used to confirm that the glacier bed was

reached in boreholes that were to be instrumented.

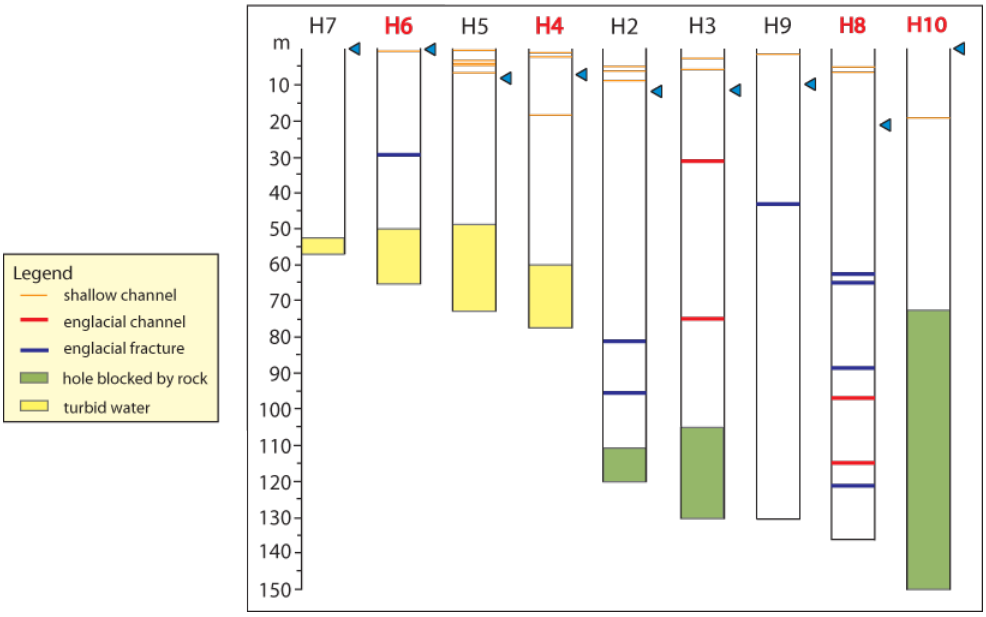

Figure 3.1: Video camera logs for the nine surveyed boreholes at WWG. The boreholes labeled in red are those that have been instrumented. The blue triangles indicate the water level at the time of borehole camera survey.

3.2.1 *Observed channels*

Nine boreholes drilled in 2007 were surveyed with the borehole video camera. In these surveys, 22 identifiable channels were observed. In the discussion that follows, channels located in the top 25 m will be referred to as 'shallow channels'; channels at greater depths will be referred to as 'englacial channels'. This distinction is based upon the argument by Paterson (1994) that measured surface crevasses rarely exceed a depth of 25 m.

Shallow channels

In total, 18 shallow channels were identified in the nine boreholes, with the majority seen in H2, H4 and H5, as shown in Figure 3.1. Of these shallow

channels, 13 had water flowing through them, detected only when the borehole camera was above the borehole water level and water could be observed pouring out of the channels; most of the remaining shallow channels were open but not filled with water. The shallow channels had a generally circular cross-section with diameters ranging ∼2-5 cm (estimated by visual comparison with the 2.5 cm-wide compass attached to the borehole video camera and the ∼12 cm diameter of the drilled borehole).

Englacial channels

In total, 4 englacial channels (i.e. channels located at depths greater than 25 m) were observed at WWG: 2 in H3 and 2 in H8 (Fig. 3.1). The englacial channels are labeled as CH1-CH4 and are described in Table 3.1. The dip (from horizontal) and dip direction of the englacial channels were estimated in relation to the borehole camera compass attachment and across-borehole trend of the features.

Table 3.1: Englacial channel characteristics

	CH1	CH2	CH3	CH4
Borehole	H3	H3	H8	H8
Depth	31.5 m	75 m	97 m	114 m
Height above bed	75.8 m	32.3 m	40 m	23 m
Dip	n/a	∼ 33°	∼ 5°	∼ 38°
Dip direction	n/a	NW	SW	SW
Diameter	∼2 cm	∼0.5 cm	∼0.5 cm	∼2 cm
Ice type	white	white	blue	white
Water flow?	no	no	bubble emerged from the southern end of the channel	no
Water level drop during drilling?	no	no	no	no
Notes	Only one end of the channel can be seen			

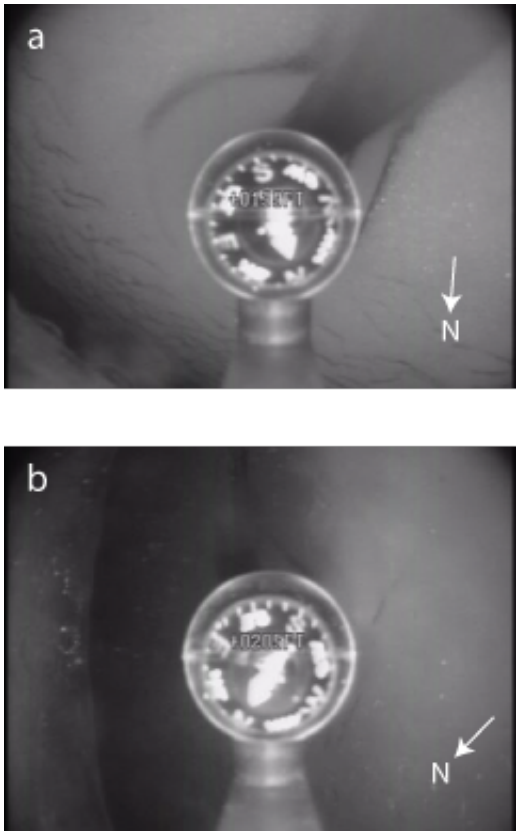

Figure 3.2: Frames from the borehole video. a) Englacial fracture observed 43 m below the surface in H9. This fracture is ∼12 cm wide and dips ∼45° with a north-west strike. b) Englacial fracture observed at a depth of 63 m in H8. The fracture is ∼8 cm wide and dips ∼20° with a north-west strike. The white arrows point to true north

3.2.2 *Englacial fractures*

The most striking features encountered in the borehole video footage were open crevasses or fractures. These features were located, for the most part, more than 30 m below the surface of the glacier (Fig. 3.2). In total, 8 open fractures (labeled F1-F8) were intersected. Characteristics of these crevasses are described in Table 3.2.

Table 3.2: Englacial fracture characteristics

	F1	F2	F3	F4	F5	F6	F7	F8
Borehole	H2	H2	H6	H8	H8	H8	H8	H9
Fracture depth	82 m	98 m	30 m	63 m	65 m	89 m	122 m	43 m
Height above bed	31 m	15 m	35.3 m	74 m	72 m	48 m	15 m	93 m
Dip	~ 45° E	~ 45° E	~ 20° NE	~ 20° NE	~ 10° SW	~ 45° NE	~ 10° E	~ 45° NE
Strike	S	S	NW	NW	NW	NW	S	NW
Width	~3 cm	~1 cm	~10 cm	~8 cm	~8 cm	~6 cm	~10 cm	~12 cm
Debris?	yes	yes	no	no	no	yes	no	no
Water flow?	no	no	no	no	no	no	no	rippled refrozen water?
Water drop during drilling?	no	no	no	yes	no	no	no	yes, refills soon after

3.3 Weather stations

Comparison of air temperature values recorded on the moraine by AWS 1 with those recorded on-glacier by AWS 2 show that there were only insignificant lags between measurements at the two weather stations. The temperature at AWS 2 was generally lower than at AWS 1 by ∼1-2°C, as can be seen in Figure 3.3. AWS 2 only recorded until 28 August, '07 whereas AWS 1 recorded year-round. As a result, in order to have a standard temperature comparison for instrument records, the AWS 1 surface air temperature record is used. The annual AWS 1 hourly air temperature record is shown in Figure 3.4a.

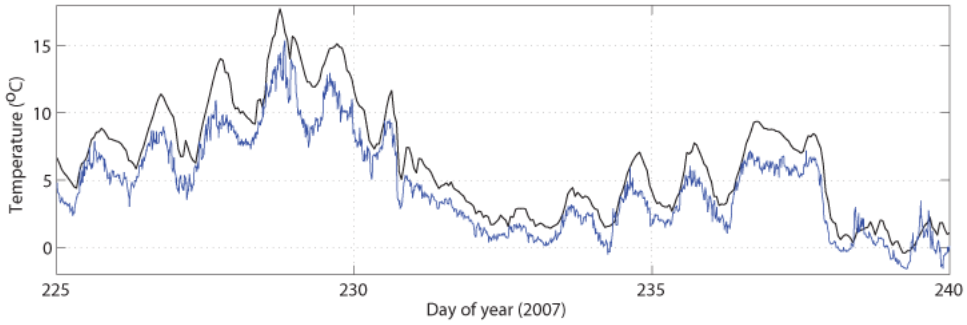

Figure 3.3: Average surface air temperature records for summer 2007. The black line represents the data from AWS 1 (hourly average), located on a moraine to the east of WWG . The blue line is from AWS 2 (15 minute average), which was located on the glacier, several hundred meters to the south-west of the boreholes.

3.4 Borehole instrument data

Records for most of the subglacial instruments span an approximately one-year period between August 2007 and August 2008 (Table 2.1). Figure 3.4b-e shows the annual borehole pressure records, Figure 3.5 shows the annual conductivity data series, and Figure 3.6 shows the annual basal temperature records. For clarity, these one-year records will be divided into three periods: summer 2007 (∼August-November), winter 07/08 (∼December-March), and summer

2008 (∼April-August). For each season, the pertinent pressure, conductivity, and temperature records from H4, H6, H8 and H10 are presented; only the information useful for later discussion is presented here. These results are followed by comparisons of the pressure, conductivity and temperature records between boreholes.

All of the instrument records varied on a range of timescales, including diurnal in most of the sensor records. Here, I focus primarily on diurnal signals within the records, as the changes in water input in relation to diurnal air temperature cycles are one of the most recognisable forcings within glacial hydrology, and are the most readily understood in relation to subsurface glacial hydrology.

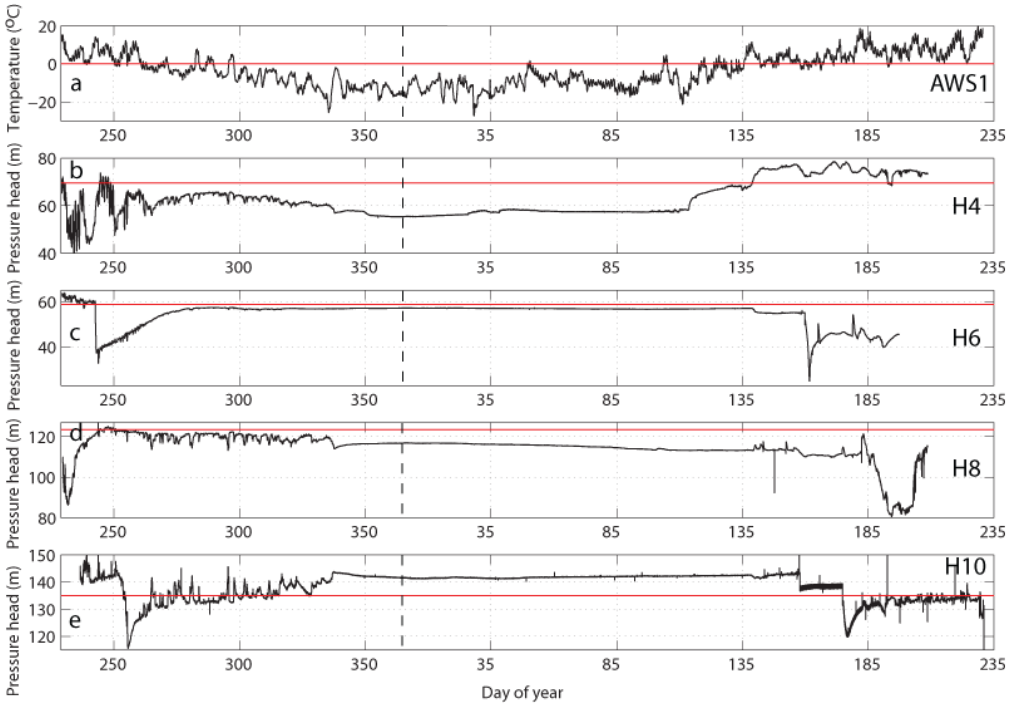

Figure 3.4: Annual pressure records for all instrumented boreholes from August 2007-August 2008. The start of the new year is indicated by the dashed line. a) Hourly average air temperatures from AWS 1. b) P4 record (black) with the overburden pressure in red. c) P6 record (black) with the overburden pressure in red. d) P8 record (black) with the overburden pressure in red. e) P10 record (black) with the overburden pressure in red.

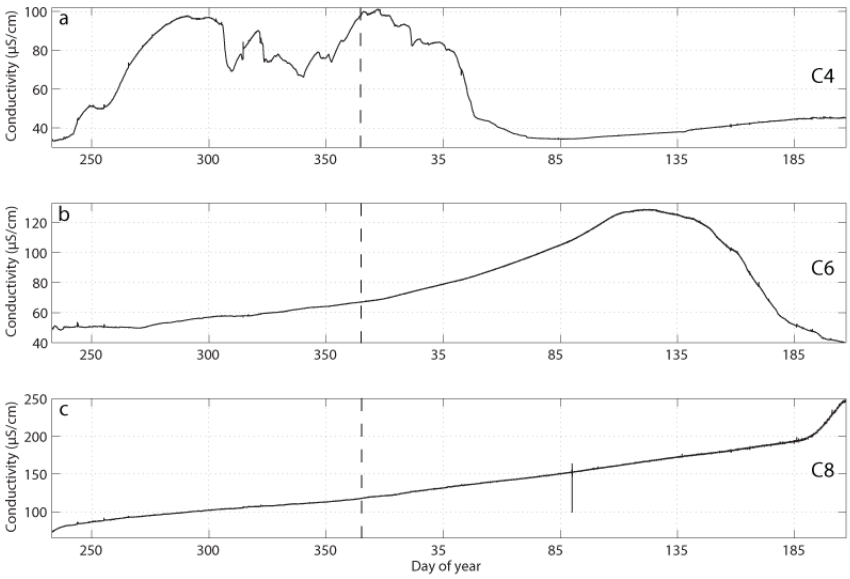

Figure 3.5: Annual electrical conductivity records from August 2007-August 2008. The start of the new year is indicated by the dashed line. a) C4 record. b) C6 record. c) C8 record.

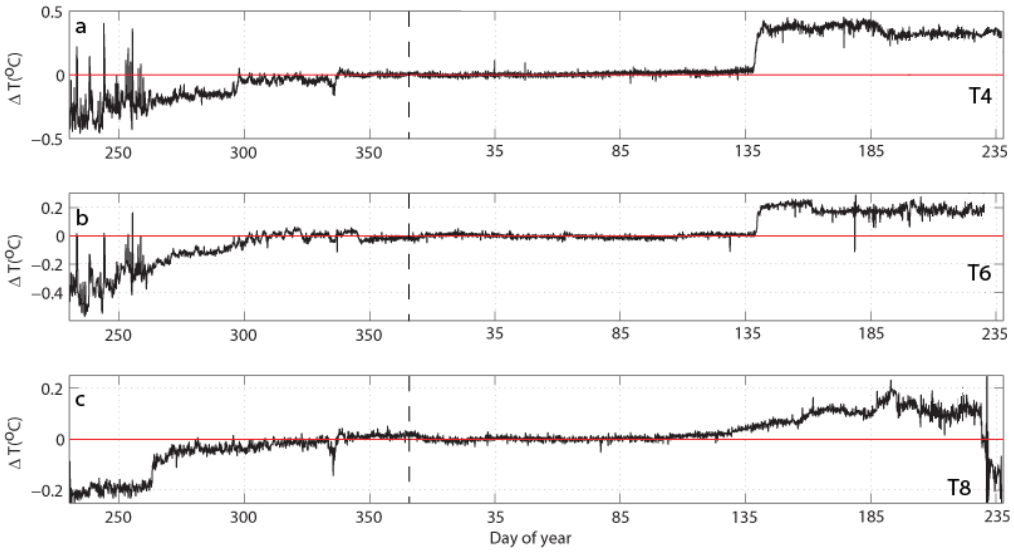

Figure 3.6: Annual basal water temperature series from August 2007-August 2008 plotted relative to the mean over-winter temperature for each borehole (in red). The start of the new year is indicated by the dashed line. a) Basal water temperatures in H4. b) Basal water temperatures in H6. c) Basal water temperatures in H8.

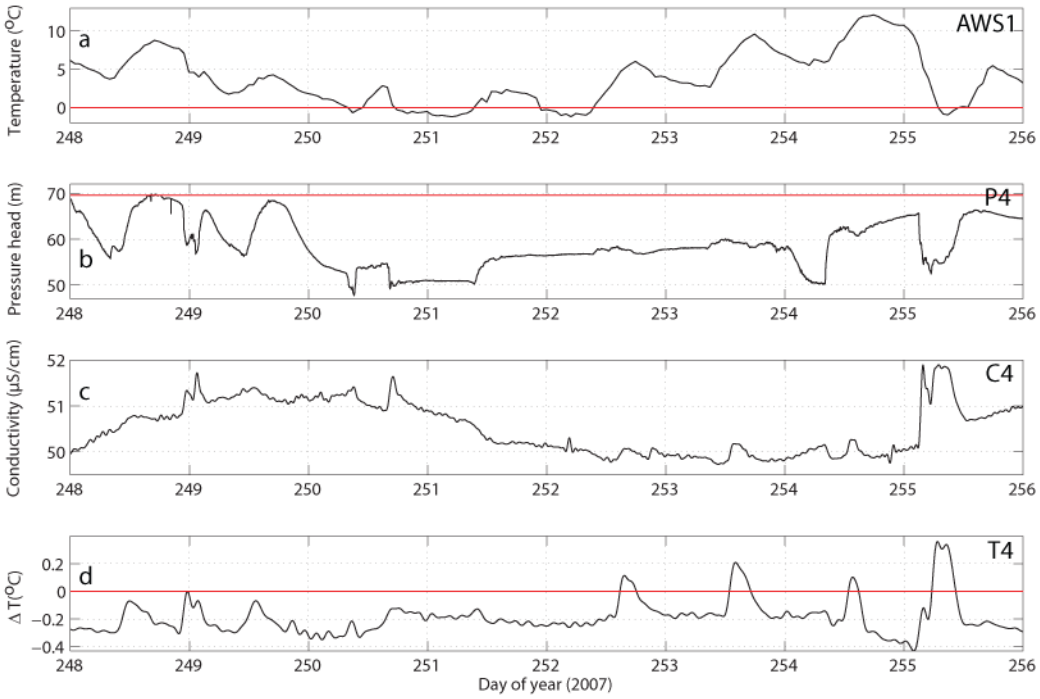

Figure 3.7: Instrument records from the base of H4 during an eight-day period in early September 2007. a) Hourly average air temperatures from AWS 1. b) Pressure record (black line) with the overburden pressure (red line). c) Electrical conductivity record. d) Water temperature record plotted with respect to the mean over-winter temperature value (red line).

3.4.1 *Summer 2007*

H4

H4 was a ∼77 m-deep borehole, located towards the northern margin of WWG, relatively close the riegel (Fig. 2.5). ***Pressure*:** H4 diurnal pressure swings in August 2007 were on the order of ∼20 m and varied in-phase with changes in AWS 1 temperature (Fig. 3.7a, b). After 17 September (day 260), P4 diurnal pressure fluctuations became smaller. This decrease in amplitude coincided with the first significant drop of surface air temperatures below 0°C (Fig. 3.4a, b). For most of the 2007 melt-season, P4 pressure fluctuated within 40-100% of overburden pressure. ***Conductivity*:** Conductivity sensor C4 recorded

diurnal variations over a small range of several μS cm^{-1}; these fluctuations were out-of-phase with P4 pressure change (Fig. 3.7b, c). ***Temperature*:** T4 temperature varied out-of-phase with P4 pressure change on diurnal timescales (Fig. 3.7b, d), up to 0.8°C (maximum amplitude on day 255). Strong diurnal temperature variability continued until 18 September (day 261), when the signal became more muted (Fig. 3.6a).

H6

H6 was a ~65 m-deep borehole, drilled close to the northern margin of WWG, approximately 100 m up-glacier from H4 (Fig. 2.5). ***Pressure*:** Pressure, following installation of P6 on day 227, varied diurnally by ~4 m, in-phase with changes in AWS 1 air temperature. Pressure remained above overburden until 30 August (day 242), when the water level dropped ~22 m below flotation. P6 water pressure then increased by ~20 m between early-September and mid-October. During this period, diurnal fluctuations decreased in amplitude from ~2 m to ~0.5 m (Fig. 3.4c). ***Conductivity*:** The C6 conductivity record indicates an out-of-phase relationship with respect to changes in P6 pressure (Fig. 3.8b, c), although H6 conductivity varied only slightly on the diurnal scale (<1 μS cm^{-1}). ***Temperature*:** Changes in T6 temperature were out-of-phase with changes in P6 pressure (Fig. 3.8b, d). Temperatures were observed to vary on diurnal timescales, up to 0.58°C (maximum amplitude on day 255). Average T6 temperature gradually increased between early-September and late-October from approximately -0.35°C to approximately -0.1°C below the mean over-winter base-line (Fig. 3.6b). During this time the amplitude of diurnal water temperature fluctuations became increasingly muted.

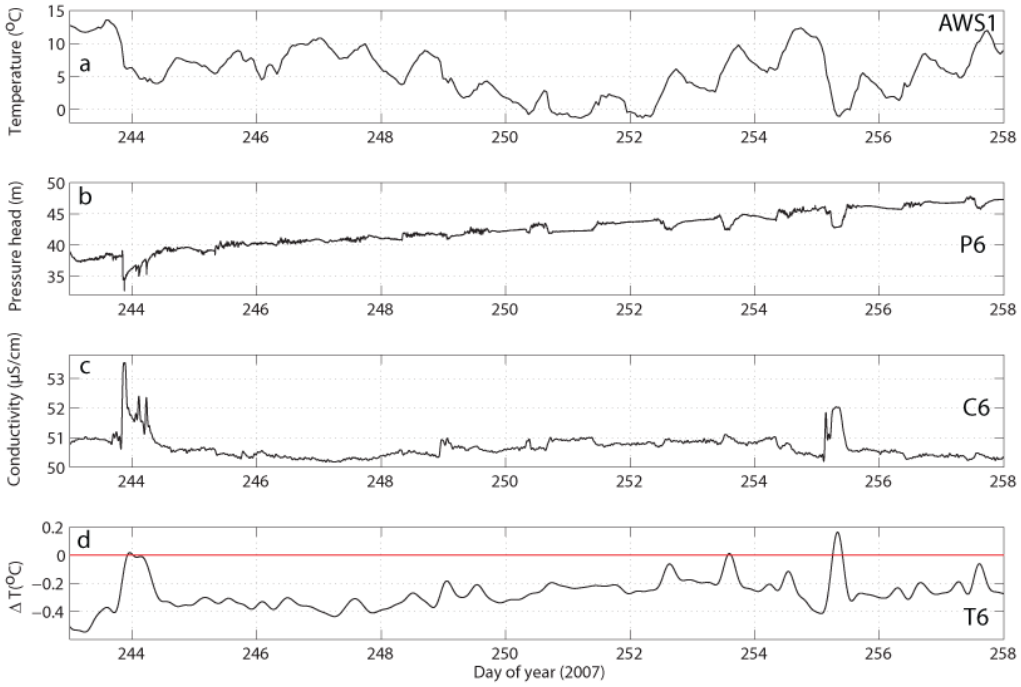

Figure 3.8: Instrument records from H6 during a fifteen-day period in September 2007. a) Hourly average air temperatures from AWS 1. b) Pressure record. c) Electrical conductivity record. d) Water temperature record plotted with respect to the mean over-winter temperature value (red line).

H8

H8 was located ∼100 m to the SSE of H4, in a deeper area of the cirque than H4 and H6 (Fig. 2.5). ***Pressure*:** After installation of P8 in this 137 m-deep borehole, no clear relationship between pressure variation and air temperature change could be observed until 33 days after installation (day 262; Fig. 3.4d). After this time, P8 water pressure varied diurnally by 3-8 m (Fig. 3.9b), in-phase with AWS 1 air temperature change. Diurnal pressure fluctuations for the remainder of the melt-season were within 93-98% of the flotation pressure. ***Conductivity*:** Following installation of C8, there was only minimal correspondence between C8 conductivity and changes in surface air temperature or P8 pressure (Fig. 3.9a-c); brief events of correlation indicated an out-of-phase relationship. ***Temperature*:** In summer 2007, T8 water temperature fluctu-

ated over a 0.05°C range, ∼0.2°C below the mean over-winter temperature. After 20 September (day 263), T8 water temperature began to gradually rise towards the over-winter level (Fig. 3.6c). There was little discernible correspondence between T8 temperature and changes in P8 pressure (Fig. 3.9b, d), although one event with out-of-phase correspondence between T8 temperature and P8 pressure occurred on 22 October (day 295).

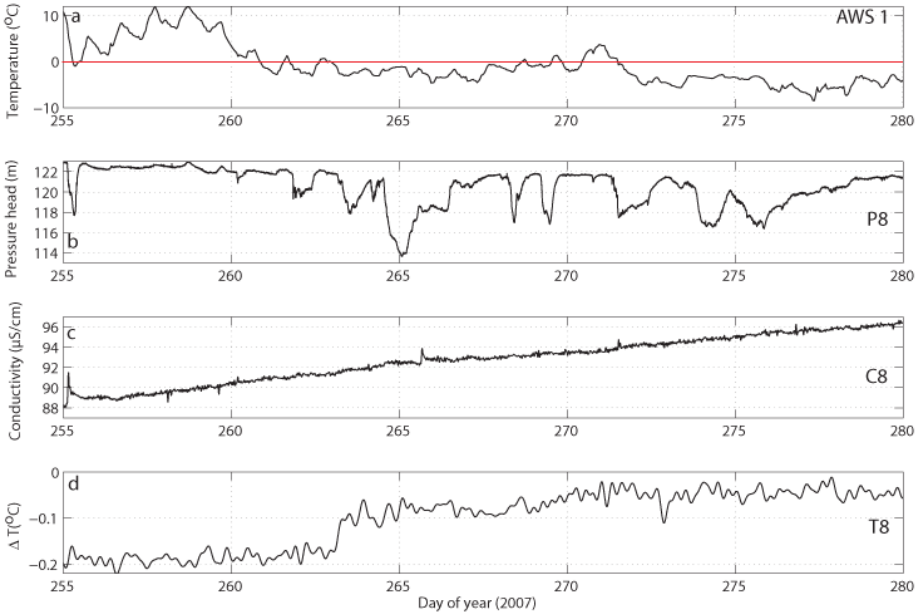

Figure 3.9: Instrument records from H8 in September 2007. a) Hourly average air temperatures from AWS 1. b) Pressure record. c) Electrical conductivity record. d) Water temperature record plotted with respect to the mean over-winter temperature value.

H10

H10 was the deepest instrumented borehole (∼150 m), and was located farthest from the glacier margin, directly up-glacier from the riegel (Fig. 2.5). ***Pressure*:** Following installation of P10 on day 236, water pressure fluctuated within ∼100-110% of the H10 overburden pressure. Variations in P10 pressure were out-of-phase with changes in surface air temperature (Fig. 3.10). After 19 September (day 262), pressure dropped to fluctuate within 95-108%

of overburden, with a diurnal range of 5-10 m (Fig. 3.4e).

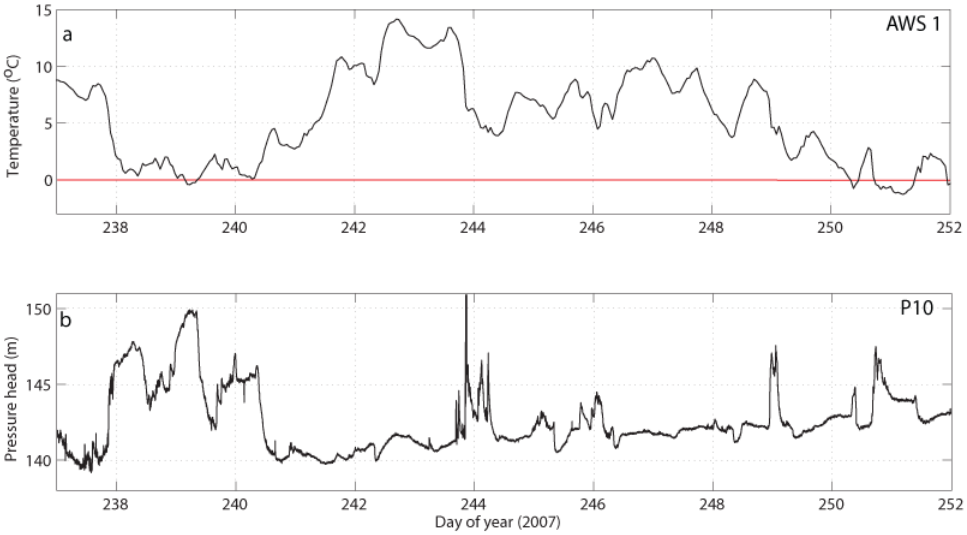

Figure 3.10: H10 pressure record during summer 2007. a) Hourly average air temperatures from AWS 1. b) P10 pressure record.

3.4.2 *Winter 07/08*

H4

***Pressure*:** P4 pressure fluctuations ceased on 3 December (day 337), over a month after air temperatures dropped continuously below 0°C and three days after air temperature dropped to a minimum of -25°C (Fig. 3.11a, b). Following cessation, little change was observed in water pressure values (Fig. 3.4b). ***Temperature*:** After 3 December (day 337), T4 water temperature ceased to fluctuate diurnally. The over-winter temperature was approximately 0.2°C above the average summer 2007 temperature (Fig. 3.6a).

H6

***Pressure*:** The P6 record shows a cessation of pressure fluctuations on 12 November (day 316), as can be seen in Figure 3.11c. The over-winter pressure

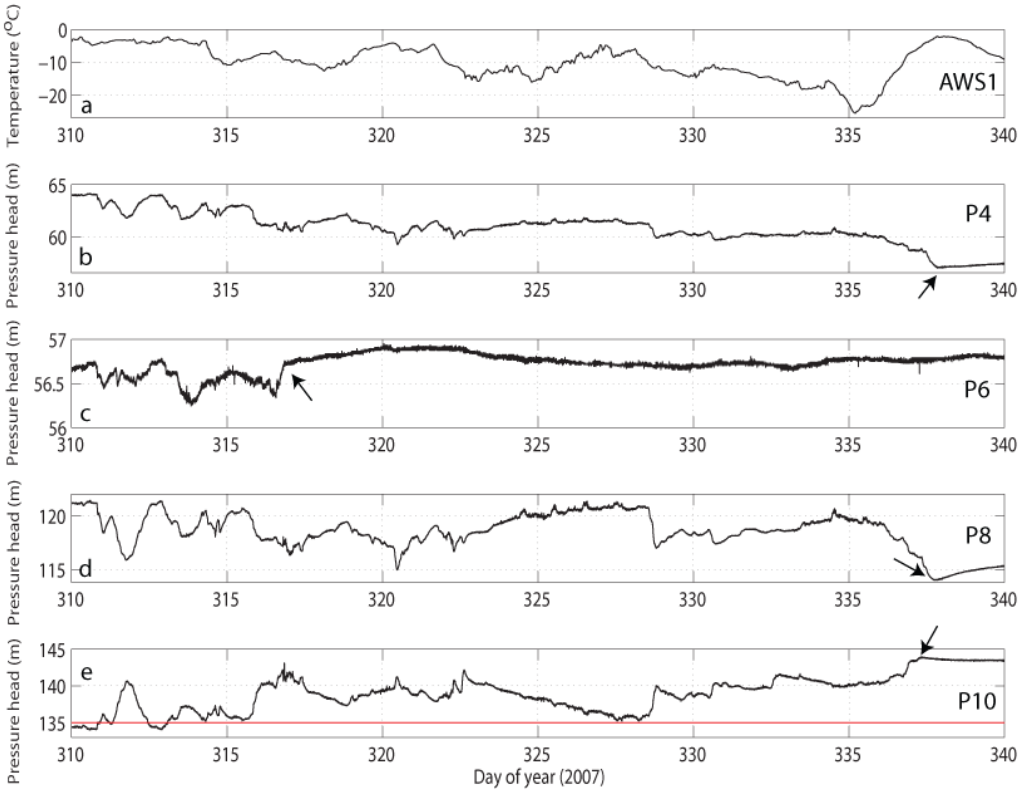

Figure 3.11: Pressure records covering the shut-down of the hydrological system, ranging over a month from early November to early December 2007. a) Hourly average air temperatures from AWS 1. b) P4 records with shut-down in early December. c) P6 records with shut-down in mid-November. d) P8 records with shut-down in early December. e) P10 records with shut-down in early December. The arrows indicate the time of hydrological shut-down for each borehole.

maintained a level of <2 m below H6 flotation level (Fig. 3.4c). ***Conductivity*:** Several days after H6 pressures ceased to fluctuate on day 316, the C6 conductivity began to increase at a rate of $\sim 0.5\,\mu\mathrm{S\,cm^{-1}}$ per day. Conductivity values continued to rise at approximately this rate throughout the winter period (Fig. 3.5b). ***Temperature*:** The average over-winter T6 water temperature was reached on 6 November (day 310). This occurred 6 days before P6 pressure ceased to fluctuate. As shown on Figure 3.6b, there were occasional fluctuations in temperature until 12 December (day 346).

H8

***Pressure*:** P8 pressure ceased fluctuating on 3 December (day 337), as shown in Figure 3.11d. Over winter, the pressure was maintained ∼6-8 m below overburden (Fig. 3.4d). ***Temperature*:** There was a temporary drop in T8 water temperature on 30 November (day 334). After this time, the average over-winter temperature was maintained (Fig. 3.6c).

H10

***Pressure*:** P10 pressure fluctuations ceased on 3 December (day 337), approximately 12 hours prior to P4 and P8 pressure fluctuation cessation (Fig, 3.11e). Over winter, P10 pressure was maintained ∼7 m above overburden (Fig. 3.4e).

3.4.3 *Summer 2008*

H4

***Pressure*:** P4 pressure began to rise at a rate of 0.5 m per day after 22 April (day 113). At this time, the ambient air temperature was approximately -10°C (Fig. 3.4a, b). In-phase correspondence between pressure and surface air temperature change was noticeable after 10 July (day 192), as shown in Figure 3.12a and b. ***Conductivity*:** After 9 July (day 191), an out-of-phase relationship between the C4 conductivity and P4 pressure records can be seen, with diurnal conductivity variation on the scale of 0.2-0.4 μS cm^{-1}. ***Temperature*:** T4 water temperature rose 0.4°C over 4 days after 17 May (day 138). The temperature rise coincided with a rise in P4 pressure (Fig. 3.13a). There was no discernible relationship between the T4 temperature and P4 pressure records during the summer 2008 season.

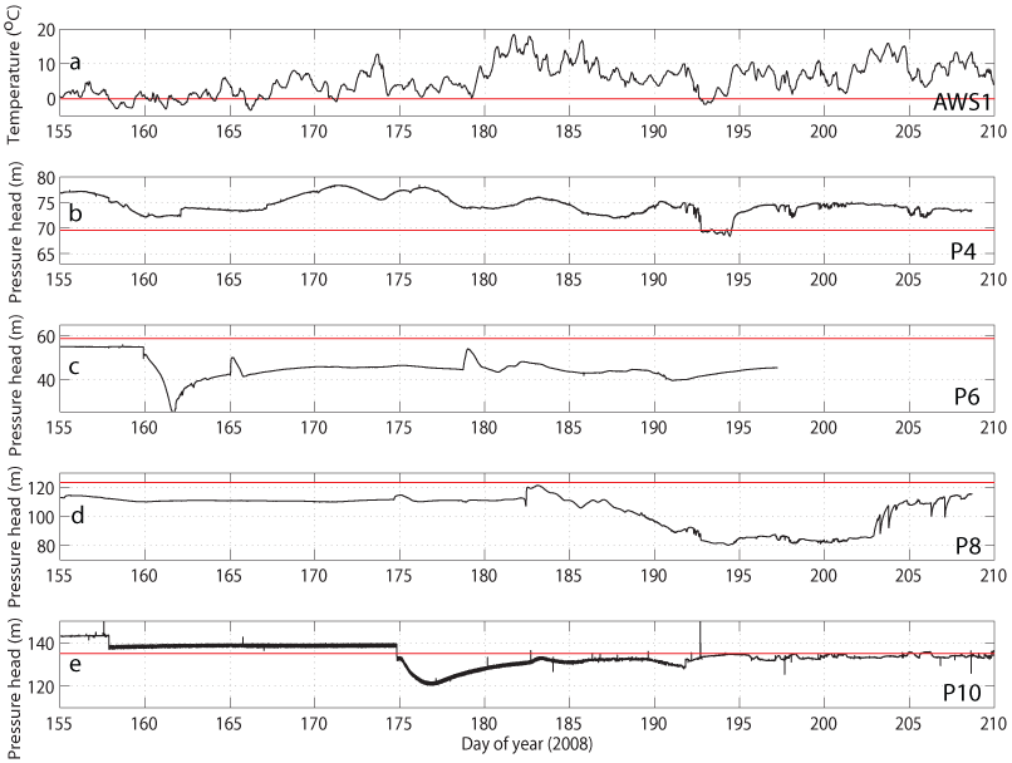

Figure 3.12: Pressure records from all the instrumented boreholes. Data from June and July 2008. a) Hourly average air temperatures from AWS 1. b) P4 record (black) with the overburden pressure in red. c) P6 record (black) with the overburden pressure in red. d) P8 record (black) with the overburden pressure in red. e) P10 record (black) with the overburden pressure in red.

H6

***Pressure*:** P6 pressure change began on 6 June (day 158; Fig. 3.4c). There was no obvious correspondence between changes in pressure in H6 and surface air temperature during summer 2008, prior to failure of P6 on 15 July (day 197), as can be seen in Figure 3.12a and c. ***Conductivity*:** During summer 2008 there was no clear relationship between the C6 conductivity and P6 pressure records. However, diurnal variability on the scale of $\sim 1\,\mu\mathrm{S\,cm^{-1}}$ can be seen after 15 July (day 197) in the C6 conductivity record. ***Temperature*:** After 18 May (day 139), T6 water temperature rose 0.2°C over 2 days. The rise in temperature occurred at the same time as a small drop of 1.5 m in P6 pressure (Fig. 3.13b). In summer 2008 there were no diurnal fluctuations

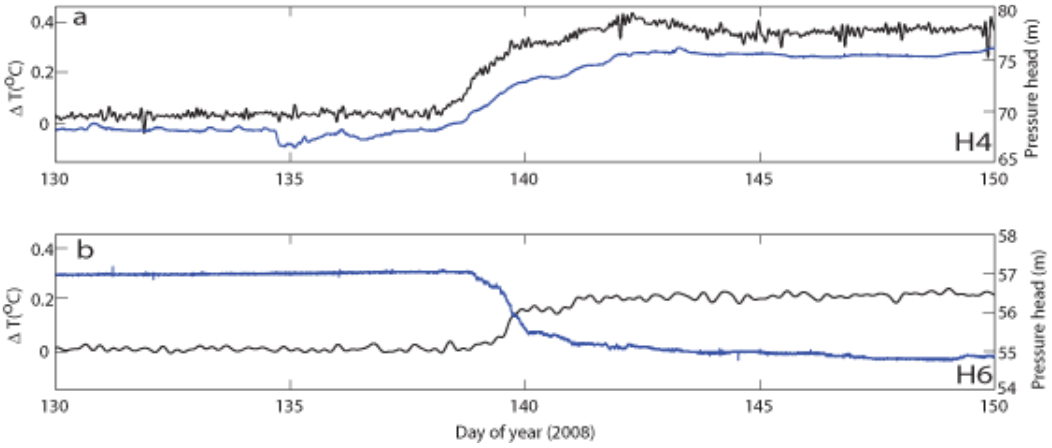

Figure 3.13: Pressure and temperature records from H4 and H6 during a 20-day period in May 2008. a) T4 temperature (black) and P4 pressure (blue) records. b) T6 temperature (black) and P6 pressure (blue) records.

recorded and no discernible correspondence between the T6 temperature and P6 pressure records.

H8

***Pressure*:** Changes in P8 pressure began on 18 May (day 139; Fig. 3.4d). However, there was no in-phase correspondence between surface air temperature change and pressure until 4 July (day 186). ***Conductivity*:** In summer 2008 there was a small (1-1.5 μS cm^{-1}) indication of diurnal variability in the C8 conductivity record superimposed on a background of steadily rising conductivity. ***Temperature*:** After 14 April (day 105), T8 water temperature began to rise. By 11 July (day 193) the T8 maximum temperature of 0.24°C above the mean over-winter temperature was reached. After this time, temperature dropped to fluctuate ∼0.1°C above the over-winter temperature. After 16 August (day 229), the temperature dropped further to ∼0.1°C below the mean over-winter temperature (Fig. 3.6c).

H10

***Pressure*:** P10 pressure variation began on 22 May (day 143; Fig. 3.4e). After 15 July (day 197), P10 pressure began fluctuating around overburden; these diurnal variations were out-of-phase with changes in surface air temperature.

3.4.4 *Comparison of instrument data*

1) Pressure

Figure 3.14 shows the pressure records plotted as a percentage of overburden for each borehole. Expressed in this manner, the amplitude of diurnal pressure variations in H4 are seen to encompass a much larger fraction of the overburden pressure than was recorded in the other boreholes.

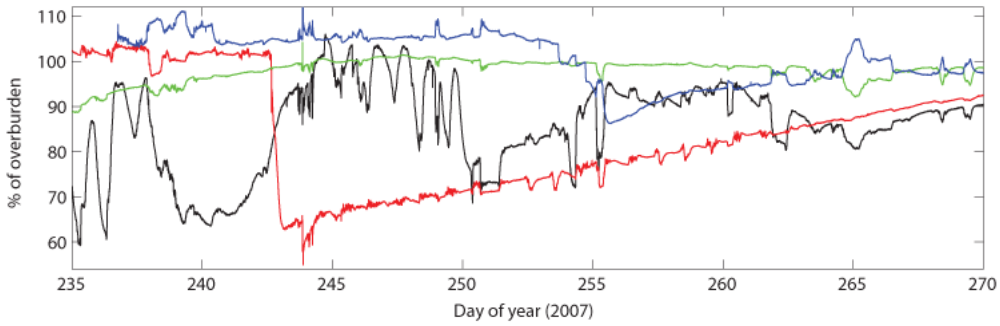

Figure 3.14: Pressure records for a 35-day period in late August and September 2007 from P4 (black), P6 (red), P8 (green) and P10 (blue) plotted as a percentage of the overburden pressure for each borehole.

P4, P6 and P8 pressure records varied nearly in-phase; differences in response were less than 20 minutes. P10 pressure varied very close to anti-phase with the other pressure transducers. The out-of-phase peak-trough lag is up to 10 minutes with P10 lagging the other pressure transducers. The phase relationships between P10 and the other pressure transducers are discussed further in Chapter 5.

2) Conductivity

There are two 'conductivity events' in summer 2007 that can be identified in all of the C4, C6 and C8 conductivity records. The first event occurred on 31 August (day 243); the second on 12 September (day 255). These events involved a temporary abrupt conductivity increase of approximately 2.5 μS cm^{-1} that lasted $\sim$12 hours and corresponded with drops of pressure in each borehole (Figs. 3.7b, c; 3.8b, c; 3.9b, c). There was a short lag between the conductivity sensors' responses during these events (the C4 and C8 records followed within 15 minutes of the C6 record).

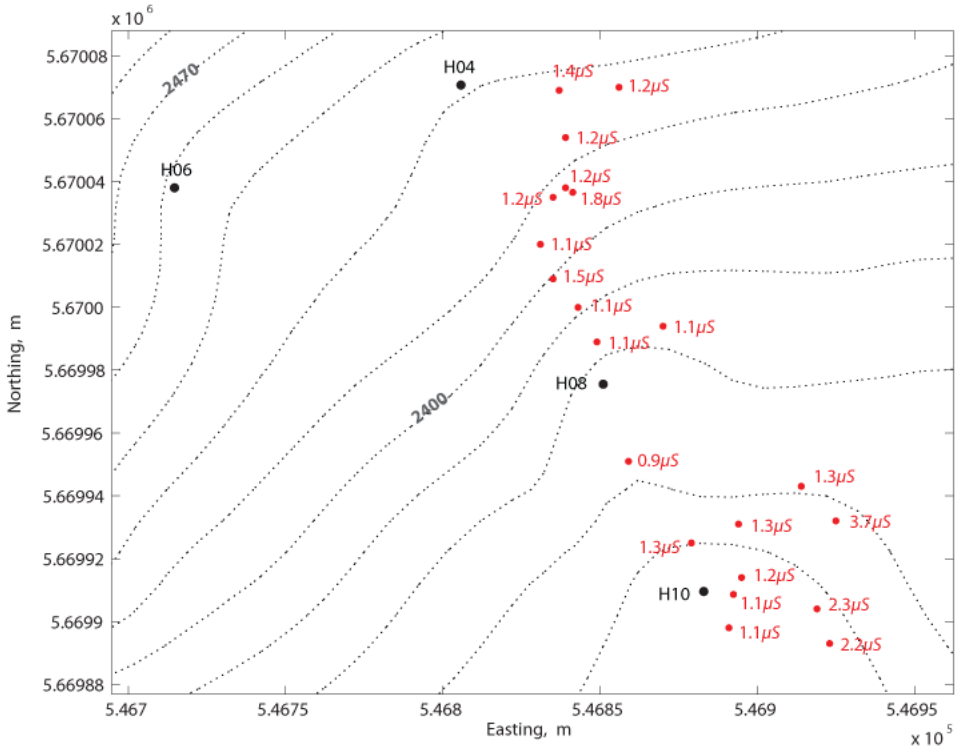

Figure 3.15: Contour map of the instrumented borehole sites at WWG; contours are at 14 m intervals. Boreholes are labeled in black. Red points denote the sites of electrical conductivity measurements taken in surface meltwater streams on day 237, 2007.

As a reference for measurements of basal conductivity, supraglacial water conductivity was measured. The results are reported in Figure 3.15. Most

surface stream measurements indicated low meltwater conductivity (averaging $1.4\,\mu\mathrm{S\,cm^{-1}}$).

3) Water temperature

As shown in Figure 3.16, basal water temperatures recorded in boreholes H4 and H6 exhibited similar variations; however, the diurnal variations recorded by T6 were smaller in amplitude than those recorded by T4. On longer timescales (Fig. 3.6), temperature changes in H4, H6 and H8 all showed similar characteristics: the water temperatures in H4 and H8 reached a steady over-winter value on day 337, the same day that pressure fluctuations ceased in these boreholes (basal temperature in H6 reached a steady over-winter level by day 346, 30 days after pressure fluctuations ceased in H6). Water temperatures then rose again once basal pressure activity was re-initiated in the Spring of 2008 (Fig. 3.6).

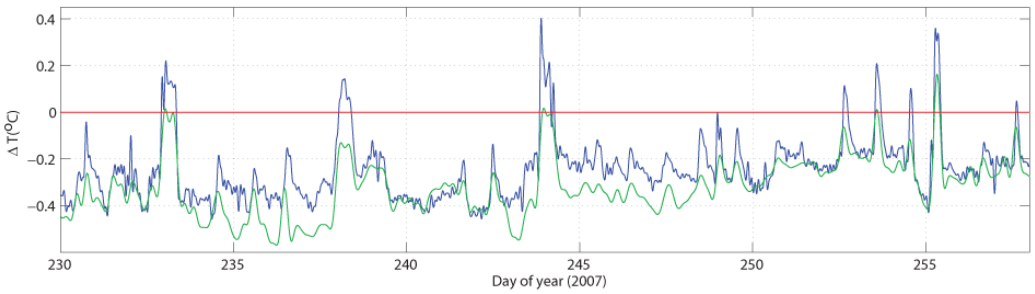

Figure 3.16: Basal temperature records showing both diurnal variability and similarity between the borehole temperature changes. The blue line is the T4 record. The green line is the T6 record. Temperatures are presented as values relative to the mean over-winter values recorded for each borehole.

Due to calibration problems with the thermistors (see Appendix A), the exact temperatures of basal water at WWG are not known. I will therefore discuss three temperature scenarios for WWG (Fig. 3.17):

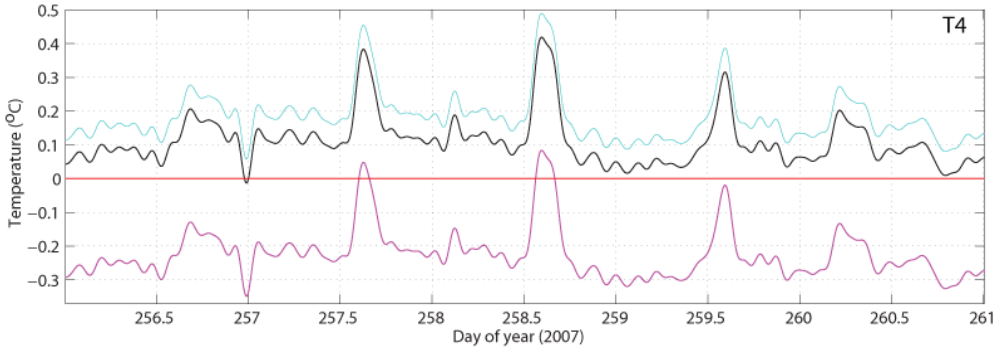

Figure 3.17: Plot of the different temperature scales for T4. The pink line is the T4 record with the over-winter temperature set at 0°C (red line). The black line is the T4 record with the lowest temperature set at the WWG supercooling minimum of -0.12°C. The blue line is the T4 record with the lowest temperature set at the H4 PMP of -0.06°C.

1. The mean over-winter temperature recorded by each thermistor is taken to be 0°C. In this case, the y-axes of Figures 3.7d, 3.8d, 3.9d, 3.6, and 3.16 represent true values (in °C) as opposed to changes relative to the mean over-winter temperature.

2. The local pressure melting point is assumed to be the lowest temperature seen in each thermistor record.

    - In H4, setting the minimum water temperature to the local pressure melting point (PMP) of -0.06°C results in an over-winter temperature averaging ∼0.4°C. The average H4 2008 summer temperature is then ∼0.75°C.
    - In H6, when the minimum water temperature is set at the local PMP (-0.04°C), the over-winter mean temperature is just above 0.5°C. The 2008 summer season then has an average water temperature of ∼0.7°C.
    - In H8, the local pressure melting point is -0.09°C. With the minimum water temperature set at the PMP, the average over-winter

temperature is ∼0.15°C. Summer 2008 temperatures then range from 0.2-0.35°C.

3. The lowest temperature in each thermistor record is assumed to correspond with the PMP of the greatest ice thickness at WWG (-0.12°C; Fig. 3.18). I refer to the lowest WWG PMP as the supercooling minimum. As can be seen in Figures 3.18 and 3.17, applying the supercooling minimum to the thermistor records only lowers the temperature of the water in the boreholes slightly from the local pressure melting point minima.

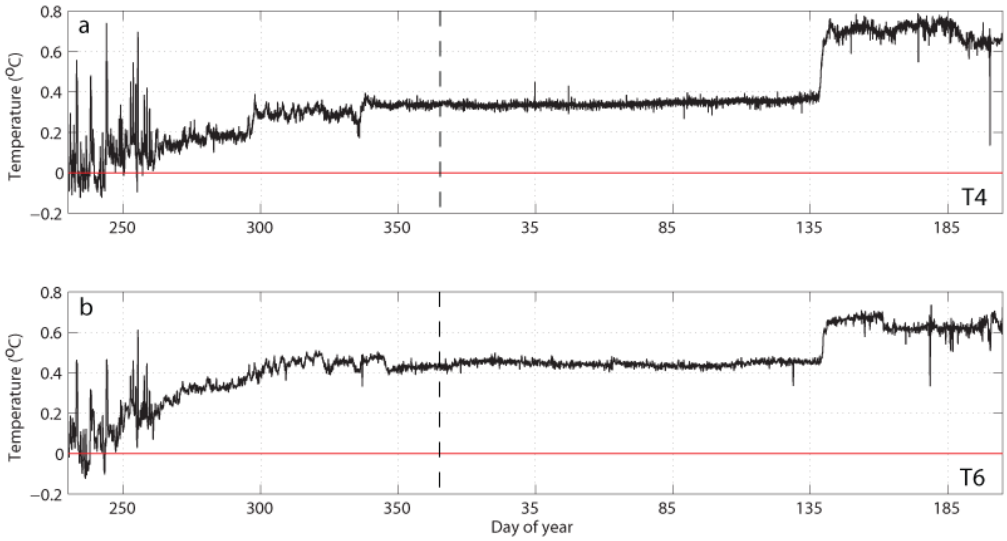

Figure 3.18: Annual basal water temperature records. The scale is set so that the lowest temperature spike (in summer 2007 for both records) is at the lowest possible supercooled temperature for WWG. a) T4 water temperature (black line) with 0°C in red. b) T6 water temperature (black line) with 0°C in red. The start of the new year is indicated by the dashed line.

Pro-glacial stream temperatures are noted on Figure 3.19. Pro-glacial water temperatures range between 0.22-0.49°C. The highest temperatures, at 0.42°C and 0.49°C, were measured directly at subglacial water outlets. The remaining pro-glacial water temperatures were recorded slightly down-stream of the glacier outlets.

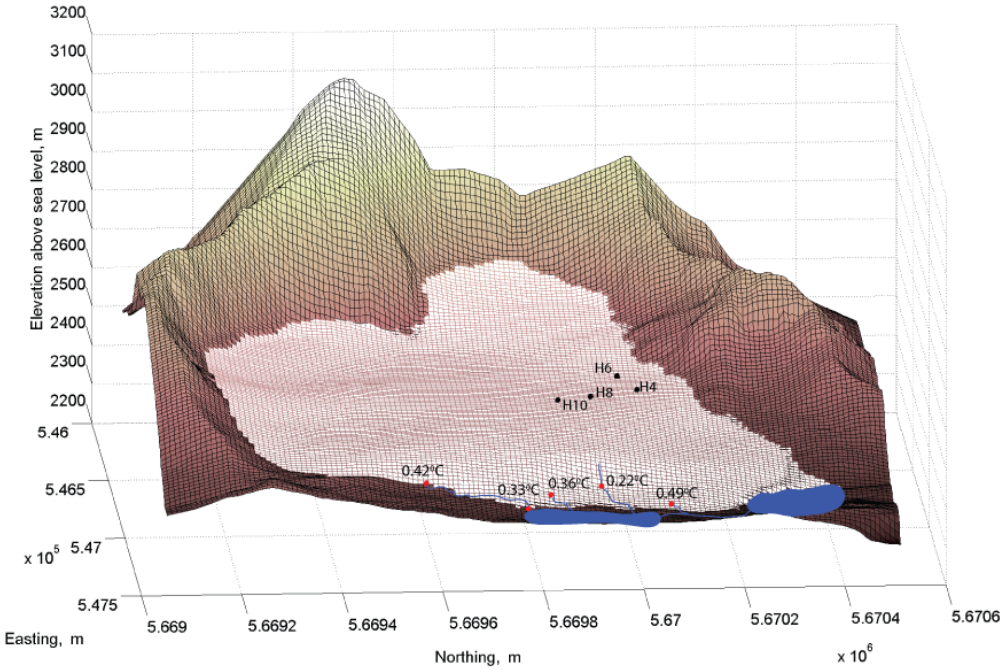

Figure 3.19: Schematic of West Washmawapta Glacier. The instrumented boreholes are marked and labeled in black. The glacier outlet streams are drawn in blue and the points of water temperature measurement are denoted by the red points.

3.5 Summary

The primary results from the summer 2007 field season at WWG and the annual instrument records are summarized as follows:

3.5.1 *Borehole video study*

1. Very few channels were seen in the borehole video footage, and most of those observed were shallow channels located within 25 m of the ice surface.

2. Several open fractures were observed in the boreholes, at depths of up to 120 m.

3.5.2 *Borehole instrument studies*

1. P4, P6 and P8 pressure varied diurnally, in-phase with surface air temperature during summer 2007.

2. P10 pressure varied diurnally, out-of-phase with surface air temperature and P4, P6 and P8 pressure.

3. Conductivity varied out-of-phase with basal pressure in all instrumented holes.

4. Water temperatures in H4 and H6 varied out-of-phase with basal pressure and showed strong diurnal variability in summer 2007. Over the year, the temperature rose in all instrumented boreholes to a stable over-winter level, and then again to a warmer summer 2008 temperature level.

5. Instrument records indicate a cessation of pressure fluctuations in mid-November or early December for all instrumented boreholes.

6. Summer 2008 instrument records show less diurnal variability than the summer 2007 records. Out-of-phase pressure fluctuations in the P10 record with respect to the P4 and P8 pressure records are re-established by mid-July 2008.

Chapter 4

Overdeepening hydrology

4.1 Introduction

The englacial overdeepening drainage hypothesis (EODH) developed by Hooke and others through studies at Storglaciären (Hooke *et al.*, 1988; Hooke, 1989; Hooke and Pohjola, 1994; Hanson *et al.*, 1998) has been widely cited by researchers of overdeepening hydrology and glaciohydraulic supercooling (e.g. Alley *et al.*, 1997, 1998; Fountain and Walder, 1998; Lawson *et al.*, 1998; Hock *et al.*, 1999; Cook *et al.*, 2006; Creyts, 2007). This EODH argues that water primarily traverses an overdeepening via an englacial drainage system, due to blockage of basal water flow pathways on a riegel that reaches the supercooling slope threshold (SST).

It is necessary to establish whether an englacial system is the primary drainage network for glacier overdeepenings in order to understand ice dynamics in these areas. The aim of this chapter is to examine the application of the EODH to West Washmawapta Glacier (WWG). As a result, I will take the interpretation of the Storglaciären drainage system provided by Hooke and others (Hooke *et al.*, 1988; Hooke, 1989; Hooke and Pohjola, 1994) at face

value. Without the data from Storglaciären, it is not possible to question the interpretation of the drainage system by Hooke and others. Here I will address the following questions for WWG: 1) Does the riegel block basal water flow at WWG? 2) How does the riegel affect the configuration of the subsurface hydrological system? 3) Is there a significant englacial component to the draining network in the cirque glacier? 4) Is supercooling a prominent and influential phenomenon in the hydrological system at WWG?

4.2 The englacial overdeepening drainage hypothesis

There are three primary scenarios that have been proposed in the literature by which water in an overdeepened bowl could begin to flow englacially:

a) Hooke (1991) suggested that when basal water pressures increase due to blockage of flow up a sufficiently steep adverse riegel slope, englacial channels form at the head of overdeepenings (Fig. 4.1a (i)); Hooke and Pohjola (1994) argued that englacial channels close more slowly than broad, low basal channels and will therefore have a lower pressure, encouraging flow from the subglacial system to the englacial system. There are, however, a couple of issues with this hypothesis for englacial flow. First, it is unclear how englacial channels initiate at the head of the overdeepening. (This is demonstrated by Equation 1.15: with an initial water flux of $Q = 0$, there is no heat energy available to form the englacial channels.) Second, the dip of equipotential planes must be oriented such that water is driven down-glacier to the riegel tip. As shown in Figure 4.1a (ii), however, equipotential contours for a typical overdeepening would instead drive water towards the bed of the glacier. Under

most circumstances, it is therefore unlikely that englacial channels could form from a subglacial origin at the head of an overdeepening.

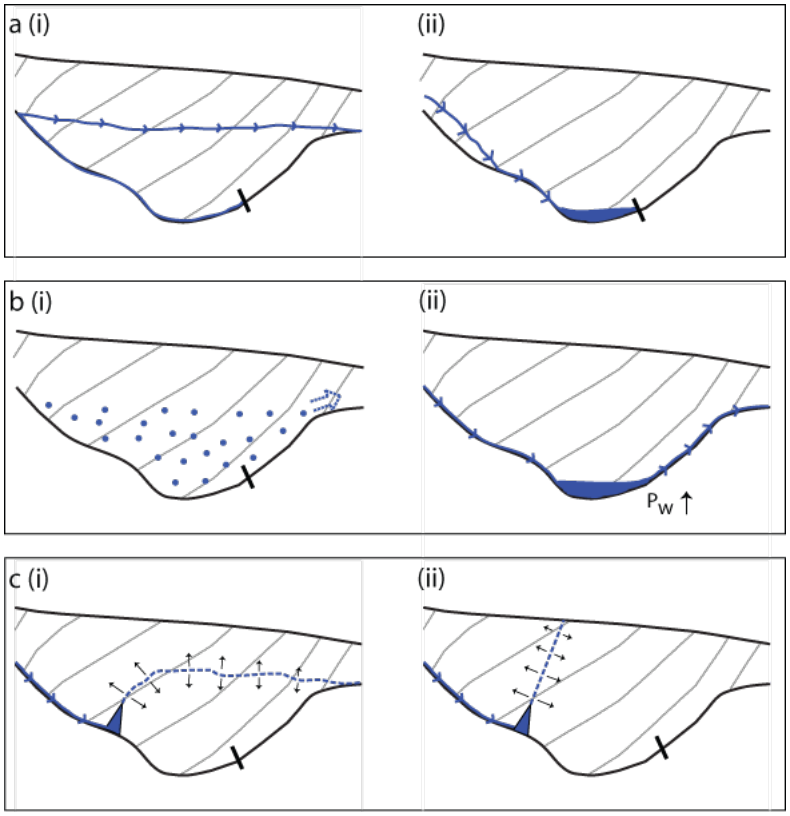

Figure 4.1: Schematics of possible drainage networks in an overdeepening. a(i) Subglacial drainage is blocked by the riegel and englacial channels form at the head of the overdeepening. a(ii) Subglacial drainage is blocked by the riegel and pools in the overdeepening, building up pressure. b(i) Water flows into an englacial aquifer via pores in the ice and finds a pathway over the riegel. b(ii) Water pools at the base of the riegel until the pressure rises to the level that water can flow up the riegel. c(i) Subglacial water flows up a basal fracture. The fracture is extended over the riegel. c(ii) Subglacial water flows up a basal fracture. The fracture propagates along a plane of weakness in the ice towards the surface.

b) Figure 4.1b (i) shows a scenario where water at the bottom of a simplified overdeepening flows through pores in the ice as part of an englacial aquifer until it reaches the tip of the riegel (Creyts, 2007). For water to move into an englacial water table, ice would have to be sufficiently permeable to allow flow. Lliboutry (1971), however, argued that refreezing in ice grain intersec-

tions limits the permeability of ice. Pore flow from the bed of an overdeepening is therefore unlikely to initiate an englacial flow network.

c) The third scenario for englacial water flow involves basal fractures that allow access of subglacial water in the overdeepening to an englacial system. For water to cause ice fracturing at the bed of the glacier, stress conditions must be suitable at that location, including high basal water pressures and significant tensile stress, which could be caused either by longitudinal extension (van der Veen, 1998) or strong vertical shear (Paterson, 1994). Fractures form along planes of weakness (such as cracks; van der Veen, 1998), and tend to propagate perpendicularly to the plane of greatest tensile stress (Roberts *et al.*, 2000). However, such planes of weakness will not always be co-planar with the regions of maximum tensile stress and, as such, it would be possible for a fracture to propagate in a direction that differs somewhat from that suggested by the stress field. On the other hand, it is unlikely that stress-induced fractures would travel horizontally (or near-horizontally), for example across an overdeepening (Fig. 4.1c (i)). Instead, it is more likely basal fractures would propagate towards the ice surface (van der Veen, 1998), as depicted in Figure 4.1c (ii).

Although basal fractures are unlikely to constitute an independent drainage network that would allow water to move from the base of an overdeepening to the riegel tip, it is possible that basal fractures in the overdeepening could intersect an active englacial network, such as an arborescent network originating from the glacier surface. As such, there could be a connection between a basal and englacial drainage system that facilitates the flow of water from the base of the overdeepening. There are, however, two limitations for flow via basal fractures to an englacial system:

1. Flow of water up basal fractures, according to Equation 1.19, will be subject to similar supercooling slope thresholds described for subglacial adverse slopes. The angle of the fracture would therefore have to be less than ∼1.2-1.7 times the surface slope (and in the opposite direction) to allow water flow at overburden pressure; otherwise water would potentially freeze within the basal fracture. However, observations of artesian fountains, such as during the 2006 field season at WWG (pers. communication, J. Kavanaugh), suggest that water flow through fractures is more complex than suggested by Equation 1.19. Instead, freezing is likely dependent on the water velocity and volume of water flowing through the fractures to the ice surface. This point will be revisited in the discussion of glaciohydraulic supercooling (Section 4.3).

2. van der Veen (1998) has argued that basal crevasses are unlikely to form on grounded glaciers, especially those that are slow-moving, unless they are at or above flotation pressure. He argued that ice streams are the only glaciers likely to form basal fractures. Given that englacial fractures have been seen in borehole footage at Storglaciären (Fountain *et al.*, 2005a,b) at a significant depth (at 96% of the ice thickness), and at WWG at ∼90% of the ice thickness, it is not clear that van der Veen (1998)'s assessment of the conditions necessary for basal crevassing is applicable to WWG.

Formation of an englacial drainage system in line with these scenarios would be likely to occur only under very limited circumstances. The alternative is that water finds a way to flow over, or around, the riegel in the subglacial system, as shown in Figure 4.1b (ii). In the following sections, I will discuss the characteristics of subsurface flow in the overdeepened WWG, in-

cluding a) the glaciohydraulic supercooling thresholds on the riegel at WWG, b) whether an englacial drainage system is present at WWG that could constitute a Storglaciären-type englacial overdeepening drainage network, c) the significance of the hydraulic potential gradients at WWG, and d) the effect of basal water temperature on supercooling at WWG.

4.3 Glaciohydraulic supercooling

The riegel at West Washmawapta Glacier is too shallow to prevent basal water flow hydrostatically at overburden pressure as defined by Equation 1.12. However, Figure 4.2 shows a plot of the regions on the WWG riegel that exceed the supercooling slope threshold according to Equation 1.18. Assuming water is flowing from the overdeepened region and is at overburden pressure, flow of both air saturated water (Fig. 4.2a) and pure water (Fig. 4.2b) appears to be blocked by the riegel.

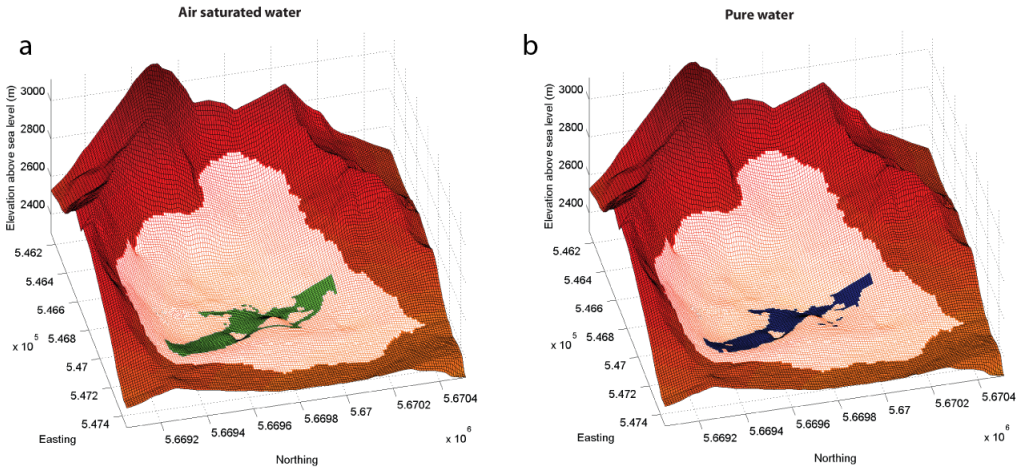

Figure 4.2: Map of the regions of the WWG riegel that are subject to supercooled freeze-on with water at overburden pressure. The white area represents the extent of the glacier in the cirque bowl. a) The area subject to freezing when subglacial water is air saturated (green shading). b) The area subject to freezing when subglacial water is pure (blue shading).

The equations from Alley *et al.* (1998) that I use to calculate supercooling slope thresholds for WWG are limited in their applicability. For example, as noted in Chapter 1, geothermal heating and heating associated with sliding are not incorporated within the equations. Perhaps more importantly, the volume and velocity of water flowing through the system are not taken into account with Equation 1.18. With greater velocity of water flow, frictional heating is increased and water can flow along a longer length scale before equilibrating to the local temperature; with greater water volumes, it is less likely that all the water would freeze within flow pathways (Creyts, 2007). As a result, the thresholds reported in this thesis might not prevent all water flow out of the overdeepening. However, given that no information could be collected about the water volumes or velocity of water flowing through the WWG overdeepening, it is not possible to ascertain how much water would freeze on the riegel. The thresholds calculated from Equation 1.18 are therefore assumed to be the areas on the riegel where water might potentially freeze.

A second limitation of Equation 1.18 is that the supercooling slope threshold is usually determined assuming basal water pressures are at overburden throughout. This pressure scenario is rarely found in reality (at least in summer months), as evidenced by borehole pressure measurements presented in Chapter 3. In order to investigate the impact of changing water pressure conditions on the supercooling slope threshold, Equation 1.18 can be reconfigured to incorporate a scaling factor (γ) that adjusts basal pressures as a uniformally varied fraction of overburden:

$$\alpha^{\dagger}_{b\gamma} = -\frac{\gamma\left(g\rho_i K\alpha_s\right)}{g\left[\rho_w - \gamma\left(\rho_i K\right)\right]}. \tag{4.1}$$

It should be noted that, as basal water pressures rarely vary uniformally within glacial systems, Equation 4.1 also has limitations. Equation 4.1 and the follow-

ing analysis are also based on the assumption that water within the overdeepening is at the local pressure melting point. If subglacial water is warmer than this temperature, the supercooling slope threshold will be steeper; with sufficiently warm water, no supercooling will occur.

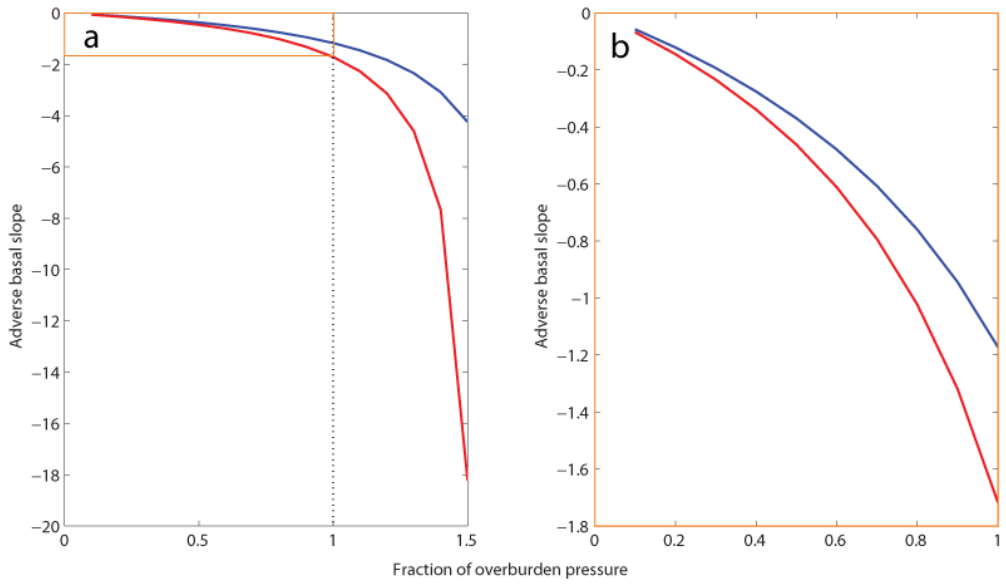

Figure 4.3: Supercooling slope thresholds at uniformally varied basal pressures, with an ice surface slope of -0.05. The thresholds are in relation to water pressures as a fraction of overburden pressure. The blue indicates the thresholds for air-saturated water, and the red line are the thresholds for pure water. a) SSTs for basal water at pressures 0-150% of overburden. b) A close-up of plot a, with basal water pressures at 0-100% of overburden.

Figure 4.3 shows SSTs for different values of γ for both air-saturated and pure water. At lower pressures, the adverse basal slope necessary for supercooling freeze-on is shallower. At higher pressures, water can flow up steeper adverse slopes without freezing. The relative importance of the air content of subglacial water is seen to be more influential at higher pressures. With changes in basal water pressure often occurring on diurnal time-scales, glacial systems with variable basal topography might experience periodic freezing and thawing on adverse basal slopes within the subglacial drainage system (see e.g. Iken, 1981). Such freeze/thaw cycles could potentially occur both on the scale

of days and on a seasonal basis, depending on the configuration of the basal hydrological system.

Figure 4.4 shows a series of plots of areas on the WWG riegel that reach the SST at different values of γ. These plots show that once basal water pressure rises significantly above overburden level, water flow is possible over the riegel at WWG. For air saturated water, flow occurs above $\sim$130% of overburden (Fig. 4.4c) and for pure water, above 150% (Fig. 4.4j). On the other hand, none of the borehole pressure records indicate that basal water pressures significantly exceed the overburden level at WWG. For this overdeepening, the adverse slope therefore seems too steep for thermally equilibrated water flow in most circumstances; this issue will be revisited later in the context of the observed WWG basal water temperatures.

The calculations of SSTs for WWG demonstrate that at sufficient pressures, water will flow up and over the riegel. This is a viable alternative for overdeepening hydrology that does not involve water entering an englacial network to traverse the overdeepening. I therefore argue that Figure 4.1b (ii) is the most likely scenario for overdeepening hydrology. However, it is important to establish whether the drainage system at WWG is in fact primarily subglacial, to verify this basal flow hypothesis for overdeepening hydrology.

4.4 WWG englacial flow

This section determines whether an englacial flow network is present at WWG and, if so, how influential it is for transporting meltwater through the glacial system. The englacial network is discussed first in terms of englacial channels

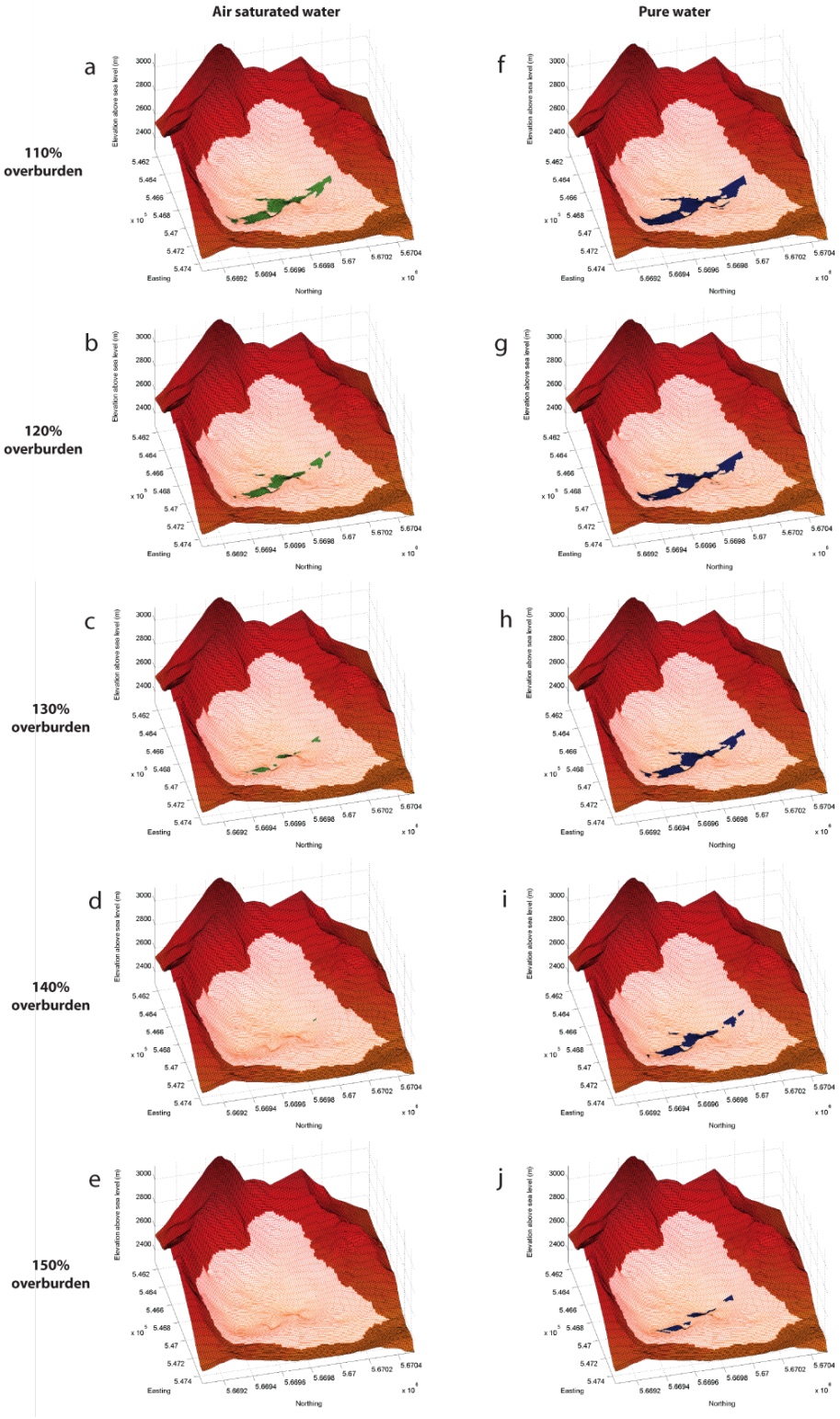

Figure 4.4: Maps of WWG showing the areas on the riegel subject to freezing as basal water pressure increases above the overburden level. The SSTs are calculated with uniformally varied water pressure as a percentage of overburden. a) Air saturated water: 110% of overburden. b) Air saturated: 120%. c) Air saturated: 130%. d) Air saturated: 140%. e) Air saturated: 150%. f) Pure water: 110%. g) Pure: 120%. h) Pure: 130%. i) Pure: 140%. j) Pure: 150%.

and then in terms of englacial fractures observed at WWG.

4.4.1 *Englacial channels*

The number of WWG boreholes surveyed with the borehole camera is too small to establish an englacial drainage density for this glacier. However, in the surveyed boreholes, the borehole camera footage indicated a paucity of englacial channels. Most observed englacial drainage features were shallow (<25 m depth) channels that were associated with open surface crevasses or with palaeo-crevasses that have closed through ice deformation. The deeper englacial conduits that were observed mostly dipped steeply towards the glacier bed and did not resemble horizontal englacial conduits as depicted in Figure 4.1a (i). The englacial channels were found at sufficiently different depths within the boreholes to suggest they were not related to each other (Table 3.1). The englacial channels identified with borehole photography by Hooke and Pohjola (1994) in the main overdeepening at Storglaciären were larger than 10 cm in diameter. In contrast, no channels of this size were identified in the nine boreholes at West Washmawapta Glacier; instead, all of the conduits identified were ≤5 cm in diameter.

Video footage in four boreholes at Storglaciären revealed twelve englacial channels, of which five were argued to have active water flow through them (Pohjola, 1994). This can be compared with four englacial channels (i.e. channels deeper than 25 m) in nine holes at WWG, none of which had discernibly active water flow. Storglaciären therefore appears to have had a significantly greater density of englacial channels than seen in the boreholes at WWG. On the other hand, a borehole system only allows single point investigation of a very limited region of the glacier, and it is possible that an englacial drainage system at WWG was missed (see e.g. Sharp *et al.*, 1998), particularly since

only nine boreholes were surveyed at this glacier. In addition, investigation at depth in the WWG boreholes was often not possible due to high turbidity levels and blockage (Fig. 3.1). On the other hand, active water flow through englacial conduits would likely have reduced or eliminated turbid water at that elevation. As a result, an englacial network with active water flow is unlikely to have been present within the high-turbidity areas of the boreholes.

The observed channels at WWG were unlikely to have caused the variations in pressure recorded in the boreholes. Although water input from shallow channels (channels above 25 m in the borehole) could give rise to apparent changes in borehole pressure, such changes would last only a short period of time (likely less than one week) due to freeze-closure of the boreholes. H4 and H10 had no englacial channels or englacial fractures below 25 m in the borehole that could create the diurnal pressure signals seen in the P4 and P10 records (see Fig. 3.1). Both variations in instrument records from two holes with no observable englacial features, and the lack of observed water flow from englacial features in the remaining boreholes suggests that the diurnal pressure variations seen in the WWG records (Fig. 3.14) are part of a basal hydrological system.

This interpretation is supported by details in the conductivity and basal water temperature records. Figure 4.5b shows diurnally varying electrical conductivity signals at WWG. The electrical conductivity varied out-of-phase with basal water pressures and surface air temperatures. As low-conductivity surface water is input into the system ($\sim$1.4 μS cm^{-1} at WWG; Fig. 3.15), the water conductivity at the base of the borehole drops, concurrent with rises in borehole water pressure (e.g. Collins, 1979a). With less water input into a glacial system, water velocity is argued to generally decrease, allowing

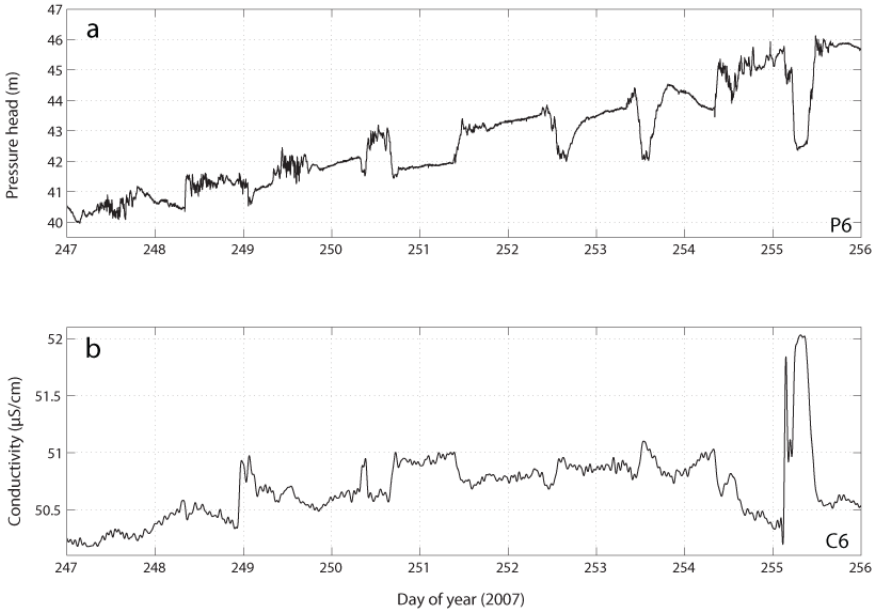

Figure 4.5: Nine-day time series of H6 instrument records in summer 2007. a) P6 pressure records, all below overburden level. b) C6 conductivity records.

increased subglacial water-sediment contact, and therefore greater chemical enrichment (Collins, 1979a; Gurnell and Fenn, 1985). The relationship between water input and basal water conductivity likely created the diurnal, out-of-phase signal seen in the WWG records. Conversely, englacial water is likely to encounter little sediment and would thus be unlikely to produce diurnal changes in conductivity (see e.g. Collins, 1979b).

Variations in basal water temperature within boreholes at WWG (Fig. 3.16) would similarly not likely be caused by englacial water flow. The large (maximum 0.8°C) diurnal swings in water temperature can, however, be explained by changes in basal water pressure; this will be discussed in detail in Chapter 5. From the borehole camera evidence of few englacial channels, and the borehole instrument evidence of diurnally varying pressure, temperature and conductivity, the hydrological system at WWG appears to be primarily subglacial.

4.4.2 *Fractures*

Englacial fractures, as defined by Fountain *et al.* (2005a,b), were visible in four of the surveyed boreholes. Such features could serve as an additional pathway for englacial water flow (Fig. 3.2). Statistically, the number of fractures observed at WWG is similar to that encountered at Storglaciären (8 in 9 holes vs. 36 in 48 holes, respectively; see Fountain *et al.*, 2005a). These features at WWG were also of a similar size as reported at Storglaciären, with widths between ∼1 cm (F2) and ∼12 cm (F8) within the borehole (Table 3.2). It is not possible to calculate the volume of water that could be transported through these fractures because, for example, their lateral and vertical extents are not known. However, the width of fractures intersected by the boreholes suggests they were capable of transmitting greater volumes of water than the observed englacial channels at WWG would be. At Storglaciären, water flow through fracture features was observed through particles moving across the camera's field of view (Fountain *et al.*, 2005a), but at WWG this was not seen for any of the fractures.

Fractures at the bed of a glacier are most likely to form in the area of maximum basal extension where there is high longitudinal tensile stress (van der Veen, 1998). In an overdeepening, longitudinal stress will likely be highest where ice flows down slope into the overdeepening; the riegel would tend to be an area of basal compression (Hooke *et al.*, 1989), which would retard formation of basal crevasses or close crevasses advected from up-glacier. Like the fractures identified by Fountain *et al.* (2005a) at Storglaciären, those seen at WWG dipped down towards the riegel. It is therefore unlikely that these features formed subglacially. Instead, they probably originated at the surface, were advected from up-glacier or were formed englacially along shear zones, and remained open either because they constitute an active hydrological sys-

tem, or became hydraulically isolated with a water packet that was sufficiently pressurized to prevent closure by ice deformation (e.g. Fountain *et al.*, 2005a).

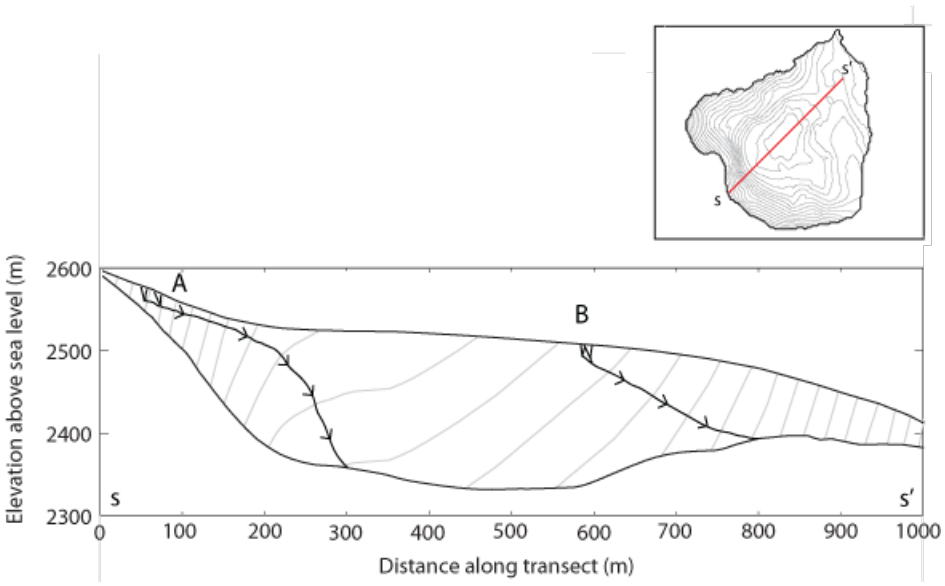

Figure 4.6: A cross-section from S to S' of WWG with equipotential contours. Drainage Pattern A demonstrates the pattern of englacial flow if water is input above the head of the overdeepening. Drainage Pattern B indicates the englacial networks that would develop if water input occurs further down-glacier.

The dip of the observed fractures at WWG indicates that if they did reach the glacier bed, they would intersect the adverse slope of the riegel, even when accounting for rotation of the crevasse within the ice. In order to provide an alternative (englacial) path for water flow over the riegel, they would have to also intersect an active englacial network, as described in Section 4.2 (c). As discussed above, an active englacial channel network (channels with water flow) was not observed within the WWG boreholes, which suggests that the fractures would not draw a significant volume of water away from the overdeepening. Figure 4.6 shows a cross-section of WWG with the equipotential contours plotted. As demonstrated by Drainage Pattern A, most englacial channels originating from the glacier surface would flow normal to equipotential contours, and reach the bed up-glacier of the riegel. Drainage Pattern B demonstrates the region where input of water could result in englacial chan-

nels flowing over the tip of the riegel. As a result, subglacial water that flowed through any basal fractures intersecting an englacial network within the overdeepening region of WWG would likely be redirected towards the bed.

There is little evidence of a significant englacial network at WWG. Instead, diurnally varying pressure, conductivity and temperature records suggest that the WWG drainage system is primarily basal. The presence of a major subglacial flow network at WWG contradicts the premise that glaciers with sufficiently steep riegels should develop an englacial network as suggested by Hooke and others (Hooke *et al.*, 1988; Hooke, 1991; Hooke and Pohjola, 1994). The discovery of a basal flow regime in the WWG overdeepening, however, supports other studies that have found subglacial drainage networks within glacial overdeepenings (e.g. Hodge, 1976; Hantz and Lliboutry, 1983; Iken *et al.*, 1996; Hanson *et al.*, 1998).

4.5 Overdeepening hydraulic potential

This section discusses the configuration of basal hydraulic potential gradients at WWG and the impact of this configuration on the application of the EODH. Hydraulic potential gradients for basal water flowing at a uniform overburden pressure at WWG are presented in Chapter 2 (Fig. 2.4). That figure indicates that the strongest hydraulic gradients are towards the margins of the cirque glacier, avoiding the overdeepening. Such a configuration of basal hydraulic potential is due to steeper surface slopes towards the margins of the cirque glacier, if assuming that Shreve's (1972) calculations are applicable. By calculating hydraulic potentials with Equation 1.5, the gradients with uniformally varied water pressures can be established. Figure 4.7 shows hydraulic

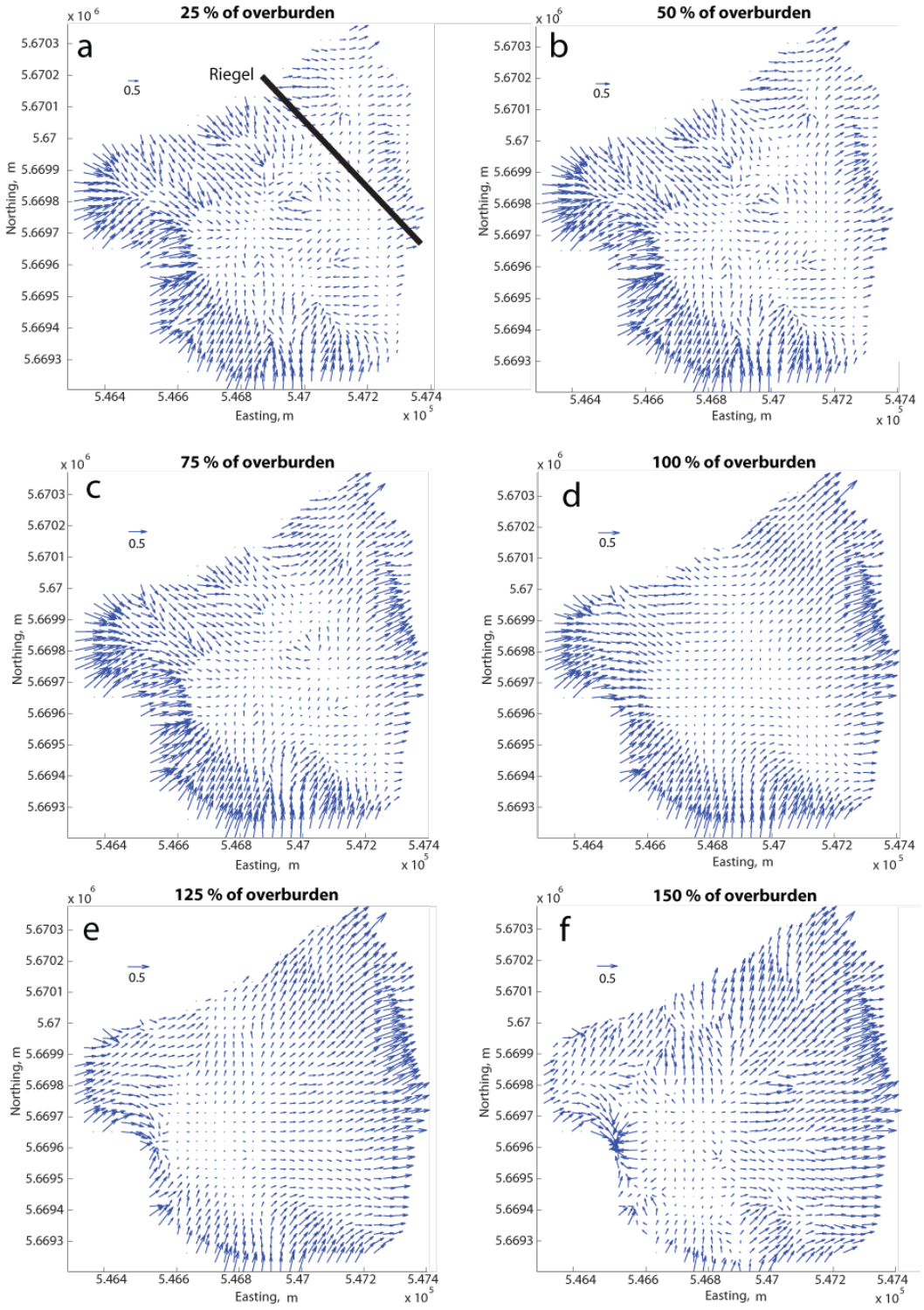

Figure 4.7: Series of hydraulic potential gradient maps for WWG. The calculated potentials are based on uniformally varied basal water pressures relative to ice overburden pressure. The scales show 0.5 m of hydraulic potential change per meter. a) 25% of overburden with the approximate location of the riegel in black, b) 50% of overburden, c) 75% of overburden, d) 100% of overburden, e) 125% of overburden and, f) 150% of overburden.

potential gradients for WWG at different basal water pressures (expressed as percentages of overburden pressure). The presence of the riegel becomes increasingly more influential with respect to potential gradients as subglacial water pressures decrease. As can be seen from Fig. 4.7a, when pressure is 25% of overburden, water is driven towards the overdeepening; at this pressure the basal topography is the main control for potential gradients. At 75% of overburden (Fig. 4.7c) water is driven somewhat towards the overdeepening, but also weakly down-glacier. Only once pressures approach overburden is water driven predominantly down-glacier (Fig. 4.7d). At levels above overburden pressure, the strongest potential gradients would act to force water out of the overdeepening towards the glacier margins, driven primarily by the surface slope gradients (Fig. 4.7e, f).

Calculations of hydraulic potential are over-simplified in that they, similarly to the supercooling equations, do not take account of changing volumes of water into and out of a system, or the velocity of the water flowing through the system. In order to establish whether ponding is occurring within the overdeepening, the flux into and out of the overdeepening would need to be established, which in a subglacial system is challenging. Assuming uniformally varied subglacial water pressures for calculation of hydraulic potential gradients has limitations in that basal water pressures are rarely uniform in connected regions of the bed during the melt season. Ideally, varying hydraulic potential gradients in relation to spatial and temporal changes in pressure could be calculated. However, with four instrumented boreholes at WWG it is not possible to establish changing hydraulic potential gradients with respect to changing basal pressure for the entire glacier. As a result, the plots of hydraulic potential at uniformally varied pressures are presented as an indication of the importance of basal pressure change for water flow in the glacial system.

Diurnal changes in pressure, in-phase with surface air temperature change, imply that H4, H6 and H8, which were all located towards the shallower margin of the cirque glacier (Fig. 2.4), were within a strongly connected zone of basal water flow (Figs. 3.7a, b; 3.8a, b; 3.9a, b). The pressure record from H10 (located deeper in the cirque bowl) suggests that there was little active water flow in this area; the P10 record will be discussed further in Chapter 5. These data indicate that basal flow at WWG was primarily near-marginal; the borehole instrument data therefore corroborate the hydraulic potential maps. Pressures in these boreholes were often greater than 75% of overburden, suggesting that hydraulic gradients were somewhat (although not entirely) driving flow down-glacier (Fig. 4.7c).

Near-marginal basal water flow has been identified at other overdeepenings, such as Glacier d'Argentière (Hantz and Lliboutry, 1983) and South Cascade Glacier (Fountain, 1994), and is argued for theoretically by Lliboutry (1983). If little water flow occurs within the deepest regions of the overdeepening, conditions would likely be unfavourable for development of an englacial flow network.

4.6 Water temperature

Thermistor records at WWG show diurnally varying water temperatures, with maximum values of $\sim$0.9°C above the local pressure melting point (Fig. 3.16). These variations will be discussed further in Chapter 5. It is worth noting here, however, that if temperatures are above the local pressure melting point within the overdeepening, the impact of supercooling on the riegel will likely be lessened or potentially absent. Given that water temperatures in WWG

vary diurnally and seasonally, supercooling might occur only during certain basal water flow conditions (e.g. times of high water pressure, when basal water temperatures are typically low). If warm basal temperatures occur at other glaciers with overdeepenings, supercooling could also be limited under these glaciers. With no supercooling freeze-on, the riegel will be less likely to block basal flow and the conditions for englacial channel formation, as defined by the EODH, would not be in place.

4.7 Conclusions

West Washmawapta Glacier appears to have a primarily subglacial drainage network; borehole instrument records at WWG show diurnal variations in temperature, conductivity and pressure, which suggest the presence of a dynamic basal hydrological system. Borehole camera footage reveals a paucity of englacial channels, and no evidence for hydrological connection of englacial fractures. These englacial features do not appear sufficiently pervasive to cause the diurnal pressure head changes recorded at WWG, nor do the features likely facilitate diurnal changes in conductivity or water temperature.

Given the evidence for a basal drainage network at WWG, the EODH does not appear to be applicable to this small cirque glacier. I argue that the EODH is not applicable to this overdeepened glacier for the following reasons:

- Englacial channels are unlikely to form at the head of an overdeepening from a subglacial origin, and run directly to the riegel tip. Englacial channels forming at the head of the overdeepening will flow perpendicular to equipotential contours. These contours will rarely allow flow within the ice across the entire overdeepening.

- Water will not likely flow from the base of an overdeepening into an englacial network through pores (due to low hydraulic conductivity) or basal fractures (which would, in many cases, propagate along a plane towards the ice surface as opposed to over the riegel), unless basal fractures intersected an established englacial drainage network. Basal fractures however, are unlikely to form within a slow-moving overdeepened system, according to van der Veen (1998).

- Evidence from WWG suggests that the strongest basal hydraulic gradients are towards the ice margins, avoiding the overdeepening, unless water pressures drop to less than 75% of overburden. Near-marginal water flow at WWG is supported by strong variations on diurnal (among other) timescales in the borehole instrument records. These obesrvations agree with other studies of overdeepening hydrology (e.g. Hantz and Lliboutry, 1983; Fountain, 1994), which also indicate near-marginal flow. With little flow through the overdeepening, the conditions are likely not present to encourage development of a significant englacial network.

- Diurnally varying basal temperatures at WWG suggest that water in a sediment aquifer at the base of an overdeepening is not necessarily at the pressure melting point. At higher water temperatures, supercooling will not occur to the same extent and water will not likely freeze while flowing up the riegel. As temperatures recorded at WWG vary diurnally, supercooling freeze-on might only occur under certain subglacial drainage conditions.

As an alternative to the EODH, I suggest that, if a riegel does block subglacial water flow through supercooling freeze-on, water will pool within the overdeepening. Equation 4.1 demonstrates that once water builds up sufficient

pressure, it can flow up and over the riegel. It is more likely that pressure build-up would allow subglacial flow up the adverse slope than through an englacial network. From evidence closer to the margin of the glacier the drainage system appears to be primarily distributed. As a result, flow over the riegel would also potentially be in a distributed system that, with lower water volumes per unit area, would likely be more subject to supercooling freeze-on than a channelized system. However, from investigation at WWG, near-marginal flow around the overdeepening and diurnally varying basal water temperatures are also likely influential in limiting the volume of supercooling freeze-on that occurs within the overdeepening.

Chapter 5

West Washmawapta Glacier Hydrology

5.1 Introduction

The formation and development of an overdeepening, whether in a cirque bowl or under a valley glacier, is likely influenced by subglacial hydrological conditions. Basal water will affect both the ice velocity (Bindschadler, 1983) and erosive power (Alley *et al.*, 1997) of the glacier. There has been little research into cirque glacier hydrological conditions. Instead, most cirque research has focused on aspect and elevational controls of cirque location (e.g. Chueca and Julián, 2004; Evans, 2006; López-Moreno *et al.*, 2006), and the initiation of cirque hollow formation (e.g. Holmlund, 1991; Bennett *et al.*, 1999; Turnbull and Davies, 2006).

This chapter explores the subglacial hydrological characteristics of West Washmawapta Glacier and suggests effects of basal water flow on weathering and erosion of the cirque bowl. The following sections include discussions of 1) field data from summer 2007, 2) field data from winter 2007/2008, 3) field

data from summer 2008, 4) H10 hydraulic jacking signals, and 5) implications of these observations for cirque erosion.

5.2 Basal hydrological characteristics: Summer 2007

The WWG field data from summer 2007 are here used to discuss a) the basal hydrological system at WWG, b) drainage in a sediment-based macroporous horizon, c) diurnally varying basal water temperatures, d) sediment flow into boreholes at WWG, and e) basal conductivity variations.

5.2.1 *Subglacial drainage*

Three of the four instrumented boreholes at WWG connected to a basal drainage system, as indicated by diurnal changes in borehole pressure, conductivity and temperature (Figs. 3.7; 3.8; 3.9). If the basal water network was composed of discrete channels by the late melt-season, rather than a distributed drainage network, it is unlikely that three boreholes would have made a good drainage connection (see Shreve, 1972). In a channelized system, pressures will often be substantially below overburden level (although this is based on flow under thin ice), and have a lagged or out-of-phase response with respect to changes in surface water input. The lagged response is due to the increased melt of channels with greater volumes of water that expands the channels faster than ice creep can close them (e.g. Röthlisberger, 1972; Shreve, 1972; Bindschadler, 1983; Röthlisberger and Lang, 1987; Fountain, 1993; Paterson, 1994; Mair *et al.*, 2002a; Schuler *et al.*, 2004). Instead, the WWG pressure records from H4, H6 and H8 varied in-phase with surface air temperature changes, with pressures mostly fluctuating within ∼65-105% of overburden

(Fig. 3.14). These characteristics have been argued to indicate the presence of a distributed hydrological system (Harper *et al.*, 2005; Lappegard and Kohler, 2005).

The large diurnal changes in basal water pressure, of up to 27 m in H4 (Fig. 3.14), suggest that the drainage network was sensitive to changes in water input (e.g. Bindschadler, 1983). The borehole instrument records provided no information about the volume of water passing through WWG. However, the steep headwall contributes little water directly to the glacial system following snow-melt in June and July, and the surface area of the glacier is just $\sim$1 km^2. As a result, it is likely the total volume of water input into the subglacial network at WWG is low in comparison to larger valley glacier systems. To initiate large swings in diurnal water pressure from little water flow, the system must be substantially constricted (Bindschadler, 1983; Rutter, 2005). Low volumes of water input into the WWG drainage network would likely reduce the potential for channelized system development under the cirque glacier, even by the late 2007 melt-season. As discussed in Chapter 4, the WWG riegel is sufficiently steep to block water flow at up to 130% of overburden (if basal water is both air-saturated and at the pressure melting point in the overdeepening). Given that the observed water pressures at WWG rarely exceeded 110% of overburden, the riegel could be affecting the formation of drainage networks; such restriction could prevent the development of a channelized drainage system and instead encourage distributed flow. Blockage of flow by the riegel, however, depends on the volume of water flowing through the overdeepening. If, as suggested by Figure 4.7d, water is directed more strongly towards the margin of the cirque glacier at basal water pressures near overburden, it is possible that little water is flowing into the riegel. Without additional information, it is not possible to ascertain the effect that small volumes of water

flow into the overdeepening would have on development of drainage networks in the glacier.

At WWG, the lag time between air temperature change at AWS 1 and basal pressure change in summer 2007 was short (maximum of 2 hours). Because air temperature values were averaged over one hour by AWS 1, it is not possible to determine phase differences smaller than this between basal pressure and air temperature. In a highly constricted drainage system, it is plausible that peaks in water pressure could lead air temperature maxima; maximum pressure does not necessarily directly indicate maximum water input volumes (given that drainage system capacity likely changes with fluctuations in pressure). Distributed drainage systems often have long lags between air temperature change and basal pressure change. For example, South Cascade Glacier had lags of up to 2 days (Hodge, 1976). However, because WWG is less than a kilometer in length, the phase differences between air temperature and subglacial pressure can be expected to be much shorter.

5.2.2 *Macroporous horizon*

All of the WWG boreholes that intersected the bed had columns of turbid water at the base; this was likely due to disturbance of basal material by the hot water drill as the turbidity was too great to have been created from the melting of dirty basal ice. In addition, an unfrozen wedge of sediment was observed at the base of H8. Given that the H8 instruments displayed diurnal variations in conductivity and pressure, and seasonal variation in basal water temperature, it is possible there was a connection to the basal system through the sediment wedge. This wedge, and the turbidity in the directly connected boreholes, suggest that there was a basal sediment layer in the study area (see e.g. Engelhardt *et al.*, 1978). If WWG is largely sediment-based (at least

in the northern region), the distributed drainage system identified from the borehole pressure records was probably not linked-cavity as the latter is usually associated with bedrock-based glaciers (e.g. Harper *et al.*, 2007), and in sediment-based systems is argued to be an unstable drainage configuration (Paterson, 1994). Walder and Fowler (1994) argued that canals will preferentially form in sediment-based systems that have significant fluxes of basal water, if the sediment is not too permeable. Such canals, however, would tend towards a channelized type of drainage system within the sediment, which, as seen, does not seem to occur at WWG. In addition, as discussed above, WWG likely has a relatively low volume of water input that would limit the flux of water through the subglacial drainage system.

Instead, it is likely that basal water flow at WWG is primarily within a subglacial sediment aquifer (e.g. Stone and Clarke, 1993; Fountain and Walder, 1998; Jansson *et al.*, 2003). It is not possible from the measurements taken at WWG to establish the permeability of the basal sediment; however, the velocity of sediment pore-flow is generally thought to be low (e.g. Lliboutry, 1983; Iken and Bindschadler, 1986; Walder and Fowler, 1994). Given the very short lag times between AWS 1 air temperature change and reaction of the basal water pressure at WWG, it is plausible that water is flowing in a macroporous (or multiporous) horizon (see Clarke, 1987b). These hydraulically permeable horizons form when sediment grains are re-aligned by water flow and fines are eluviated (Hubbard *et al.*, 1995); larger pore spaces and pipes are created within the sediment and allow faster water transmission through the system (Clarke, 1987b). Water therefore does not necessarily flow in direct contact with the base of the ice. Such a sediment-based drainage system was identified at Trapridge Glacier, Yukon Territory, and was described by Murray and Clarke (1995) as consisting of a layer of larger clasts (2-16 mm diameter)

between the base of the ice and the underlying sediment.

At WWG, it is not known whether sediment is present throughout the overdeepening or whether sediment cover is limited to the northern margin of the glacier where the boreholes were drilled. There might therefore be concurrent types of drainage networks operating in different areas of the glacier (e.g. Fountain, 1993; Hubbard *et al.*, 1995; Hubbard and Nienow, 1997; Fountain and Walder, 1998). Development of drainage systems within the overdeepening at WWG is potentially strongly influenced by the presence of the riegel preventing continuous flow at basal pressures below 130% of overburden (if water is equilibrated to the PMP in the overdeepening).

5.2.3 *Basal water temperature*

The basal water temperature records from H4 and H6 at WWG show substantial (up to 0.8°C) diurnal variations in temperature that fluctuated out-of-phase with basal water pressure changes. Interpretations of data from both field-based (Iken and Bindschadler, 1986) and modelling (Röthlisberger, 1972; Shreve, 1972; Clarke, 1987b; Flowers and Clarke, 2002; Bates *et al.*, 2003) studies generally assume that water flowing at the ice-bed interface is at the local pressure melting point (PMP). Any excess heat in basal water (i.e. that available to raise water temperature above the PMP) that could be gained from downhill flow, geothermal heating, or viscous friction is rapidly utilized for melting or warming surrounding ice, if colder than the melting point (Alley *et al.*, 2003a; Clarke, 2005; Tweed *et al.*, 2005).

The greatest ice thickness at WWG is ∼200 m, which corresponds to a minimum pressure melting point of -0.12°C (this value neglects any freezing point depression due to the effect of solutes; basal conductivity values of be-

tween 30-100μS cm^{-1} in H4 and H6 during the summer melt-season, as shown in Figure 3.5a and b, suggest that this is a reasonable assumption). As a result, this value reflects the minimum temperature at which supercooled water would be expected to flow in the vicinity of the boreholes. However, even when the thermistor records are adjusted to incorporate this supercooling minimum for low temperatures, maximum temperatures still reach ~0.9°C above this supercooling minimum (as seen in Fig. 3.18a). It is possible that warm basal temperatures are due to one or a combination of the following processes:

- The primary source of heat for warming subglacial water is likely to be geothermal (Zotikov, 1986). Additional heat could be created within the sediment from friction between the grains and the water, heating due to loss of potential energy as water flows downhill, or through sediment deformation (Murray and Porter, 2001). Basal water could maintain temperatures above the local PMP with a combination of warm water input and insulation from the ice by basal sediment. Isenko *et al.* (2005) conducted lab experiments for supraglacial water flow through sediment and found that even a thin insulating layer of sediment could raise the water temperature by several tenths of a degree. Studies at Dzhankuat Glacier in the Central Caucasus recorded water temperatures of 0.15-0.2°C in the streams emerging from the base of the glacier. The high temperatures were explained by water flow that had little contact with basal glacier ice as it flowed through the system (Zotikov, 1986).

- Upwelling from deeper geothermally-heated groundwater sources into the subglacial sediment aquifer could provide warmer water to the subglacial drainage system at WWG. Groundwater flow elsewhere has been reported to raise subglacial water above the local PMP. For example, Bayley (2007) recorded subglacial water temperatures of up to 3.5°C

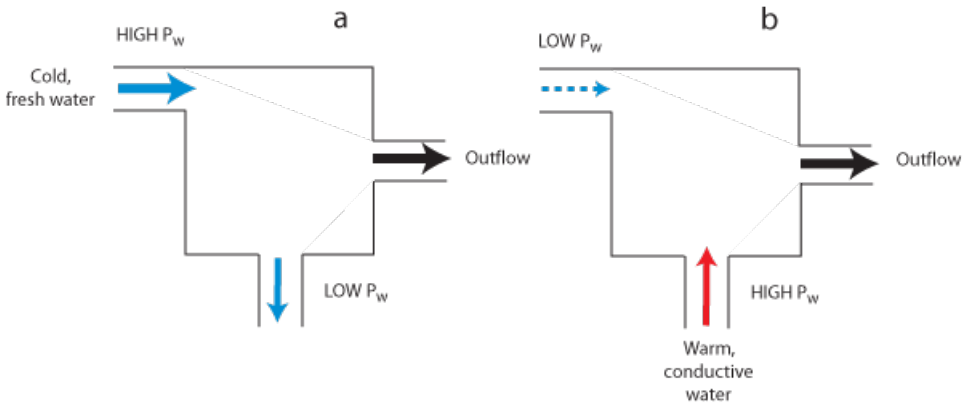

Figure 5.1: Box diagrams of the subglacial drainage system postulated for WWG. a) Cold, fresh, high pressure water enters the system. This high pressure water flows vertically down into the lower-pressure sediment aquifer. The temperature in the box is therefore cool. b) At lower pressure, less cold water enters the system and warm, conductive groundwater at higher pressure can flow vertically up into the sediment aquifer. The temperature in the box is therefore warmer.

at Glacier de Tsanfleuron, Switzerland. These high water temperatures were argued to be a result of groundwater influx through a karst system into the subglacial water network. It is not known whether there is a karst system underlying WWG.

In addition to high water temperatures, diurnal fluctuations of up to 0.8°C were recorded by the T4 thermistor. These diurnal variations could be due to the following factors:

- At low water pressure in the WWG basal sediment aquifer, water might flow largely within the material by Darcian flow (Fig. 5.2a). While flowing within the sediment, the water is insulated from the overlying ice. At high water pressures, the glacier is hydraulically lifted off the bed (as discussed later in Section 5.5), allowing water to flow at the ice-sediment interface (see e.g. Iverson *et al.*, 1995; Hubbard and Nienow, 1997; Truffer and Harrison, 2006). This could act to create or thicken a basal water film, increasing the volume of water that is in direct contact with glacier

ice and resulting in cooler water temperatures (Fig. 5.2b).

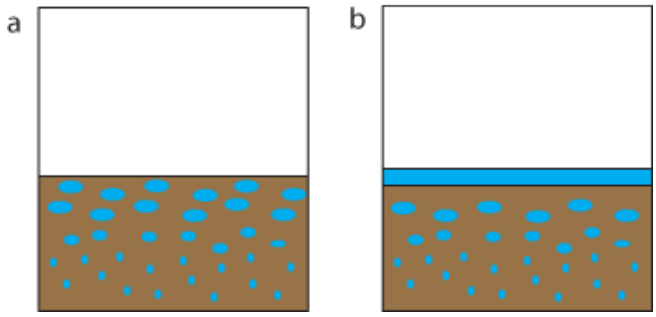

Figure 5.2: Schematics of basal water flow through a subglacial sediment aquifer. a) A sediment aquifer at lower water pressures with little direct contact between water in the aquifer and the base of the ice. b) A sediment aquifer with film flow at the ice-bed interface due to high water pressures.

- Models, supported by measurements, of pore-water flow within sediment by Kavanaugh and Clarke (2006) suggest that diurnal variations of water pressure at the ice-bed interface drive a vertical flux of water into (at times of high pressures) and out of (at time of low pressure) the sediment aquifer. The depth and rate of diffusion of the pressure signal is dependent on the hydraulic conductivity of the sediment, the temporal variation of pressure, and the duration and magnitude of changes in pressure (Kavanaugh and Clarke, 2006). As shown in Figure 5.1a, if diffusion of pressure signals at depth is an important phenomenon at WWG, input of cold meltwater (at times of higher pressure) could result in cooler temperatures within the sediment pack. As shown in Figure 5.1b, with less meltwater input there is a lower pressure zone at the ice-sediment interface, and warmer water can flow towards the ice-bed interface.

Temperatures were recorded at several pro-glacial meltwater outlets at WWG in 2008 (Fig. 3.19). The recorded temperatures, which measured between 0.22-0.49°C, suggest that water flowing through the system maintains relatively high temperatures. This could imply that a sediment aquifer is

widespread under WWG, allowing consistently high subglacial water temperatures. However, warm pro-glacial water temperatures could also result from frictional heating as water flows down the riegel; if flow is sufficiently rapid, thermal equilibration with the overlying ice would be prevented, especially if water is flowing in a partly-full channel at atmospheric pressure. Further research at WWG could include continuous temperature measurements at the meltwater outlets to establish whether diurnal variations in temperature are translated to the pro-glacial zone.

Warm, diurnally varying, subglacial water temperatures have also been recorded at Trapridge Glacier, Yukon. Temperature-measuring devices (Analog Devices AD590) were installed within basal sediments at Trapridge Glacier in order to correct for temperature sensitivity of solid-state tilt cells (pers. communication, J. Kavanaugh). As shown in Figure 5.3a, the basal water reaches maximum temperatures of 0.2°C, with diurnal swings of ∼0.25°C for sensor 98TG02; this sensor was installed at a depth of 0.19 m into the subglacial sediments. A second temperature sensor (98TG05) was installed at a depth of 0.15 m in the sediment, and recorded a maximum temperature of 1.1°C with diurnal swings of ∼0.4°C (Fig. 5.3b). Basal water temperatures and diurnal signals recorded at Trapridge Glacier are similar to those seen at WWG. It is therefore possible that the two glaciers experience similar relationships between water pressure, sediment porosity and water temperature. That similar temperature signals were observed in two very different types of glacier (a polythermal, surging valley glacier vs. a temperate, slow-flowing cirque glacier) suggests that variations in basal water temperature could potentially be a common feature for other sediment-based glaciers. Further research is necessary to establish whether this is the case, and also the potential impacts of basal temperature variations on basal melt characteristics and drainage sys-

tem development.

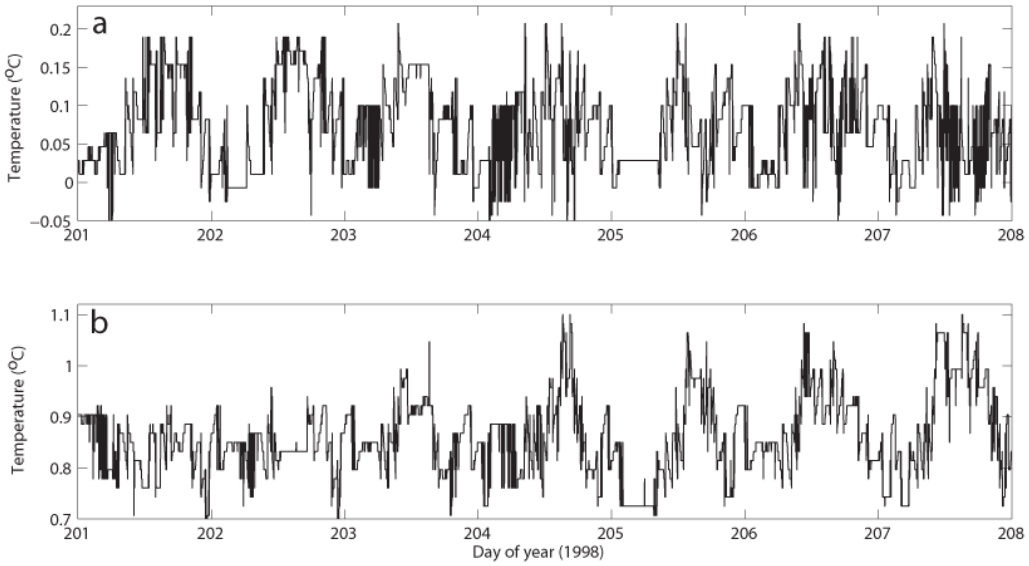

Figure 5.3: Pore-water temperatures at Trapridge Glacier recorded in July 1998. a) 98TG02 temperatures. b) 98TG05 temperatures. Data provided by J. Kavanaugh.

Given the noise and capacitance-driven voltage offset issues with the borehole instrument data (described in Appendix A), it is important to rule out the possibility that the basal water temperature signals are measurment artefacts. Several factors indicate that the water temperature signals at WWG are real:

1. The effect of capacitance on the data series was in the form of sudden, one-time offsets that are associated primarily with installation or removal of sensors from the dataloggers.

2. The temperature signals were diurnally repeating and varied in time (though anti-phased) with changes in basal water pressure observed in the same boreholes.

3. T4 and T8 were attached to the same datalogger, and while T4 showed

diurnal variations in temperature, T8 did not. It is unlikely that the two sensors would have had such different responses to changes in capacitance.

4. T4 and T6 were attached to two separate data loggers, but recorded very similar variations in temperature. Such an in-phase response is unlikely to occur through independent changes in capacitance (Fig. 3.16).

5.2.4 *Basal sediment intrusion into boreholes*

The WWG thermistors were installed ∼65 cm above the base of the boreholes and not within basal sediment. With direct contact between water and ice, diurnal temperature signals would likely be dampened within the borehole. However, there are instances where borehole video footage have shown sediment forced up into glacier boreholes (pers. communication, N. Humphrey). As an open borehole has a lower overburden stress than the surrounding ice (unless the water pressure within the borehole is higher than the overburden stress), sediment in the vicinity could potentially flow into the borehole, perhaps as much as several meters depending on the stress conditions, sediment properties, and sediment availability. At WWG, repeat inclinometry of H5 in August 2008 revealed a change in depth of the borehole by ∼8 m. The repeat inclinometry re-drilling created a ∼20 cm diameter hole, so it is unlikely that the inclinometer was simply unable to pass a constriction within the re-drilled borehole. Such a significant change in depth could have resulted from substantial sediment flow into the borehole, which neither the hot water drill nor inclinometer could penetrate. In addition, recovery of the inclinometry wire weight, which was initially located 30 cm above the base of H5, 'felt like pulling an object from soft mud' (pers. communication, J. Kavanaugh); the wire weight was sediment-covered upon retrieval. Encasement of the weight

in sediment at this height in the borehole implies that the material was forced up into H5, as postulated for H4, H6 and H8. If sediment flow into boreholes occurred at WWG, the basal thermistors could become encased in sediment and potentially record warmer temperatures due to insulation, provided warm water was flowing into the area.

With sediment intrusion into the boreholes, the records from the pressure transducers and conductivity sensors would perhaps also be affected. Regarding the pressure records, diurnal fluctuations would likely then represent changes in pore water pressure communicated through the macro-porous horizon; as noted by Kavanaugh and Clarke (2006), burial in sediment does not preclude variations in basal water pressure. However, the pressure records might be expected to be dampened with perhaps an increased lag between air temperature change and water pressure change. It is not possible to determine whether this is the case from the borehole records, although the lag between air temperature and pressure change is very short. For conductivity, the effects of sediment burial would depend on whether the conductivity sensor cell became packed with material. In the latter case it might be expected that the conductivity sensor sensitivity would be reduced (through changes in the cell constant); conductivity values could also potentially be higher. Again, from the borehole records it is not possible to ascertain the effect of sediment burial on the conductivity sensors.

5.2.5 *Conductivity*

At WWG, the electrical conductivity records vary out-of-phase with basal water pressures and surface air temperatures. As described in Chapter 4, this is often ascribed to influx of fresh, low-conductivity surface water into

a subglacial system that also results in higher water pressures. At times of decreased meltwater input, pressures drop and conductivity increases due to greater contact time with sediment (Collins, 1979a; Gurnell and Fenn, 1985). However, influx of high-conductivity groundwater into a subglacial aquifer at times of lower subglacial water pressure could create a similar out-of-phase response of conductivity in relation to water pressure (as discussed in Section 5.2.3 and shown in Fig. 5.1b). From the records at WWG, it is not possible to distinguish between these two factors for conductivity change; the fluctuations in the conductivity records are therefore only minimally discussed.

5.3 Hydrological shut-down

5.3.1 *Basal pressure*

Following summer 2007, the WWG hydrological system remained active (in terms of basal pressure fluctuations) until early December. The cessation of pressure fluctuations in H6 occurred almost a month before the cessation of pressure fluctuations in H4 and H8, suggesting that H6 had a weaker connection to the distributed drainage system than the other boreholes. (H6, however, is still likely part of the same general drainage system as H4 and H8, as the pressure fluctuations in all these boreholes occurred at similar times with similar patterns of variation). In contrast, the termination of pressure fluctuations in H4 and H8 occurred within ∼2.5 hours of one another, implying a strong connection of these two boreholes to the hydrological system.

In comparison to other glacial systems, the hydrological shut-down at WWG occurred late. For example, at Bench Glacier in Alaska, largely stable winter conditions have been observed to be established around the end of September (Fudge *et al.*, 2008). Basal pressure fluctuations at Trapridge

Glacier have been seen to cease in mid-September (Flowers, 2000). It is unclear what caused continued fluctuations of borehole basal pressures at WWG into mid-November and early December; the air temperature dropped consistently below 0°C on 24 October (day 297), more than a month before the cessation of pressure fluctuations in H4 and H8. The late-season basal signals at WWG could be due to a combination of the following processes:

- Water stored in the surface snow aquifer and englacial system could slowly percolate to the ice-bed interface (e.g. Hodge, 1976; Lingle and Fatland, 2003). However, after 10 November (day 314), the air temperatures consistently remained below -5°C; after this time, and especially once air temperatures approached -25°C at the beginning of December, any remaining water stored in a firn or surface snow aquifer would likely have frozen.

- Pressure signals could occur due to mechanical adjustments of the ice as diminishing subglacial water flow allowed the ice to settle onto the bed. As no mechanical sensors were installed in the boreholes it is not possible to determine whether this is a viable explanation.

- Water at the glacier bed might gradually flow through the system, long after surface input has ceased (e.g. Hubbard and Nienow, 1997; Lingle and Fatland, 2003); groundwater flowing from Helmet Mountain might also continue to contribute to the basal hydrological system until the subglacial drainage network becomes excessively constricted.

- The barrier to supercooled water flow at pressures <130% overburden imposed by the riegel (see Section 4.3 and Fig. 4.4a-c) could prevent drainage of the basal water from the system, once the water input volumes began to drop towards the end of the melt-season. This could

involve the filling and bursting of ponds or storage sites within the overdeepening even after surface air temperatures dropped well below freezing.

5.3.2 *Basal water temperature*

Basal water temperatures in borehole H4 ceased fluctuating within a day of cessation of P4 pressure fluctuations in December 2007. As seen in Figure 3.6, water temperatures in H6 and H8 settled to a relatively steady over-winter value soon after (within nine days). If the lowest temperature for the boreholes is assumed to be the supercooling minimum (see Section 4.4.3 and Fig. 3.18), the over-winter temperatures are approximately 0.12°C (T8), 0.34°C (T4), and 0.44°C (T6). These relatively high over-winter values could be due to the low volume of water likely flowing through the WWG drainage system during the winter season; with little water flow, there is unlikely to be active flow of warm groundwater into the boreholes. Instead, insulation from sediment in the boreholes potentially allows relatively high water temperatures, likely heated from geothermal sources, to be maintained throughout the winter season.

5.4 Spring drainage re-establishment

5.4.1 *Basal water pressure*

Diurnal pressure variations in H4 and H8 re-appeared by mid-July 2008; P4 and P8 pressure changes varied in-phase with change in AWS 1 air temperature, while P10 pressure again demonstrated anti-phased fluctuations with respect to P4 and P8 pressures. Although changes in pressure were recorded in H6, that borehole apparently did not connect to an active diurnally-varying hydrological system prior to failure of sensor P6 on 15 July, 2008. However,

diurnal variability observed in late July 2008 in the C6 record implies that H6 eventually re-connected to an active hydrological system.

5.4.2 *Basal water temperature*

In the spring of 2008, the basal water temperature in boreholes H4 and H6 rose at approximately the same time (days 138 and 139; Fig. 3.6a, b). In H4, this temperature rise (of 0.4°C) occurred at the same time as a rise in P4 pressure and C4 conductivity (Fig. 3.13a); in H6, the water temperature rose 0.2°C at the same time as a drop in P6 pressure (Fig. 3.13b). The air temperature rose consistently above 0°C several days prior to these events (day 135). The T8 temperature rise was more gradual, and began significantly earlier on day 105. This suggests that the spring 2008 reorganization was complex, and developed over a substantial period of time in the study region.

The rise in water temperatures might be the result of influx of warm groundwater into the subglacial system; such water influx could have resulted from the re-charge of the Helmet Mountain groundwater system through melt of snow on the cirque headwall, which might occur substantially earlier than surface melt on the glacier itself. The different pressure responses recorded by P4 and P6 could therefore reflect re-organizational changes in the basal drainage system resulting from this groundwater influx.

A drop in water temperature in H8 to the summer 2007 value occurred at the end of the T8 record on 16 August (day 229; Fig. 3.6c). This temperature drop suggests that by mid-August the subglacial drainage system at WWG had perhaps reached a similar stage of development as that observed in August 2007. A more fully-developed drainage system would allow greater influx of cooler surface water and therefore cooler basal water temperatures.

5.5 Hydraulic Jacking

5.5.1 *Mechanism*

The H10 pressure record indicates an anti-phased response with respect to the H4, H6 and H8 pressure records during the 2007 and 2008 summer seasons. Figure 5.5 shows the P10 records plotted against the P4 and P8 records. These 'phase diagrams' show an out-of-phase, nearly-linear relationship between the pressure records. Clockwise hysteresis in the phase diagrams indicates that pressure changes occur first in boreholes H4 and H8; responses in H10 occur several minutes later. Changes in the vicinity of H4 and H8 (i.e. in what appears to be the main distributed drainage system at WWG) therefore seem to be driving an inverse response in the vicinity of H10. This anti-phased response can be explained by hydraulic jacking. As water pressure rises in the main distributed drainage system, the subglacial water there supports greater parts of the overburden pressure, and the ice is lifted off the bed. In such a distributed system, the hydraulic jacking can potentially occur over a sufficiently large region that surrounding ice can also be lifted off the bed (e.g. Bindschadler, 1983; Iken *et al.*, 1983; Murray and Clarke, 1995; Gordon *et al.*, 1998).

I argue that, with hydraulic jacking in the WWG near-marginal drainage system, the full overburden weight of the ice no longer pressed on an isolated region of water at H10, and so the water pressure decreased. Once pressures decreased in the vicinity of H4 and H8, the ice settled back onto the bed at H10, and the overburden pressure in that region increased resulting in re-pressurization of the isolated water. Figure 5.4 demonstrates this hydraulic jacking process. The P10 pressure record displayed neither substantially lagged nor dampened pressure fluctuations, and out-of-phase responses

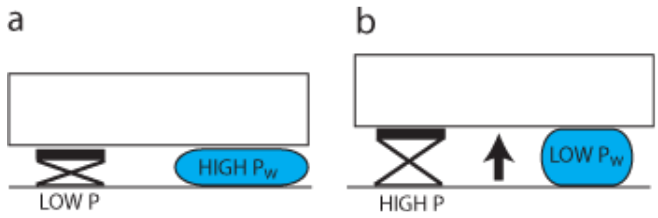

Figure 5.4: Schematic of hydraulic jacking. The jack and related pressure (P) represents the hydrologically connected areas of WWG. The blue balloon represents the isolated region of water intersected by H10 and the related water pressure (P_w). a) The jack at low pressure only holds some of the weight of the overlying block. Therefore, the water pressure in the balloon is high. c) The jack lifts the box up and holds a greater percentage of the weight. The water pressure in the balloon is therefore lower.

were not limited to times of high pressure in H4 and H8. Such a response would be expected if there was active water flow in the vicinity of H10, or water flow from the near-marginal distributed system towards H10 when the ice was lifted off the bed. This suggests that at H10 there was a hydraulically isolated region of water and that the above hydraulic jacking mechanism is plausible.

An interesting feature in these data is that hydraulic jacking occurred even though the basal pressures in H4, H6 and H8 rarely exceeded overburden during summer 2007; anti-phased responses in H10 even occurred when basal pressures in H4 were only ∼60% of flotation. Although the ice overburden would only be fully supported by water pressures at or above the flotation pressure, changes in force spatially integrated over the area of the instrumented boreholes could impact the distribution of normal stresses, which could then be transmitted to larger areas of the bed through the mechanical strength of the ice. (It is worth noting that there might be regions of the bed, not intersected by boreholes, where the water pressure is higher than the ice overburden pressure.) It seems that the distributed system at WWG maintains

sufficiently high pressures to be above some hydraulic jacking threshold at most times during the melt-season. This explains the sensitive anti-phased response of the pressure signal in H10 late into the melt-season in December 2007. Anti-phased pressure signals were re-established in H10 by mid-July 2008, apparently once the distributed system had become sufficiently developed in the vicinity of H4 and H8. The hydraulic jacking phenomenon might therefore be a common feature at WWG.

Hydraulic jacking within the overdeepening at WWG might affect the flow of water over the riegel. If space is created at the glacier bed during hydraulic jacking the flow of water through the system might be altered. For example, hydraulic jacking could potentially change the pressure at the ice-bed interface on the riegel which, as demonstrated in Section 4.3, could affect the flow of water over the adverse slope depending on the volume and velocity of water within the overdeepening and on the riegel. Further investigation is necessary to establish the impact that hydraulic jacking might be having on subglacial water flow pathway development at WWG.

5.5.2 *Soft-bed hydraulic jacking*

Most studies of glacial hydraulic jacking involve hard-bedded glaciers with linked-cavity drainage systems (e.g. Iken and Bindschadler, 1986; Mair *et al.*, 2002b). In fact, Iken and Bindschadler (1986) and Riihimaki *et al.* (2005) have suggested that vertical motion of a glacier indicates that a widespread basal sediment layer is absent. The evidence from WWG, however, suggests that a hard bed is not a pre-requisite for hydraulic jacking. Hydraulic jacking has been observed at other soft-bedded glaciers. Murray and Clarke (1995) reported data from Trapridge Glacier, where unconnected boreholes demonstrated strong anti-correlation to water pressure changes in connected bore-

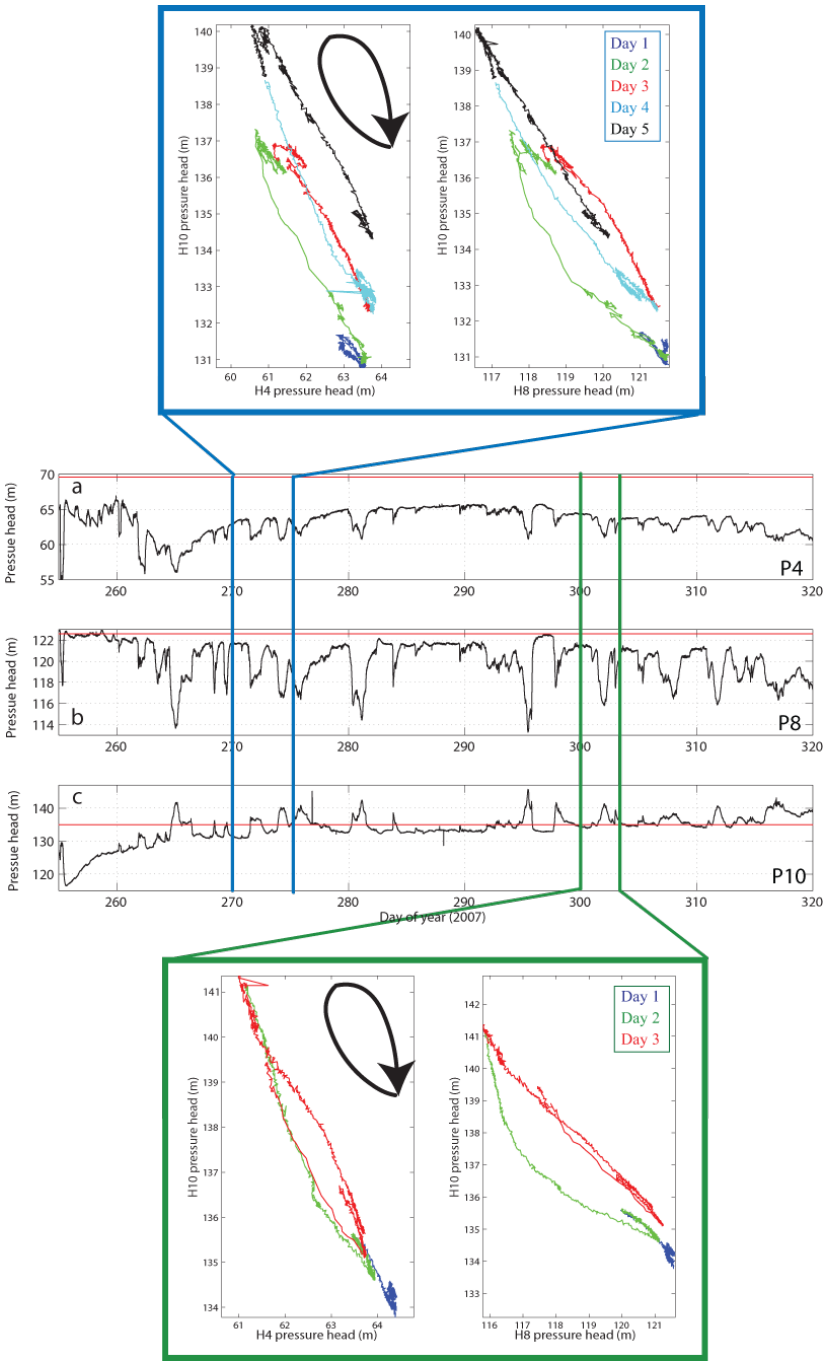

Figure 5.5: Data series of pressure records from mid-September to late November 2007, and related phase plots. a) P4 records (black line) with overburden in red. b) P8 records (black line) with overburden in red. c) P10 records (black line) with overburden in red. The blue phase plots shows data from days 270-275 with each day as a separate colour. The first plot is P4 against P10. The second plot is P8 against P10. The green phase plots are from days 300-303 with each day in a separate colour. The first plot is P4 against P10. The second plot is P8 against P10. The direction of hysteresis is indicated by the black arrows.

holes. Murray and Clarke (1995) explained the observed inverse pressure signals at Trapridge Glacier as follows:

- Changes in basal pressure in some regions impacted the vertical force balance in neighbouring areas of the glacier bed. This resulted in an inverse response between connected and unconnected sensors.

- Large pressure gradients were maintained between the connected and unconnected sensors due to a low-permeability substrate, which restricted water flow.

- At low pressures, a smaller area of the glacier bed at Trapridge was connected to the hydrological system, and therefore had less of an influence on the force balance at the base of the glacier. The hydraulic jacking signal became muted as a result.

- With hydraulic jacking, the ice was decoupled from the basal sediment, and the driving stress was transferred elsewhere.

My explanation for hydraulic jacking at WWG is similar to that suggested by Murray and Clarke (1995). However, at WWG there is no indication that hydraulic jacking became muted at lower basal pressures. The nearly continuous anti-phased signal during the summer months of 2007 and 2008 at H10 indicates the basal network at WWG was almost always above a threshold pressure that would allow hydraulic jacking. The presence of the riegel at WWG, which blocks flow of basal water at low pressures could be contributing to the relatively high basal pressures at WWG that, in turn, facilitate continuous hydraulic jacking cycles during the melt-season. Over winter, the anti-phased hydraulic jacking signal was not apparent in H10, likely due to insufficient variation in basal pressures within the drainage system.

5.6 Implications for cirque erosion

It is widely argued that basal water flow is one of the most important mechanisms for subglacial erosion (Iverson, 1991; Alley *et al.*, 1997, 2003b; Cohen *et al.*, 2006). The hydrological system identified at WWG thus has several implications for the erosion of the cirque glacier:

1. Evidence from temperature, conductivity and pressure records suggests that there was an active basal hydrological system at WWG; an englacial drainage system did not seem prevalent. Basal water flow is an important mechanism for subglacial erosion, especially through quarrying (enhanced by rapid changes in basal water pressure; Hooke, 1991; Iverson, 1991; Alley *et al.*, 1997; Cohen *et al.*, 2006).

2. The drainage network at WWG appeared to be distributed, as evidenced from the discovery of soft sediments at the base of boreholes and the good connections to the hydrological system by three of the boreholes. The removal of sediment from the base of WWG will therefore be relatively inefficient (Alley *et al.*, 2003a), as the most efficient transportation of subglacially weathered material is through a fast-flowing channelized system (Riihimaki *et al.*, 2005).

3. With sediment at the base of the glacier, the capacity for subglacial erosion is reduced. There are two main schools of thought regarding erosion through subglacial sediment:

    - The first school argues that it is difficult to achieve joint breakage in rocks when they are covered by a layer of sediment (Alley *et al.*, 1997). In addition, in a sediment-based system, abrasion and

plucking are not likely to occur as there is little direct contact with rock faces (Alley *et al.*, 1997).

- The second school argues that pressure pulses through sediment could have enough force to quarry underlying rock through changing the distribution of stress at the rock interface (Iverson, 1991; Kavanaugh, 2009). Pressure pulses under Trapridge Glacier were found to reach levels of twice overburden, corresponding to a transient stress of ∼75 times the driving stress (Kavanaugh, 2009). If similar pressure pulses are present at WWG, the stress could be sufficient to enhance weaknesses and cracks in basal rocks underlying the sediment (Kavanaugh, 2009).

4. The observed hydraulic jacking might significantly impact erosion at WWG, as repeated unloading and loading of the glacier bed could enhance erosion of basal material. In addition, when ice is lifted off the bed, the driving stress is transferred to pinning points. This stress transfer to different areas of the glacier might be important for temporal and spatial erosion patterns. It is not known how widespread hydraulic jacking is within the overdeepening as there is only one instrumented hole in the deeper part of the cirque glacier; further research is necessary to establish the extent of hydraulic jacking and its impact on erosion.

5. The riegel at WWG is sufficiently steep to prevent the flow of supercooled water over the riegel at pressures lower than 130-150% of overburden, based on variations of equations developed by Alley *et al.* (1998). Pressures this high were rarely observed in the borehole instrument records. However, with the presence of warm water in the overdeepening, likely facilitated by sediment insulation and groundwater influx, supercooling

probably does not occur and instead the limit to water flow up the adverse slope is based on the hydraulic slope threshold (HST), af following Shreve's (1972) assumptions. As a result, active water flow up the riegel could allow continued erosion of the riegel and transportation of basal sediment from the overdeepening.

6. At WWG, both the strongest hydraulic gradients and the strongest hydraulic connections of boreholes are towards the margin of the glacier. Near-marginal flow could imply that once the ice surface flattens out to a particular gradient in an overdeepening, water preferentially flows towards the edge; this might focus erosion in these regions.

5.7 Conclusions

I suggest that the main hydrological features of WWG from August 2007 through August 2008 consisted of the following:

1. A distributed basal water flow system that resulted from limited water input (given the small size of the cirque), and from the hydrological barrier imposed by the riegel.

2. Sediment-based drainage through a macroporous horizon.

3. Diurnal temperature variations above the pressure melting point within the subglacial sediment aquifer. This was likely due to influx of groundwater and insulation of water by the sediment. Due to hydraulic jacking, a film at the ice-sediment interface could have been formed or increased at high water pressures, allowing cooler water temperatures. Vertical flow deeper into (and out of) the sediment pack might also have contributed to diurnal temperature changes.

4. Hydraulic jacking over a significant portion of the glacier. The hydraulic jacking system was very sensitive to pressure changes in the near-marginal areas, and was observed during the summers of both 2007 and 2008.

5. Late hydrological shut-down. This could be due to a constricted hydrological network that was sensitive to basal water moving slowly through the system long after direct surface water input had ceased; the riegel could have also restricted basal water flow. Additionally, groundwater influx might have contributed to pressure variations late in the melt-season.

6. Re-initiation of a diurnally varying basal hydrological system in July 2008, once surface snow melt allowed greater volumes of water to flow through the cirque system.

The hydrological characteristics of WWG likely have impacts on the erosion of the cirque glacier:

- Basal as opposed to englacial drainage in the overdeepening would allow greater erosion.

- Mechanical hydraulic jacking a) continually loads and unloads the sediment pack and b) shifts overburden stress to pinning points on the glacier bed.

- Flow up the riegel at WWG is possible at high water pressures and when the water temperature is warmer than the local PMP, allowing further erosion of the riegel and transportation of sediment from the overdeepening.

- Near-marginal flow at WWG is suggested by strong hydraulic gradients and the borehole hydrological data, and suggests that erosion is focused towards the margins of the cirque glacier.

Chapter 6

Conclusions

6.1 Summary

This thesis examines the hydrological characteristics of West Washmawapta Glacier, a small overdeepened cirque glacier in the Vermillion Range, B.C., Canada. Installation of pressure transducers, conductivity sensors and thermistors into boreholes drilled to the base of the glacier, along with borehole camera surveys, allowed an assessment of the primary characteristics of the cirque glacier's drainage system.

6.2 WWG hydrology

Despite the fact that it is operating within a small system, the hydrology of West Washmawapta Glacier is complex. The main features of the hydrological system are as follows:

1. Analysis of WWG DEM models shows that, following adaptations of Shreve's (1972) equations, at pressures lower than ∼75% of overburden, the hydraulic potential gradients would act to drive basal water

flow towards the overdeepening. At pressures equal and greater than overburden, the strongest potential gradients are towards the margin of the cirque glacier, driving water flow primarily down-glacier. Assuming the classical view of supercooling (i.e. that basal waters are at the local pressure melting point and at overburden throughout), the adverse slope of the WWG riegel is sufficiently steep to block water flow. However, by modifying the supercooling calculations, I show that once basal water pressures exceed 130-150% of overburden, water can flow up and over the adverse slope. This assumes that water is at the pressure melting point within the overdeepening. However, although water pressures might occasionally reach levels significantly above overburden for a short period, such high pressures would not likely be maintained. Disregarding other factors such as water temperature and water volume within the overdeepening at WWG, this suggests that the riegel could potentially have a significant impact on the subsurface drainage system at this glacier.

2. The *in situ* instrument records indicate that the glacier hydrological system was primarily subglacial. This is suggested by diurnally varying pressure, conductivity and water temperature records, and by a paucity of englacial water passageways identified within the boreholes. Those englacial channels and fractures observed showed little evidence of being connected to a hydrological system.

3. Comparison of borehole records show that hydraulic jacking occurred during both the 2007 and 2008 melt seasons. This is indicated by anti-phased pressure signals in the deepest borehole with respect to pressure changes in the shallower boreholes. Hydraulic jacking also suggests that

the system is primarily basal.

4. The WWG drainage system was distributed and sediment-based, with flow likely occurring through a macroporous horizon. Evidence for a sediment base in the study area include columns of turbid water in boreholes following drilling, a sediment wedge observed at the base of one borehole, and the apparent infill of the base of one borehole with soft sediment. A sediment base, along with strong connection of the three near-marginal boreholes, indicates distributed drainage. The near-synchronicity of water pressure changes in the near-margin boreholes, and basal pressure fluctuations primarily within 60-110% of overburden, also demonstrate that the system was distributed, as channelized systems would be expected to exhibit generally lower diurnal minimum pressures. The very short lag times observed between changes in surface air temperature and basal water pressures suggest flow through a macroporous horizon, allowing relatively rapid transit times within the sediment.

5. Near-marginal flow at WWG is suggested by the strong connections of boreholes towards the glacier margin, along with evidence for little water flow in the deeper regions of the glacier (i.e. the H10 anti-phased pressure signals). These observations provide confirmation for near-marginal flow indicated by the hydraulic potential maps.

6. The WWG hydrological system shut down at the beginning of December, over a month after air temperatures dropped continually below freezing. This is late relative to many valley glacier shut-downs, which are commonly observed to occur in mid- to late-September. The late shut down at WWG was potentially due to the presence of the riegel that bounds the overdeepening affecting the flux of water through the basal

system; groundwater influx into the subglacial hydrological system could also cause fluctuations in basal pressure even after surface temperatures dropped below 0°C.

7. During summer months, basal water temperatures at WWG varied diurnally. These variations were usually nearly anti-phased with changes in basal water pressures, and had amplitudes as large as 0.8°C. The warm temperatures were potentially due to a combination of insulation of basal water within a subglacial sediment aquifer and influx of deeper, geothermally-heated groundwater. Two potential causes for the observed diurnal variations in temperature are 1) hydraulic jacking, which at higher water pressures could create a film of water at the ice-sediment interface, resulting in greater ice-water contact and hence lower water temperatures at higher pressures, and 2) vertical water flow within the sediment pack, where higher meltwater input could drive fluxes of cold water down into the sediment at higher pressures and allow an influx of warm deeper groundwater at lower pressures.

The observed characteristics of the WWG hydrological system suggest that the assumptions underlying the classical hydraulic potential equations and supercooling theory for glacial hydrology are overly-simplified. In both cases, varying basal water pressures significantly change the calculated slope thresholds for water flow over an adverse slope. For overdeepening hydrology, variations in basal pressure therefore appear to be very important for establishing flow pathways in the glacier. I also note here that, to fully establish the water flow thresholds on a riegel, information is required about the volume and velocity of water flowing through the system. The latter are difficult to come by in subglacial investigations but in the future should be taken into

account as much as possible. With varying basal water temperatures in the overdeepening, in addition to the above factors, the occurrence and impact of supercooling is potentially highly variable.

6.3 Implications for erosion at WWG

The erosion of WWG is likely affected by the hydrological characteristics identified in this study. It is possible that some of the hydrological characteristics and related potential erosional impacts also occur at other cirque glaciers. The following are the postulated effects of the hydrological system on the erosion of WWG:

1. Basal (rather than englacial drainage) in the cirque glacier system is likely to impact the location and rate of subglacial erosion. However, a distributed, sediment-based drainage system suggests that removal of sediment from the base of WWG is inefficient, and it is not yet clear whether erosion can occur through a sediment pack. Further investigation though *in situ* measurements of basal sediment properties and deformation (e.g. with plough-meters and tilt cells) could provide additional information about basal conditions of the glacier and also the characteristics of the subglacial material.

2. The observed hydraulic jacking might significantly impact erosion at WWG, as jacking would repeatedly load and unload the glacier bed, and would change the distribution of resistive stresses at the glacier bed. Drilling of additional boreholes at WWG could reveal the true extent of the hydraulic jacking signal. High-resolution ice surface GPS measurements could also illuminate hydraulic jacking behaviours.

3. Primarily near-marginal flow at WWG suggests that erosion might be currently focused towards the margins of the cirque glacier, as basal water flow is widely argued to be a major agent of subglacial erosion (Iverson, 1991; Alley *et al.*, 1997, 2003b; Cohen *et al.*, 2006).

6.4 Implications for overdeepened glaciers

The results from this study of WWG glacier hydrology could be applicable to other glaciers, in particular those with overdeepenings. The wider implications for other glaciers are as follows:

1. As mentioned above, from this study at WWG, it seems that the classic view of supercooling blockage of flow up a riegel is overly-simplified. This is suggested by two main factors: 1) Water at pressures higher than overburden can flow up adverse riegel slopes that prevent flow at overburden pressure; and 2) water at temperatures warmer than the local pressure melting point in the overdeepening will likely limit freezing while flowing up the riegel. Conversely, at water pressures below overburden, slopes significantly shallower than the classic overburden supercooling slope threshold can create thermodynamic barriers to flow. Supercooling freeze-on might therefore be both spatially and temporally variable, determined by drainage conditions and subglacial topography.

2. Models that incorporate water flow through subglacial sediment (e.g. Flowers and Clarke, 2002; Flowers *et al.*, 2003) do not generally consider the possibility that water can be warmer than the pressure melting point. In addition to affecting the thresholds of flow up adverse basal slopes, temperature fluctuations of subglacial water could potentially impact the rate of melt of basal ice and the development of subglacial drainage sys-

tems. Measurements of basal water temperatures should be performed at other glaciers to determine the importance of these temperature effects.

3. A primarily englacial drainage system, suggested by Hooke and others (Hooke *et al.*, 1988; Hooke, 1989; Hooke and Pohjola, 1994) to be the principal mechanism for drainage in overdeepenings, is apparently not in place at WWG, and might occur only at a subset of overdeepened glaciers, if any. Other overdeepenings, such as at Matanuska Glacier (Lawson *et al.*, 1998) and a smaller overdeepening at Storglaciären (Hanson *et al.*, 1998), also appear to have basal hydrological systems. Further investigations of overdeepened systems is necessary to establish whether basal or englacial drainage systems are the more prevalent. Basal drainage systems will directly impact subglacial erosion rates and ice dynamics whereas an englacial system typically has little effect on glacial dynamics.

6.5 Overview

This study into the subsurface hydrology of an overdeepened cirque glacier constitutes one of a very small number of investigations into cirque glacier hydrology. The information gathered during this hydrological study of West Washmawapta Glacier contributes to theories of cirque hydrology, overdeepening hydrology and also potentially cirque erosion.

Bibliography

Alley, R. B., K. M. Cuffey, E. B. Evenson, J. C. Strasser, D. E. Lawson and G. J. Larson, 1997. How glaciers entrain and transport basal sediment: physical constraints, *Quaternary Science Reviews*, **16**(9), 1017–1038.

Alley, R. B., D. E. Lawson, E. B. Evenson and G. J. Larson, 2003a. Sediment, glaciohydraulic supercooling, and fast glacier flow, *Annals of Glaciology*, **36**(1), 135–141.

Alley, R. B., D. E. Lawson, E. B. Evenson, J. C. Strasser and G. J. Larson, 1998. Glaciohydraulic supercooling: a freeze-on mechanism to create stratified, debris-rich basal ice: II. Theory, *Journal of Glaciology*, **44**(148), 563–569.

Alley, R. B., D. E. Lawson, G. J. Larson, E. B. Evenson and G. S. Baker, 2003b. Stabilizing feedbacks in glacier-bed erosion, *Nature*, **424**(6950), 758–760.

Arcone, S. A., D. E. Lawson and A. J. Delaney, 1995. Short-pulse radar wavelet recovery and resolution of dielectric contrasts within englacial and basal ice of Matanuska Glacier, Alaska, U. S. A, *Journal of Glaciology*, **41**(137), 68–86.

Bates, P. D., M. J. Siegert, V. Lee, B. P. Hubbard and P. W. Nienow, 2003. Numerical simulation of three-dimensional velocity fields in pressurized and non-pressurized Nye channels, *Annals of Glaciology*, **37**, 281–285.

Bayley, O. D. R., 2007. Temperature of a 'Temperate' Alpine Glacier: Glacier de Tsanfleuron, Switzerland, *Ph.D.thesis (unpublished)*, Aberystwyth University, UK.

Benn, D. I. and D.J.A. Evans, 1998. Glaciers and Glaciation, London: Arnold.

Bennett, M. R., D. Huddart and N. F. Glasser, 1999. Large-Scale Bedrock Displacement by Cirque Glaciers, *Arctic, Antarctic, and Alpine Research*, **31**(1), 99–107.

Bindschadler, R., 1983. The importance of pressurized subglacial water in separation and sliding at the glacier bed, *Journal of Glaciology*, **29**(101), 3–19.

Boon, S. and M. Sharp, 2003. The role of hydrologically-driven ice fracture in drainage system evolution on an Arctic glacier, *Geophysical Research Letters*, **30**(18), 1916, doi:10.1029/2003GL018034.

Boulton, G. S. and A. S. Jones, 1979. Stability of temperate ice caps and ice sheets resting on beds of deformable sediment, *Journal of Glaciology*, **24**(90), 3–24.

Chueca, J. and A. Julián, 2004. Relationship between solar radiation and the development and morphology of small cirque glaciers (Maladeta Mountain Massif, Central Pyrenees, Spain), *Geografiska Annaler*, **86**(A), 81–88.

Clarke, G. K. C., 1987a. A short history of scientific investigations on glaciers, *Journal of Glaciology*, **Special Issue**, 4–24.

Clarke, G. K. C., 1987b. Subglacial till: A physical framework for its properties and processes, *Journal of Geophysical Research*, **92**(B9), 9023–9036.

Clarke, G. K. C., 2005. Subglacial Processes, *Annual Review of Earth and Planetary Sciences*, **33**(1), 247–276.

Cohen, D., T. S. Hooyer, N. R. Iverson, J. F. Thomason and M. Jackson, 2006. Role of transient water pressure in quarrying: a subglacial experiment using acoustic emissions, *Journal of Geophysical Research*, **111**(F03006), doi:10.1029/2005JF000439.

Collins, D. N., 1979a. Hydrochemistry of meltwaters draining from an Alpine glacier, *Arctic and Alpine Research*, **11**(3), 307–324.

Collins, D. N., 1979b. Quantitative determination of the subglacial hydrology of two Alpine glaciers, *Journal of Glaciology*, **23**(89), 347–362.

Cook, S. J., R. I. Waller and P. G. Knight, 2006. Glaciohydraulic supercooling: the process and its significance, *Progress in Physical Geography*, **30**(5), 577–588.

Copland, L., J. Harbor, S. Gordon and M. Sharp, 1998. The use of borehole video in investigating the hydrology of a temperate glacier. In M. Sharp, K. S. Richards and M. Tranter (eds.), *Glacier hydrology and hydrochemistry*, Chichester: J. Wiley, 191–203.

Creyts, T., 2007. A Numerical Model of Glaciohydraulic Supercooling, *Ph.D.thesis (unpublished)*, University of British Columbia, Canada.

Currie, K. L., 1975. The Geology and Petrology of the Ice River Alkaline Complex, British Columbia, *Geological Survey of Canada Bulletin*, **245**.

Elliston, G. R., 1973. Water movement through the Gornergletscher, *Proceedings of the Symposium on the Hydrology of Glaciers, Cambridge, 7-13 September 1969*, International Association of Scientific Hydrology Publications, No. 95, 79–84.

Engelhardt, H. F., W. D. Harrison and B. Kamb, 1978. Basal sliding and conditions at the glacier bed as revealed by bore-hole photography, *Journal of Glaciology*, **20**(84), 469–508.

Evans, I. S., 2006. Allometric development of glacial cirque form: geological, relief and regional effects on the cirques of Wales, *Geomorphology*, **80**(3-4), 245–266.

Fenn, C. R., 1987. Electrical Conductivity. In A. M. Gurnell and M. J. Clark (eds.), *Glacio-Fluvial Sediment Transfer: An Alpine Perspective.*, New York: John Wiley and Sons, 377–414.

Fischer, U. H. and G. K. C. Clarke, 2001. Review of subglacial hydromechanical coupling: Trapridge Glacier, Yukon Territory, Canada, *Quaternary International*, **86**(1), 29–43.

Flowers, G. E., 2000. A Multicomponent Coupled Model of Glacier Hydrology, *Ph.D.thesis (unpublished)*, University of British Columbia, Canada.

Flowers, G. E., H. Björnsson and F. Pálsson, 2003. New insights into the subglacial and periglacial hydrology of Vatnajökull, Iceland, from a distributed physical model, *Journal of Glaciology*, **49**(165), 257–270.

Flowers, G. E. and G. K. C. Clarke, 2002. A multicomponent coupled model of glacier hydrology: 1. Theory and synthetic examples, *Journal of Geophysical Research*, **107**(B11), 2287, doi:10.1029/2001JB001122.

Fountain, A. G., 1993. Geometry and flow conditions of subglacial water at South Cascade Glacier, Washington State, U.S.A.: an analysis of tracer injections, *Journal of Glaciology*, **39**(131), 143–156.

Fountain, A. G., 1994. Borehole water-level variations and implications for the subglacial hydraulics of South Cascade Glacier, Washington State, U.S.A., *Journal of Glaciology*, **40**(135), 293–304.

Fountain, A. G., 1998. Effect of snow and firn hydrology on the physical and chemical characteristics of glacial runoff. In M. Sharp, K. S. Richards and M. Tranter (eds.), *Glacier Hydrology and Hydrochemistry*, Chichester: J. Wiley, 15–28.

Fountain, A. G., R. W. Jacobel, R. Schlichting and P. Jansson, 2005a. Fractures as the main pathways of water flow in temperate glaciers, *Nature*, **433**(7026), 618–621.

Fountain, A. G., R. B. Schlichting, P. Jansson and R. W. Jacobel, 2005b. Observations of englacial water passages: a fracture-dominated system, *Annals of Glaciology*, **40**, 25–30.

Fountain, A. G. and J. S. Walder, 1998. Water flow through temperate glaciers, *Reviews of Geophysics*, **36**(3), 299–328.

Fudge, T. J., N. F. Humphrey, J. T. Harper and W. T. Pfeffer, 2008. Diurnal fluctuations in borehole water levels: configuration of the drainage system beneath Bench Glacier, Alaska, U.S.A., *Journal of Glaciology*, **54**(185), 297–306.

Gordon, J. E., 1977. Morphometry of cirques in the Kintail-Affric-Cannich area of northwest Scotland, *Geografiska Annaler. Series A. Physical Geography*, **59**(3/4), 177–194.

Gordon, S., M. Sharp, B. Hubbard, C. Smart, B. Ketterling and I. Willis, 1998. Seasonal reorganization of subglacial drainage inferred from measurements in boreholes, *Hydrological Processes*, **12**(1), 105–133.

Gordon, S., M. Sharp, B. Hubbard, I. Willis, C. Smart, L. Copland, J. Harbor and B. Ketterling, 2001. Borehole drainage and its implications for the investigation of glacier hydrology: experiences from Haut Glacier d'Arolla, Switzerland, *Hydrological Processes*, **15**(5), 797–813.

Gurnell, A. M. and C. R. Fenn, 1985. Spatial and temporal variations in electrical conductivity in a pro-glacial stream system, *Journal of Glaciology*, **31**(108), 108–114.

Hammar, L. and H. T. Shen, 1995. Frazil evolution in channels, *Journal of Hydraulic Research*, **33**(3), 291–306.

Hanson, B., R. L. Hooke and E. M. Grace, 1998. Short-term velocity and water-pressure variations down-glacier from a riegel, Storglaciären, Sweden, *Journal of Glaciology*, **44**(147), 359–367.

Hantz, D. and L. Lliboutry, 1983. Waterways, ice permeability at depth, and water pressures at Glacier d'Argentière, French Alps, *Journal of Glaciology*, **29**(102), 227–239.

Harper, J. T., N. F. Humphrey, W. T. Pfeffer, T. Fudge and S. O'Neel, 2005. Evolution of subglacial water pressure along a glacier's length, *Annals of Glaciology*, **40**(1), 31–36.

Harper, J. T., N. F. Humphrey, W. T. Pfeffer and B. Lazar, 2007. Two modes of accelerated glacier sliding related to water, *Geophysical Research Letters*, **34**(L12503), doi:10.1029/2007GL030233.

Harrison, W. D. and A. S. Post, 2003. How much do we really know about glacier surging?, *Annals of Glaciology*, **36**(1), 1–6.

Hasnain, S. I., P. G. Jose, S. Ahmad and D. C. Negi, 2001. Character of the subglacial drainage system in the ablation area of Dokriani glacier, India, as revealed by dye-tracer studies, *Journal of Hydrology*, **248**(1-4), 216–223.

Hock, R., A. Iken and A. Wangler, 1999. Tracer experiments and borehole observations in the overdeepening of Aletschgletscher, Switzerland, *Annals of Glaciology*, **28**(1), 253–260.

Hodge, S. M., 1976. Direct measurement of basal water pressures: a pilot study, *Journal of Glaciology*, **16**(74), 205–218.

Hodge, S. M., 1979. Direct measurement of basal water pressures: progress and problems, *Journal of Glaciology*, **23**(89), 309–319.

Holmlund, P., 1991. Cirques at low altitudes need not necessarily have been cut by small glaciers, *Geografiska Annaler*, **73**(A), 9–16.

Hooke, R. L., 1989. Englacial and subglacial hydrology: a qualitative review, *Arctic and Alpine Research*, **21**(3), 221–233.

Hooke, R. L., 1991. Positive feedbacks associated with erosion of glacial cirques and overdeepenings, *Bulletin of the Geological Society of America*, **103**(8), 1104–1108.

Hooke, R. L., 2005. Principles of Glacier Mechanics, Cambridge University Press, Cambridge.

Hooke, R. L., P. Calla, P. Holmlund, M. Nilsson and A. Stroeven, 1989. A 3 year record of seasonal variations in surface velocity, Storglaciären, Sweden, *Journal of Glaciology*, **35**(120), 235–247.

Hooke, R. L., S. B. Miller and J. Kohler, 1988. Character of the englacial and subglacial drainage system in the upper part of the ablation area of Storglaciären, Sweden, *Journal of Glaciology*, **34**(117), 228–231.

Hooke, R. L. and V.A. Pohjola, 1994. Hydrology of a segment of a glacier situated in an overdeepening, Storglaciären, Sweden, *Journal of Glaciology*, **40**(134), 140–148.

Hooke, R. L. B., B. Wold and J. O. Hagen, 1985. Subglacial hydrology and sediment transport at Bondhusbreen, southwest Norway, *Geological Society of America Bulletin*, **96**(3), 388–397.

Hubbard, Bryn and Peter Nienow, 1997. Alpine subglacial hydrology, *Quaternary Science Reviews*, **16**(9), 939–955.

Hubbard, B. P., M. J. Sharp, I. C. Willis, M. K. Nielsen and C. C. Smart, 1995. Borehole water-level variations and the structure of the subglacial hydrological system of Haut Glacier d'Arolla, Valais, Switzerland, *Journal of Glaciology*, **41**(139), 572–583.

Iken, A., 1981. The effect of the subglacial water pressure on the sliding velocity of a glacier in an idealized numerical model, *Journal of Glaciology*, **27**(97), 407–421.

Iken, A. and R. A. Bindschadler, 1986. Combined measurements of subglacial water pressure and surface velocity of Findelengletscher, Switzerland: conclusions about drainage system and sliding mechanism, *Journal of Glaciology*, **32**(110), 101–119.

Iken, A., K. Fabri and M. Funk, 1996. Water storage and subglacial drainage conditions inferred from borehole measurements on Gornergletscher, Valais, Switzerland, *Journal of Glaciology*, **42**(141), 233–248.

Iken, A., H. Röthlisberger, A. Flotron and W. Haeberli, 1983. The uplift of Unteraargletscher at the beginning of the melt season: a consequence of water storage at the bed?, *Journal of Glaciology*, **29**(101), 28–47.

Isenko, E., R. Naruse and B. Mavlyudov, 2005. Water temperature in englacial and supraglacial channels: change along the flow and contribution to ice melting on the channel wall, *Cold Regions Science and Technology*, **42**(1), 53–62.

Iverson, N. R., 1991. Potential effects of subglacial water-pressure fluctuations on quarrying, *Journal of Glaciology*, **37**(125), 27–36.

Iverson, N. R., R. W. Baker, R. L. Hooke, B. Hanson and P. Jansson, 1999. Coupling between a glacier and a soft bed: I. A relation between effective pressure and local shear stress determined from till elasticity, *Journal of Glaciology*, **45**(149), 31–40.

Iverson, N. R., B. Hanson, R. L. Hooke and P. Jansson, 1995. Flow mechanism of glaciers on soft beds, *Science*, **267**(5194), 80–81.

Iverson, N. R., P. Jansson and R. L. Hooke, 1994. In-situ measurement of the strength of deforming subglacial till, *Journal of Glaciology*, **40**(136), 497–503.

Jansson, Peter, Regine Hock and Thomas Schneider, 2003. The concept of glacier storage: a review, *Journal of Hydrology*, **282**(1-4), 116–129.

Kamb, B., 1987. Glacier surge mechanism based on linked cavity configuration of the basal water conduit system, *Journal of Geophysical Research*, **92**(B9), 9083–9100.

Kavanaugh, J. L., 2009. Exploring glacier dynamics with subglacial water pressure pulses: evidence for self-organized criticality?, *Journal of Geophysical Research*, **114**(F01021), doi:10.1029/2008JF001036.

Kavanaugh, J. L. and G. K. C. Clarke, 2000. Evidence for extreme pressure pulses in the subglacial water system, *Journal of Glaciology*, **46**(153), 206–212.

Kavanaugh, J. L. and G. K. C. Clarke, 2006. Discrimination of the flow law for subglacial sediment using in situ measurements and an interpretation model, *Journal of Geophysical Research*, **111**(F01002), doi:10.1029/2005JF000346.

Lappegard, G. and J. Kohler, 2005. Determination of basal hydraulic systems based on subglacial high-pressure pump experiments, *Annals of Glaciology*, **40**(1), 37–42.

Lawson, D.E., J.C. Strasser, E.B. Evenson, R.B. Alley, G.J. Larson and S.A. Arcone, 1998. Glaciohydraulic supercooling: a freeze-on mechanism to create stratified, debris-rich basal ice: I. Field evidence, *Journal of Glaciology*, **44**(148), 547–562.

Lingle, C. S. and D. R. Fatland, 2003. Does englacial water storage drive temperate glacier surges?, *Annals of Glaciology*, **36**(1), 14–20.

Lliboutry, L., 1964. Sub-glacial 'supercavitation' as a cause of the rapid advances of glaciers, *Nature*, **202**(4927), 77.

Lliboutry, L., 1968. General theory of subglacial cavitation and sliding of temperature glaciers, *Journal of Glaciology*, **7**(49), 21–58.

Lliboutry, L., 1971. Permeability, brine content and temperature of temperate ice, *Journal of Glaciology*, **10**(58), 15–29.

Lliboutry, L., 1976. Physical processes in temperate glaciers, *Journal of Glaciology*, **16**(74), 151–158.

Lliboutry, L., 1983. Modifications to the theory of intraglacial waterways for the case of subglacial ones, *Journal of Glaciology*, **29**(102), 216–226.

López-Moreno, J. I., D. Nogués-Bravo, J. Chueca-Cía and A. Julián-Andrés, 2006. Change of topographic control on the extent of cirque glaciers since the Little Ice Age, *Geophysical Research Letters*, **33**(L24505), doi: 10.1029/2006GL028204.

Mair, D., P. Nienow, M. Sharp, T. Wohlleben and I. Willis, 2002a. Influence of subglacial drainage system evolution on glacier surface motion: Haut Glacier d'Arolla, Switzerland, *Journal of Geophysical Research*, **107**(B8), 2175, 10.1029/2001JB000514.

Mair, D., M. Sharp and I. Willis, 2002b. Evidence for basal cavity opening from analysis of surface uplift during and early melt-season high velocity event: Haut Glacier d'Arolla, Switzerland, *Journal of Glaciology*, **48**(161), 208–216.

Matsuoka, K., T. Thorsteinsson, H. Björnsson and E. D. Waddington, 2007. Anisotropic radio-wave scattering from englacial water regimes, Myrdalsjökull, Iceland, *Journal of Glaciology*, **53**(182), 473–478.

Murray, T. and G. K. C. Clarke, 1995. Black-box modeling of the subglacial water system, *Journal of Geophysical Research*, **100**(B7), 10231–10245.

Murray, T. and P. R. Porter, 2001. Basal conditions beneath a soft-bedded polythermal surge-type glacier: Bakaninbreen, Svalbard, *Quaternary International*, **86**(1), 103–116.

Nienow, P., M. Sharp and I. Willis, 1998a. Seasonal changes in the morphology of the subglacial drainage system, Haut Glacier d'Arolla, Switzerland, *Earth Surface Processes and Landforms*, **23**(9), 825–843.

Nienow, P. W., M. Sharp and I. C. Willis, 1998b. Velocity-discharge relationships derived from dye tracer experiments in glacial meltwaters: implications for subglacial flow conditions. In M. Sharp, K. S. Richards and M. Tranter (eds.), *Glacier Hydrology and Hydrochemistry*, Chichester: J. Wiley, 103–117.

Nye, J.F., 1973. Water at the bed of a Glacier, *Proceedings of Symposium on the Hydrology of Glaciers, Cambridge, 7-13 September 1969*, International Association of Scientific Hydrology Publications, No. 95, 189–194.

Nye, J.F. and F.C. Frank, 1973. Hydrology of the intergranular veins in a temperate glacier, *Proceedings of Symposium on the Hydrology of Glaciers, Cambridge, 7-13 September 1969*, International Association of Scientific Hydrology Publications, No. 95, 157–161.

Oldenborger, G. A., G. K. C. Clarke and D. H. D. Hildes, 2002. Hydrochemical coupling of a glacial borehole-aquifer system, *Journal of Glaciology*, **48**(162), 357–368.

Olyphant, G. A., 1981. Allometry and cirque evolution, *Geological Society of America Bulletin, Part I*, **92**(9), 679–685.

Oskin, M. and D. W. Burbank, 2005. Alpine landscape evolution dominated by cirque retreat, *Geology*, **33**(12), 933–936.

Paterson, W. S. B., 1994. The Physics of Glaciers, 3rd Edition, Oxford, U.K.: Pergamon Press.

Piotrowski, J. A., 2003. Glaciers at work, *Nature*, **424**, 737–738.

Plewes, L. A. and B. Hubbard, 2001. A review of the use of radio-echo sounding in glaciology, *Progress in Physical Geography*, **25**(2), 203–236.

Pohjola, V. A., 1994. TV-video observations of englacial voids in Storglaciären, Sweden, *Journal of Glaciology*, **40**(135), 231–240.

Raymond, C. F. and W. D. Harrison, 1975. Some observations on the behavior of the liquid and gas phases in temperate glacier ice, *Journal of Glaciology*, **14**(71), 213–234.

Riihimaki, C. A., K. R. MacGregor, R. S. Anderson, S. P. Anderson and M. G. Loso, 2005. Sediment evacuation and glacial erosion rates at a small alpine glacier, *Journal of Geophysical Research*, **110**(F03003), doi:10.1029/2004JF000189.

Roberts, M. J., A. J. Russell, F. S. Tweed and O. Knudsen, 2000. Ice fracturing during jökulhlaups: implications for englacial floodwater routing and outlet development, *Earth Surface Processes and Landforms*, **25**(13), 1429–1446.

Roberts, M. J., F. S. Tweed, A. J. Russell, O. Knudsen, D. E. Lawson, G. J. Larson, E. B. Evenson and H. Bjornsson, 2002. Glaciohydraulic supercooling in Iceland, *Geology*, **30**(5), 439–442.

Röthlisberger, H., 1972. Water pressure in intra-and subglacial channels, *Journal of Glaciology*, **11**(62), 177–203.

Röthlisberger, H. and H. Lang, 1987. Glacial Hydrology. In A. M. Gurnell and M. J. Clark (eds.), *Glacio-Fluvial Sediment Transfer: An Alpine Perspective*, New York: John Wiley and Sons, 207–284.

Rutter, N. J., 2005. Impact of subglacial hydrology on the release of water from temporary storage in an Alpine glacier, *Annals of Glaciology*, **40**, 67–75.

Schuler, T., U. H. Fischer and G. H. Gudmundsson, 2004. Diurnal variability of subglacial drainage conditions as revealed by tracer experiments, *Journal of Geophysical Research*, **109**(F02008), doi: 10.1029/2003JF000082.

Seaberg, S. Z., J. Z. Seaberg, R. L. Hooke and D. W. Wiberg, 1988. Character of the englacial and subglacial drainage system in the lower part of the ablation area of Storglaciären, Sweden, as revealed by dye-trace studies, *Journal of Glaciology*, **34**(117), 217–227.

Sharp, M., K. S. Richards and M. Tranter, 1998. Introduction. In M. Sharp, K. S. Richards and M. Tranter (eds.), *Glacier Hydrology and Hydrochemistry*, Chichester: J. Wiley, 1–14.

Shreve, R. L., 1972. Movement of water in glaciers, *Journal Of Glaciology*, **11**(62), 205–214.

Smart, C. C., 1998. Statistical evaluation of glacier boreholes as indicators of basal drainage systems. In M. Sharp, K. S. Richards and M. Tranter (eds.), *Glacier Hydrology and Hydrochemistry*, Chichester: J. Wiley, 175–189.

Stenborg, T., 1973. Some viewpoints on the internal drainage of glaciers, *Proceedings of Symposium on the Hydrology of Glaciers, Cambridge, 7-13 September 1969*, International Association of Scientific Hydrology Publications, No. 95, 117–129.

Stone, D. B. and G. K. C. Clarke, 1993. Estimation of subglacial hydraulic properties from induced changes in basal water pressure: a theoretical framework for borehole-response tests, *Journal of Glaciology*, **39**(132), 327–340.

Stone, D. B. and G. K. C. Clarke, 1998. *In situ* measurements of basal water quality and pressure as an indicator of the character of subglacial drainage systems. In M. Sharp, K. S. Richards and M. Tranter (eds.), *Glacier Hydrology and Hydrochemistry*, Chichester: J. Wiley, 205–218.

Stone, D. B., G. K. C. Clarke and E. W. Blake, 1993. Subglacial measurement of turbidity and electrical conductivity, *Journal of Glaciology*, **39**(132), 415–420.

Stuart, G., T. Murray, N. Gamble, K. Hayes and A. Hodson, 2003. Characterization of englacial channels by ground-penetrating radar: an example from austre Brøggerbreen, Svalbard, *Journal of Geophysical Research*, **108**(B11), 2525, doi:10.1029/2003JB002435.

Svensson, U. and A. Omstedt, 1994. Simulation of supercooling and size distribution in frazil ice dynamics, *Cold Regions Science and Technology*, **22**(3), 221–233.

Swift, D. A., P. W. Nienow and T. B. Hoey, 2005. Basal sediment evacuation by subglacial meltwater: suspended sediment transport from Haut Glacier d'Arolla, Switzerland, *Earth Surface Processes and Landforms*, **30**(7), 867–883.

Truffer, M. and W. D. Harrison, 2006. In situ measurements of till deformation and water pressure, *Journal of Glaciology*, **52**(177), 175–182.

Tsang, G. and T. O'D. Hanley, 1985. Frazil formation in water of different salinities and supercoolings, *Journal of Glaciology*, **31**(108), 74–85.

Turnbull, J. M. and T. R. H. Davies, 2006. A mass movement origin for cirques, *Earth Surface Processes and Landforms*, **31**(9), 1129–1148.

Tweed, F. S., M. J. Roberts and A. J. Russell, 2005. Hydrologic monitoring of supercooled discharge from Icelandic glaciers, *Quaternary Science Reviews*, **24**, 2308–2318.

van der Veen, C. J., 1998. Fracture mechanics approach to penetration of bottom crevasses on glaciers, *Cold Regions Science and Technology*, **27**(3), 213–223.

Vivian, R., 1980. The nature of the ice rock interface: the results of investigation on 20000 m^2 of the rock bed of temperate glaciers, *Journal of Glaciology*, **25**(92), 267–277.

Walder, J. and B. Hallet, 1979. Geometry of former subglacial water channels and cavities, *Journal of Glaciology*, **23**(89), 335–345.

Walder, J. S., 1982. Stability of sheet flow of water beneath temperate glaciers and implications for glacier surging, *Journal of Glaciology*, **28**(99), 273–293.

Walder, J. S., 1986. Hydraulics of subglacial cavities, *Journal of Glaciology*, **32**(112), 439–445.

Walder, J. S. and A. Fowler, 1994. Channelized subglacial drainage over a deformable bed, *Journal of Glaciology*, **40**(134), 3–15.

Weertman, J., 1972. General theory of water flow at the base of a glacier or ice sheet, *Reviews of Geophysics and Space Physics*, **10**(1), 287–333.

Weertman, J., 1973. Can a water-filled crevasse reach the bottom surface of a glacier?, *Proceedings of Symposium on the Hydrology of Glaciers, Cambridge, 7-13 September 1969*, International Association of Scientific Hydrology Publications, No. 95, 139–145.

Willis, I. C., K. S. Richards and M. J. Sharp, 1998. Links between proglacial stream suspended sediment dynamics, glacier hydrology and glacier motion at Midtdalsbreen, Norway. In M. Sharp, K. S. Richards and M. Tranter (eds.), *Glacier Hydrology and Hydrochemistry*, Chichester: J. Wiley, 119–137.

Zotikov, I. A., 1986. *The Thermophysics of Glaciers*, Norwell, MA: D. Reidel.

Zurbuchen, J. M., 2000. Precision thermistor Thermometry. Measurement science conference tutorial, *Measurement Specialties, Temperature Product Group: Application Note*, 1–26.

Appendix A

Capacitance-driven errors

Upon inspection of the WWG borehole sensor data, two issues were discovered. The first issue was that anomalous jumps and drops in the data series occurred at times of connection or disconnection of other instruments from the datalogger or when the datalogger program was changed. The second issue was that high frequency noise appeared in some of the records; in some cases, this noise also began at times of addition or removal of instruments from the dataloggers. Issues such as these are not common in other glaciological field programs, for example at Trapridge Glacier. There are two main differences between the WWG and the Trapridge field programs that might have contributed to the above issues mentioned for WWG. The first is that newer CR1000 dataloggers were used at WWG, whereas older CR10X dataloggers were used at Trapridge. The second is that the basal instrument wire lengths were substantially longer at WWG than at Trapridge ($\sim$250 m vs. 100 m; pers. communication, J. Kavanaugh).

Based on discussions with Campbell Scientific, Canada (pers. communication, C. Labine and J. Rogoza), we believe these issues primarily result from the effect of additional capacitance in the instrument wires. Capacitance is

the tendency (or 'capacity') for two neighbouring metal bodies to store electrical charge. In the WWG study, the longer wire lengths are believed to have resulted in increased capacitance, which affected the data in several ways. Below, the effect of capacitance on the necessary instrument settling times and instrument voltage jumps and drops will be discussed, followed by a discussion of noise in the data series.

Settling time

In the case of the pressure transducers and the conductivity sensors, original calibrations were carried out on CR10X dataloggers, but measurements after installation were recorded on CR1000 dataloggers. For the conductivity sensors this was determined not to be an issue (see Appendix B). However, calibrations of the WWG pressure transducers on CR10X dataloggers were not directly transferable to the CR1000 dataloggers. The inconsistency between loggers is likely due to the fact that different settling times are used by the different logger models. For the pressure transducers, the default integration time for the CR10X loggers was 2.72 ms; for the CR1000 loggers, the settling time was 450μs (in both cases, default settling times were used). Given the long wire lengths attached to the pressure transducers (185-250 m; see Table 2.1), the settling time for neither the CR10X nor the CR1000 were sufficient to allow the full voltage signals to transfer from the pressure transducers to the dataloggers (pers. communication, C. Labine and J. Rogoza, Campbell Scientific). Figure A.1 shows an illustration of a hypothetical settling time curve; the black dashed lines indicate different points of the curves measured by the CR1000 and CR10X dataloggers. Ideally, sufficient time should be allowed for the curve to level off so that the full voltage output signal can be recorded.

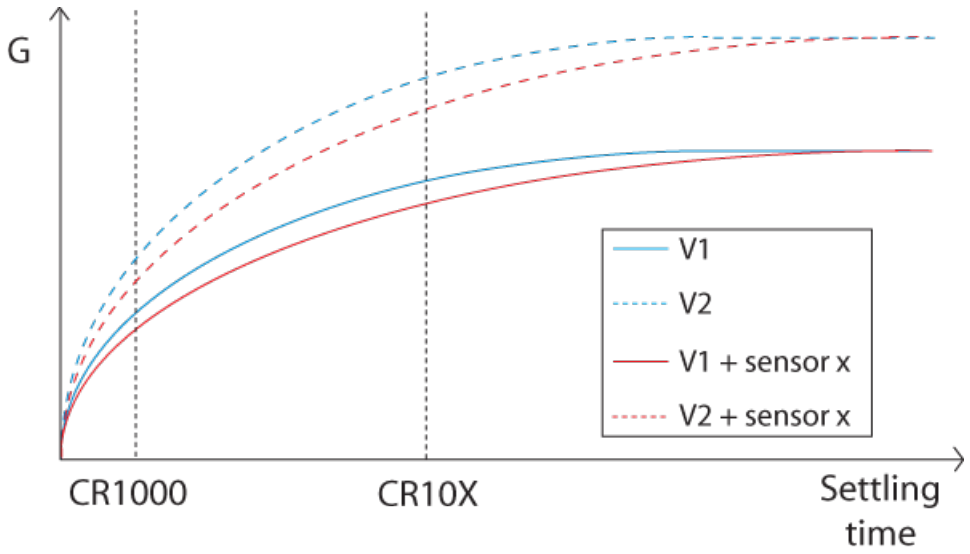

Figure A.1: A plot of the changes in instrument gain (G = Voltage out/Voltage in) with increased settling time. V1 (blue solid) is the settling curve for a single instrument on the datalogger. With higher pressures, the settling curve outputs a higher voltage V2 (blue dashed). V1 + sensor x (red solid) shows the change in the curve when an additional sensor is added to the datalogger; the added capacitance results in a slower rising curve. Increased pressure then produces a higher voltage output V2 + sensor x, also with a slower rising curve (red dashed). The black dashed lines illustrates the part of the curve recorded by the CR1000 and CR10X dataloggers (integration times not to scale). Ideally, measurements would be recorded once the settling curve had levelled out.

Fortunately, the Campbell Scientific dataloggers are very temporally consistent and so it can be assumed that the same point on the settling time curve is sampled at each measurement interval. As a result, individual scaling factor corrections can be applied to the instrument outputs to establish the correct voltage for each sensor (Fig. A.1). The scaling factors necessary to correct for the differences between the CR10X pressure transducer calibration output and the CR1000 measured pressure head ranged between 0.99-1.02. For descriptions on the instrument re-calibration efforts with scaling factors to compensate for the settling time, see Appendix B.

Changes associated with instrument connection/disconnection

The anomalous jumps and drops in the records of several instruments occurred within one measurement interval at times when instruments were added or removed from the dataloggers, or when the datalogger program was changed. The jumps were seen in two independent dataloggers and affected the records of the H4, H6 and H8 sensors. In some cases, the change in logger output also coincided with a significant increase in noise. Table A.1 details the changes in sensor output corresponding to times of instrument addition or removal. Figure A.2 shows one such change, with a drop in temperature and simultaneous increase in noise in T6 and C6 when an additional thermistor was added to the datalogger.

Campbell Scientific was consulted about the problems associated with instrument addition and removal. They suggested that changes in capacitance might be affecting the instruments (pers. communication, C. Labine and J. Rogoza, Campbell Scientific). The long wire lengths, either coiled up next to the datalogger, or strung alongside other instruments down the borehole, could change the capacitance of the logger/wire/instrument combination. Altering the system capacitance also changes the necessary settling time for the instruments. Figure A.1 illustrates an increase in capacitance with the addition of another sensor to a datalogger; additional capacitance causes a slower rising curve so that additional settling time would be necessary to guarantee full voltage outputs. These changes in capacitance and the settling time curve can be compensated for with scaling factors (see Appendix B).

Table A.1: Instrument addition and removal

Logger	Borehole	Instrument affected	Day of year	Voltage output	Instrument value change	Noise created?	Cause
1	H4	P4	228 (07)	jump	+7.1 m	no	P tested in logger/program changed
1	H4	C4	229 (07)	jump	-0.86 μS cm^{-1}	no	C8 added to logger
1	H4	C4	229 (07)	drop	+0.84 μS cm^{-1}	no	T8 added to logger
1	H4	C4	229 (07)	jump	-1.4 μS cm^{-1}	no	T8 fully wired in logger
1	H4	T4	229 (07)	drop	+1.3°C	yes	C8, P8 and T8 added to logger
1	H4	C4	229 (07)	drop	+0.9μS cm^{-1}	no	C8, P8 and T8 installed in H8
1	H4	T4	208 (08)	jump	-1.34°C	yes	P4 and P8 removed from logger
1	H4	C4	208 (08)	no change	no change	yes	P4 and P8 removed from logger
1	H8	C8	208 (08)	no change	no change	yes	P4 and P8 removed from logger
1	H8	T8	208 (08)	no change	no change	yes	P4 and P8 removed from logger
2	H6	C6	228 (07)	jump	-1.2 μS cm^{-1}	no	T6 program changed
2	H6	C6	229 (07)	drop	+2.25 μS cm^{-1}	no	C removed from logger
2	H6	T6	229 (07)	drop	+0.9°C	no	C removed from logger
2	H6	P6	229 (07)	drop	-3.9 m	no	C removed from logger
2	H6	T6	236 (07)	jump	-1.25°C	no	T removed from logger
2	H6	C6	236 (07)	jump	-0.27 μS cm^{-1}	yes	T removed from logger
2	H6	T6	236 (07)	drop	+1.15°C	yes	T added to logger

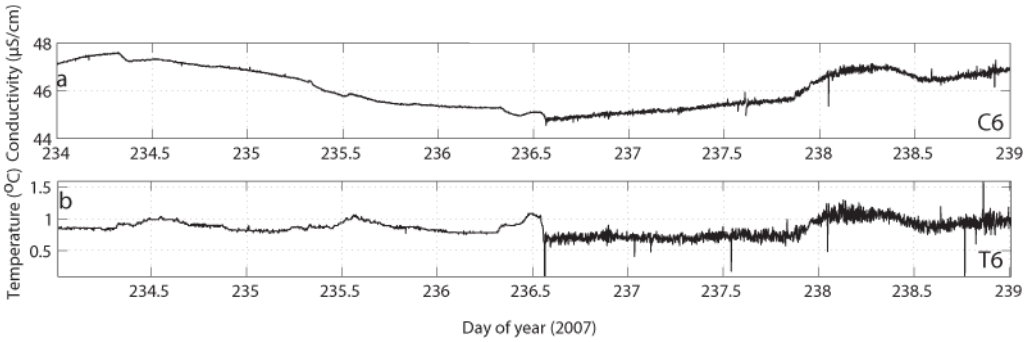

Figure A.2: Data plots from H6. a) C6 record with a slight drop and increase in noise on day 236 when a thermistor was removed from the datalogger. b) T6 record with a drop and substantial noise increase on day 234 when the thermistor was removed.

Noise in the data series

Campbell Scientific suggested that the noise created at the times of instrument addition or removal (see Fig. A.2) was due to the ungrounded nature of dataloggers situated on ice (pers. communication, C. Labine and J. Rogoza, Campbell Scientific). This is potentially made more severe by the fact that the wires were both unshielded and long, and thus acted as antennae. It is not clear what the environmental source of the noise is. For details on filtering used to remove this noise see Appendix B.

Recommendations for future work

The instrument data problems have been compensated for in this study (see Appendix B). However for future work, ideally an appropriate settling time would be calculated prior to installation of instruments. With a sufficiently long settling time, shielded wire could be used to reduce the noise (shielded wire increases capacitance effects and so longer settling times would be needed).

Appendix B

Calibrations

The calibration procedures for WWG pressure transducers, thermistors and conductivity sensors are explained in this Appendix.

Pressure transducer

Omega Engineering Inc. (PX302-300AV) pressure transducers measure changes in pressure head in a borehole by sensing deflection of a thin diaphragm. The circuit used to sense this deflection is a full-bridge (Fig B.3).

Pressure transducers were calibrated in a 50 m deep borehole (H1) at WWG. Measurements at 5 m intervals were recorded on a CR10X Campbell Scientific datalogger. Data were recorded both while the transducers were lowered and raised up the borehole to calculate the error. Linear relationships between the borehole depth and recorded gain ($G = V_{out}/V_{in}$) were calculated through least squares fitting (Fig. B.2). The pressure transducer random errors are described in Table B.1. An offset was added to each pressure transducer record to account for the additional depth of the borehole below the instrument (see Fig. 2.7). For the majority of boreholes, calculating the offset was

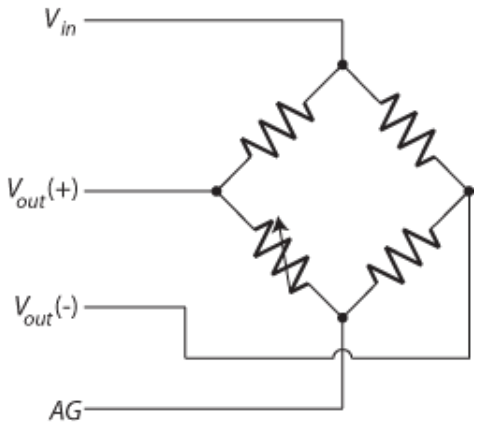

Figure B.1: Diagram of a full bridge circuit. V_{in} is the excitation voltage from the datalogger. V_{out} is the output voltage from the pressure transducer. AG is ground.

straightforward as the base of the borehole could be felt while installing the instrument. The sensors were then raised a known distance (∼0.2 m) above the bed (see Table 2.1). For H10, the offset was significantly larger at ∼80 m due to blockage of the hole by a rock. The depth of H10 has been estimated from a combination of the drilling record, the basal DEM and the estimated over-winter pressure head. As the exact depth of H10 is not known, the systematic error for H10 is fairly large (Table B.1).

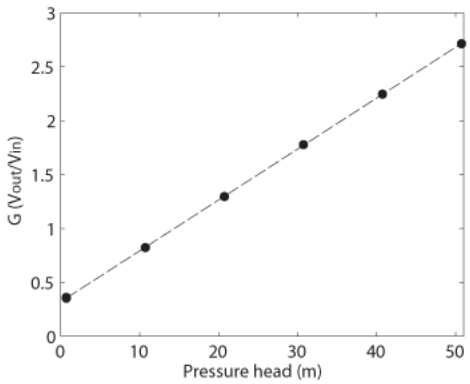

Figure B.2: Calibration of pressure transducer P6. The black dots represent the depths used in calibration; the dashed line is the least-squares fitted calibration line.

As described in Appendix A, calibrations of instruments from Campbell Scientific CR10X dataloggers did not always translate directly to Campbell Scientific CR1000 datalogger measurements. Given that the pressure transducers were calibrated with the former, but wired to the latter, additional calibration steps were taken. The correction was made using borehole water levels indicated by the borehole video camera. To account for the lag between the video survey and the installation of the pressure transducers, the trends in the initial borehole pressure records were extrapolated back to the time of the video survey. The lags between borehole camera survey and pressure transducer installation can be seen in Table B.1.

Comparing the estimated pressure head and borehole camera water depth allowed the pressure transducer records to be re-adjusted with scaling factors (as the pressure transducers operate on a full-bridge, the settled value can be either lower or higher than the recorded value depending on the charging of various wire pairs). The scaling factors used to compensate for the change in measurement between the CR10X and CR1000 dataloggers ranged between 0.92-1.06. The resulting systematic errors are described in Table B.1. Additional scaling factors were applied to remove changes in voltage output caused by the addition or removal of instruments from the datalogger (see Appendix A). Noise was not a problem for the pressure transducer records at WWG and therefore no filtering of the pressure data was necessary.

Conductivity sensors

The electrical conductivity sensors consisted of a half-bridge AC circuit (Fig. B.3) and operated with a 10,000 Ω, 1% reference resistor. With increasing conductivity in the water at the base of the borehole, the current between electrodes

at the base of the conductivity sensors increases and therefore the conductivity sensor's resistance decreases; this is translated to the dataloggers as a reduction in output voltage.

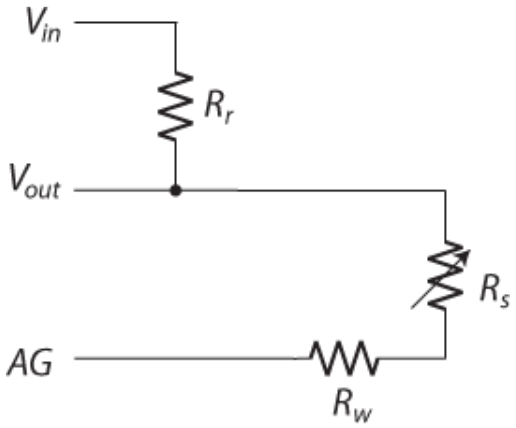

Figure B.3: Diagram of a half bridge circuit. V_{in} is the excitation voltage from the datalogger. V_{out} is the output voltage from the sensor. AG is ground. R_r is the reference resistor, R_s is the alternating resistance from the sensor and R_w is the resistance from the wire. The parallel lines indicate long wire lengths.

Prior to installation, the conductivity sensors were calibrated against an HI 8733 Multi-range Conductivity Meter (accuracy: $\pm 1\%$ at 20°C). The gain ($G = V_{out}/V_{in}$) from borehole conductivity sensors and the conductivity displayed on the hand-held probe were measured simultaneously in low-conductivity water taken from a pro-glacial lake. Salt was incrementally added to the water to

Table B.1: Borehole pressure head error

	P4	P6	P8	P10
Random error				
Least squares fitting	± 0.03 m	± 0.02 m	± 0.05 m	± 0.06 m
Systematic error				
Borehole depth	± 1 m	± 0.5 m	± 2 m	± 20 m
Camera-pressure transducer delay	17 mins	1 hr 45 mins	2 hr 38 mins	36 mins
Camera depth error	± 0.3 m	± 0.3 m	± 0.3 m	± 0.3 m
Camera re-calibration	± 2 m	± 0.7 m	± 2.5 m	± 8 m
Total systematic	± 3.3 m	± 1.5 m	± 4.8 m	± 28.3 m

increase the conductivity. The voltage outputs from the borehole conductivity sensors were recorded on a Campbell Scientific CR10X datalogger.

The gain from the borehole conductivity sensors was converted to conductivity as shown in the following equations:

$$G = \frac{V_{out}}{V_{in}} = \frac{R_s}{R_r + R_s}. \tag{B.1}$$

Here R_s is the resistance measured as 'voltage out' by the datalogger, R_r is the reference resistor in the half-bridge circuit. Re-arranging Equation B.1 to find R_s yields

$$R_s = \frac{G}{1 - G} R_r. \tag{B.2}$$

The resistance of the sensor is related to the conductivity of the water in the following manner. First, it is noted that the conductance (C_c) is the reciprocal of the resistance:

$$C_c = \frac{1}{R_s}. \tag{B.3}$$

Next, the conductance is related to the conductivity σ by a cell constant B (determined by the form of the conductivity sensor):

$$C_c = B\sigma. \tag{B.4}$$

Therefore, by Equations B.3 and B.4, σ is

$$\sigma = \frac{1}{B}\frac{1}{R_s}. \tag{B.5}$$

By substituting in Equation B.2 we find the following relationship:

$$\sigma = \frac{1}{B}\frac{1-G}{G}\frac{1}{R_r}. \tag{B.6}$$

For the WWG calibration, B was calculated by least squares fitting of the conductance from the individual borehole conductivity sensors against the conductivity readings from the HI 8733 meter (Fig. B.4). The slopes of the resulting lines are B. The random errors produced using this method were calculated using linear regression with two standard deviations: C4 ($\pm$ 0.09 μS cm^{-1}), C6 ($\pm$ 0.16 μS cm^{-1}) and C8 ($\pm$ 0.0822 μS cm^{-1}).

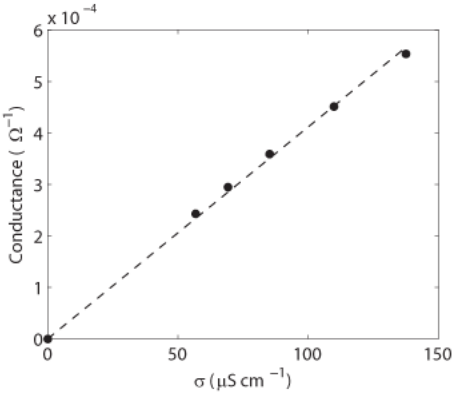

Figure B.4: A plot of the C4 least squares fitting curve. The dashed line is the calibration curve. The black dots shows the conductance from the borehole conductivity sensors with respect to conductivity measured with a hand-held conductivity meter.

Given the issues experienced with other instruments when switching between CR10X and CR1000 calibrations (see Appendix A), one of the calibrated borehole conductivity sensors was re-calibrated with a CR1000 datalogger using similar calibration procedures. For this test, a Cole Parmer 1500-32 Conductivity Meter (accuracy = $\pm$ 2%) was used. The Cole Parmer meter was calibrated in Fisher Scientific Traceable One-shot^{TM} conductivity standard at 10.4 μS cm^{-1} and 100.9 μS cm^{-1}. Measurements from the borehole conduc-

tivity sensor and the Cole Parmer meter were recorded in low-conductivity pro-glacial lake water with small volumes of salt added. Least squares fitting of the CR1000 output showed that there was insignficant change in output between the CR10X and the CR1000 dataloggers for the borehole conductivity sensors. Therefore the original calibration for the conductivity sensors are likely valid, and have been used to determine the conductivity values presented in this thesis.

Noise on the electrical conductivity time series has been removed with a Butterworth low-pass filter with a cut-off frequency of 1 hour. The changes in capacitance with addition and removal of instruments from the dataloggers had only a small impact on the conductivity values, with the largest such change measuring just $2.25\,\mu\mathrm{S\ cm^{-1}}$. As a result, not all of the changes in output were corrected. Because the conductivity record is used to examine general trends in basal conditions, not small scale adjustments, such omissions do not impact the interpretation presented here.

Thermistors

The YSI 44033 RC thermistors operated on a half-bridge circuit (Fig. B.3) using a $1000 \pm 5\,\Omega$ resistor. The voltage output from the thermistors represents changes in temperature; as the temperature increases, the resistance (and therefore output voltage) of the thermistor decreases.

YSI 44033 RC thermistors are curve-matched for resistance over a range of temperatures. However, as the thermistors installed in WWG were attached to wires of lengths between 185 m and 250 m before being connected to the

logger (for exact lengths, see Table 2.1), it was discovered that they needed individual calibration. The thermistors were initially calibrated by placing them in supraglacial water (assumed to be 0°C) for approximately half an hour before installation. However, the thermistor calibrations did not settle sufficiently around 0°C to determine the exact temperature. Further calibration of the thermistors was attempted by removing the resistance of the wire, which would otherwise artificially lower the indicated temperature. Additionally, ice baths were used to calibrate the remaining thermistors after the 2007 field season against a Traceable RTD Platinum Thermometer (model 15-077-55). The ice-bath calibrations indicated that additional resistance needed to be removed from the series, which, when applied to the borehole thermistor records, raises the temperature higher.

Unfortunately, the changes in voltage associated with sensor connection /disconnection described in Appendix A significantly affected the thermistor results. Although the jumps and drops were removed from the data with scaling factors for each change in voltage, the calibrations could not be applied to the thermistors. The exact temperature is therefore not known for any of the thermistors.

Although the true temperature values are poorly known, the indicated *changes* in measured temperatures are well constrained. As noted above, the thermistors are 'curve-matched' and are therefore interchangeable to ± 0.1°C. The random error and the thermal drift of thermistors are very low (e.g. mK per year at room temperature; Zurbuchen, 2000).

Noise in the thermistor record was not likely caused by the properties of the thermistors, which are usually very stable (the source of noise is discussed in Appendix A). Thermistor record noise was removed with a Butterworth low-

pass filter. The cut-off frequencies for each thermistor were as follows: T4 (2 hours from day 226(07)-day 199(08), 8 hours from day 200(08)-day 237(08)), T6 (6 hours) and T8 (6 hours). Note that after noise in the records became significantly extensive (from day 140 for T6, and day 208 for T4 and T8), the temperature curves were not analyzed for diurnal variation and were only considered in terms of general trends.